CALIFORNIA ENERGY COMMISSION

CALIFORNIA NATURAL RESOURCES AGENCY

Energy Research and Development Division

FINAL PROJECT REPORT

Advanced Statistical-Dynamical Downscaling Methods and Products for California Electricity System Climate Planning

February 2024 | CEC-500-2024-012

PREPARED BY:

Cayan, D., Pierce, D., DeHaan, L., Guzman-Morales, J., Gershunov, A.,
Clemesha, R., Martin, A., Ullrich, P., Shu, L., Ajami, H., Schreiner-McGraw, A.

University of California, San Diego
University of California, Davis
University of California, Riverside
Portland State University, Portland OR
Primary Authors

Martine Schmidt-Poolman
Project Manager
California Energy Commission

Agreement Number: EPC-16-063

Kevin Uy
Branch Manager
Energy Generation Research Branch

Jonah Steinbuck
Deputy Director
ENERGY RESEARCH AND DEVELOPMENT DIVISION

Drew Bohan
Executive Director

ACKNOWLEDGEMENTS

The authors thank Professor Alex Hall and Drs. Stefan Rahimi-Esfarjani and Neil Berg of the Atmospheric Science Department, University of California Los Angeles for supplying nine-kilometer weather research and forecasting downscaled North American Regional Reanalysis data, along with helpful advice in using that data. We also thank Dr. Tim Brown and staff at the Desert Research Institute for providing a weather research and forecasting regional atmospheric model wind, temperature, and humidity reanalysis dataset. Daily balloon-borne soundings, collected by National Weather Service observers, were obtained from the University of Wyoming.

PREFACE

The California Energy Commission's (CEC) Energy Research and Development Division supports energy research and development programs to spur innovation in energy efficiency, renewable energy and advanced clean generation, energy-related environmental protection, energy transmission and distribution and transportation.

In 2012, the Electric Program Investment Charge (EPIC) was established by the California Public Utilities Commission to fund public investments in research to create and advance new energy solutions, foster regional innovation and bring ideas from the lab to the marketplace. The CEC and the state's three largest investor-owned utilities—Pacific Gas and Electric Company, San Diego Gas & Electric Company and Southern California Edison Company—were selected to administer the EPIC funds and advance novel technologies, tools, and strategies that provide benefits to their electric ratepayers.

The CEC is committed to ensuring public participation in its research and development programs that promote greater reliability, lower costs, and increase safety for the California electric ratepayer and include:

- Providing societal benefits.
- Reducing greenhouse gas emission in the electricity sector at the lowest possible cost.
- Supporting California's loading order to meet energy needs first with energy efficiency and demand response, next with renewable energy (distributed generation and utility scale), and finally with clean, conventional electricity supply.
- Supporting low-emission vehicles and transportation.
- Providing economic development.
- Using ratepayer funds efficiently.

This is the final report for the Advanced Statistical-Dynamical Downscaling Methods and Products for California Electricity System Climate Planning project (EPC-16-063) conducted by University of California, San Diego Campus's Scripps Institution of Oceanography. The information from this project contributes to the Energy Research and Development Division's EPIC Program.

For more information about the Energy Research and Development Division, please visit the CEC's research website (www.energy.ca.gov/research/) or contact the CEC at ERDD@energy.ca.gov.

ABSTRACT

Global climate models provide important information regarding projected climate change, but they do not provide the necessary fine-scale data needed to fully evaluate and prepare for extreme or impactful events. Therefore, climate projections from the global climate models need to be translated to time-scales, and regional or local spatial scales, relevant to California's electricity sector. California's complex topography and hydrological features necessitate higher resolution depictions to illuminate local and regional trends and ultimately to support adaptation planning. This report describes the development of modeling techniques applied to generate high-resolution projections of California's historical and future weather, climate, and hydrologic phenomena. The report addresses the following elements: statistical and dynamical downscaling of meteorological variables; hybrid downscaling techniques, using both statistical and dynamical methods to obtain more accurate downscaling results than would otherwise be possible, hydrological modeling, including surface and groundwater components, and more detailed groundwater modeling of selected aquifers. The report also describes complementary elements that either inform or stem from these downscaling and hydrologic modeling approaches. These include observed datasets that are used for model validation and analysis, and an assessment of variables of interest to California decision makers that can be expected from dynamical and statistical downscaling. Finally, lessons learned, including opportunities and challenges, are also summarized.

Keywords: dynamical downscaling, statistical downscaling, hydrological modeling, climate variability, climate change, California.

Please use the following citation for this report:

Cayan, Daniel, David Pierce, Laurel DeHaan, Janin Guzman-Morales, Alexander Gershunov, Rachel Clemesha, Andrew Martin, Paul Ullrich, Lele Shu, Hoori Ajami, Adam Schreiner-McGraw.*Advanced Statistical-Dynamical Downscaling Methods and Products for California Electricity System Climate Planning.* California Energy Commission. Publication Number: CEC-500-2024-012.

TABLE OF CONTENTS

LIST OF FIGURES

LIST OF TABLES

Page

EXECUTIVE SUMMARY

Introduction

To assess system and infrastructure resilience in the face of present and future climate change, California's electric investor-owned utilities, as well as other stakeholders, require spatially and temporally detailed historical and projected climate, weather, and hydrological data. These data support understanding of the historical variation and projected climate changes, as well as projected variations of temperature, precipitation, and other variables over California's complex terrain and neighboring regions. Of particular importance for risk and adaptation planning, is the understanding of factors involved in extreme climatic events. However, the fine-scale data required to fully evaluate and prepare for extremes and other impactful events are not directly provided by global and some regional climate model histories and projections. Climate projections from the global climate models, therefore, need to be translated to time- and spatial-scales relevant to the electricity sector. This translation requires downscaled weather, climate, and hydrology data from multiple climate scenarios. The techniques to produce the downscaled data are designed to simulate the range of regional climate changes and impacts that are contained in the growing set of climate projections. These techniques, on one hand, need to be sophisticated enough to represent complex regional climate structures, including extreme events, but also efficient enough that computational loads are not prohibitive.

Project Purpose

The purpose of this project was to develop downscaling techniques to provide improved resolution of California's highly variable meteorological conditions; and to conduct exploratory modeling of selected surface and ground water systems employing meteorological variables from downscaled weather and climate models. This report describes the development and use of a hybrid approach that leverages statistical and dynamical methods to improve accuracy of downscaling results and to provide improved resolution of variables of interest to a high-renewables electricity sector. This includes improvements in a gridded observational dataset, hourly statistical downscaling, consideration of vector wind variables, evaluation of downslope wind model simulations; and possible improvements in physical processes included in dynamical modeling of coastal clouds, including aerosol-aware techniques.

Downscaling of global climate model projections and historical simulations can be accomplished using statistical or dynamical modeling, along with application of the multi-decade historical datasets needed to train and validate these models. This project therefore developed *hybrid downscaling techniques,* that use statistical and dynamical methods to obtain improved downscaling results. Some atmospheric variables that are needed by electricity sector stakeholders, such as vector wind, do not have a sufficiently long observational record for training statistical models; and in many cases these variables are still not consistently observed. The output provided by dynamic models may provide a dataset that can fill this void and be used in statistical downscaling. The hybrid techniques make it possible to downscale multiple global climate models and *backcast* historical weather reanalyses, with a specific focus on statistical

and dynamical downscaling of meteorological variables, including winds and coastal cloudiness. The hybrid techniques are needed to downscale multiple emission scenarios and time periods, which will help inform and prepare California for the downscaling of the broad suite of next-generation global climate model simulations currently being developed by the Coupled Model Intercomparison Project, Phase 6. The broad suite of global climate model simulations informs the Intergovernmental Panel on Climate Change and other international and national climate assessments.

Climate projections developed to support prior California Climate Change Assessments focused primarily on daily data. However, some applications require sub-daily information such as hourly temperatures for energy applications, hourly winds for wildfire analysis, and hourly solar insolation for photovoltaic analyses. Consequently, in this project, statistical downscaling of selected variables was pushed to a sub-daily time resolution. To respond to this need, this project produced a dynamical downscaled historical weather reanalysis at hourly resolution and also pushed statistical downscaling to hourly time resolution for variables of importance to California's electricity system. These variables over a 3-kilometer (km) x 3 km grid that covers California and Nevada, include temperatures at individual California station locations, vector wind, and relative humidity.

This project also explored hydrologic phenomena using two hydrological-model systems. Policymakers and stakeholders have an ongoing and growing need for high-resolution and detailed information about stream flows and the temporal-spatial distribution of hydrologic fluxes in a watershed. Because water and energy systems are interdependent, it is expected that projected changes in water supply will impact hydropower production and energy use in the future, as with groundwater pumping. Therefore, assessments of climate change also require information on soil moisture and groundwater fluctuations, which both impact streamflow generation processes and reservoir management.

Project Approach

This project was managed by Dr. Dan Cayan of Scripps Institution of Oceanography at the University of California, San Diego, with teams of researchers from University of California San Diego, Portland State University, University of California Davis, and University of California Riverside carrying out work tasks associated with the development and exploration of components involved in hybrid downscaling, specifically:

- Localized Constructed Analogs Downscaling
- Wind and Humidity Diagnostics
- Modeling and Diagnostics of Marine Stratocumulus Cloud
- Hydrological Modeling Using Simulator for Hydrologic Unstructured Domains and Machine Learning Techniques
- Groundwater Modeling Using ParFlow.CLM software

In this research, increased spatial and temporal resolution of localized constructed analogs statistical downscaling was developed and tested. The localized constructed analogs method is a statistical scheme that produces downscaled estimates suitable for hydrological simulations,

using a multi-scale spatial matching scheme to pick appropriate analog days from observations. This process reduces the averaging across analog cases, and thus, localized constructed analogs produce better estimates of extreme days, constructs a more realistic depiction of the spatial coherence of the downscaled field, and reduces the problem of producing too many light-precipitation days.

Dynamical downscaling experiments were conducted to replicate historical climate conditions using a configuration of the Weather Research Forecasting model that is aimed at simulating Marine Stratocumulus Clouds along and above the California coast. The research team called this model "WRF-CA-CLC." Coastal low clouds (CLC), including stratus, stratocumulus, and fog, are a persistent, seasonal feature of the region's climate. A disproportionate fraction of California's population lives within the coastal zone, and growing photovoltaic electrical generation is sited there. Skill in modeling coastal low clouds along and near the coast is vital for understanding the processes that drive coastal low clouds, and to plan for impacts of its variability on California's electricity sector.

Hydrologic phenomena explored by this research include surface and groundwater components, and groundwater modeling of selected aquifers. These phenomena and aquifers were modeled using two distinct approaches. Where existing hydrologic modeling systems are unable to accommodate California's rough topography, a simulator for hydrologic unstructured domains was designed to cope with this relatively extreme regime. The other approach used in this research relied on a model called ParFlow.CLM, which is designed for massively parallel computer systems, using distributed forcing and land-cover types with the capability to simulate impacts of groundwater pumping and irrigation on exchanges between surface water and groundwater.

Project Results

The research provided a nearly 11-year (2009-2019) dynamically downscaled reanalysis. Reanalyzed datasets provide a comprehensive description of the observed climate as it has evolved. The datasets compensate for inherent biases and inconsistencies of different instruments used to take measurements at different points in weather observation. (NOAA, accessed 2023). The reanalysis supports statistical downscaling experiments and various assessments of model skill and performance. The development and testing of increased spatial and temporal resolution of localized constructed analogs statistical downscaling techniques resulted in outputs of the variables that are of importance to the electricity sector (e.g., temperature, winds, and humidity). Overall, this hourly disaggregation technique provided hourly future projected temperature values that: match observations over the historical period, correctly replicate global climate-model projected trends, and preserve realistic variability on sub-daily time scales. The downscaling was conducted at an increased gridded resolution: to 3km x 3km. This is a substantial advance from the 6km x 6 km resolution applied in the prior generation of downscaling that supported California's Fourth Climate Change Assessment. The research also achieved downscaling of vector winds, not just wind speeds.

As a test and demonstration of the hybrid downscaling procedure, historical fields of vector wind and humidity were downscaled. This was done using the global reanalyses Modern-Era Retrospective Analysis for Research and Applications, Version 2 (MERRA-2), and the European

Center for Medium Range Weather Forecasting Reanalysis, Version 5 (ERA5). The resulting historical wind and humidity records showed strong similarity with the high-resolution Weather Research and Forecasting model description of a selection of Santa Ana wind episodes, based on statistical characteristics that matched Weather Research and Forecasting model data; these data should be useful in describing other extreme events over four decades.

Comparison of the dynamical modeled winds from WRF-CA-CLC with observed winds from the San Diego Gas & Electric weather stations in the San Diego County region showed that the modeled winds were not exceedingly sensitive to the details of the Weather Research and Forecasting model physics package chosen. However, the physical parameters in the packages had a greater effect in producing differing structures of coastal stratus clouds.

WRF-CA-CLC was also used as the primary methodological tool to simulate both coastal low clouds and their brightening in response to increasing aerosol concentrations. Two simulations were run to represent both clean and polluted particulate-matter scenarios. The aerosol concentrations representing each scenario were drawn from previously published observations on the California coast and are representative of current climate and current particulate matter conditions in California. Aerosol susceptibility, defined as the relative change in albedo in response to an increase in aerosol concentration, was used as the primary metric to estimate the response in cloud brightness to particulate matter. The results indicate that polluted conditions increase warm season (May to September) coastal low clouds albedo by 15 percent to 20 percent along the California coast. Thinner clouds (by water path below 700 hPa[1]) are more susceptible to pollutant aerosols than thick clouds. Results indicate that this "aerosol aware" modeling, which allows dynamically varying cloud effective radius in response to changing aerosol concentration, produces more realistic relationships between cloud water amount and albedo. The default approach used before applying this project's methods produced clouds that were too bright, even for many polluted clouds. The project's results are expected to help inform future regional downscaling efforts whose aim is to investigate coastal low clouds and their impact on surface insolation.

The Simulator for Hydrologic Unstructured Domains model was deployed for long-term hydroclimate simulations (1979-2018) in the Sacramento River watershed. The Simulator for Hydrologic Unstructured Domains model representation of Sacramento Basin output discharge and groundwater appeared to have the correct magnitude and spatial pattern. Based on the long-term groundwater storage variation, the groundwater has been decreasing since the 1980s.

A hydrological model system known as ParFlow.CLM, was configured for the Kaweah River watershed in the Southern Sierra Nevada and in the Central Valley in California. The research examined how uncertainty in the precipitation datasets propagates through the process-based hydrologic model and results in uncertainty in the simulated hydrologic outputs. Additionally, the research investigated how combined uncertainty in precipitation and air temperature impact simulated hydrologic fluxes and states in the watershed. The primary factor that impacts water budget partitioning is the total amount of snowfall predicted by each combination of

[1] Hectopascal pressure unit 1 hPa is equal to one millibar.

datasets. These results highlight the need for developing gridded climate products that can accurately represent hydrologic processes of mountain catchments.

Knowledge Transfer and Benefits to California

The methods and results of various elements of this research have been transferred through numerous activities, including submission and publication of scientific manuscripts in peer-reviewed journals, presentations at high-profile conferences such as at the Fall meetings of the American Geophysical Union, and frequent teleconferences with staff from the California Energy Commission regarding the project's data, methodology, and findings.

Access to the regional model dynamically downscaled historical reanalysis dataset produced using the WRF-CA-CLC version of Weather Research and Forecasting model described in Section 3.2. can be arranged by request to the project investigators.

This project produced advances in dynamically informed statistical techniques to downscale relatively coarse scale climate-model simulations, which are useful for California's electric utilities and a broad set of other stakeholders. The hydrological-modeling techniques are vital for translating meteorological data into impacts over land surfaces, including the quantitative characterization of floods, runoff, drought, and groundwater stocks. The datasets describe California's surface weather and hydrology at the higher spatial (3 km x 3 km) and temporal (hourly) resolution, which are needed by California's electric and other stakeholders to examine energy demand and supply, and to assess infrastructure resilience in a changing climate.

The techniques developed in this project will advance the downscaling of projected climate data (available from a large set of global-climate models) to fine spatial and temporal resolutions that will enable California to better prepare for climate changes, including high-impact extreme weather events and compound weather and hydrological events that can impact the state's electric system. These data will also be important in disentangling long-term trends from natural variability and regional or local effects. Conclusions from development of these hybrid techniques are already being applied to two other California Energy Commission projects, which together with this and other projects will advance development of a robust and usable set of climate projections for California.

CHAPTER 1: Introduction

California's investor-owned utilities (IOU), other utility sectors, and numerous other stakeholders in California need spatially and temporally detailed historical and projected future climate, weather, and hydrological data to assess resilience to present and future climate change. Of particular importance is the spatial and temporal makeup of extreme events. However, the fine-scale data required to fully evaluate and prepare for extremes and other impactful events is not directly provided by global (or by some regional) climate model histories and projections. Downscaled weather, climate, and hydrology data from multiple climate scenarios are needed to translate global climate model (GCM) climate projections into spatial and temporal details relevant to decision makers—to understand historical variation and future projected changes and variation of temperature, precipitation, and other variables. Specifically, this project leverages statistical relationships between larger-scale processes captured by GCMs and the smaller-scale weather and climate details and uses those relationships to support understanding of weather extremes and climate trends in a topologically and hydrologically complex area such as California.

Downscaling tools and approaches are especially needed to help users process a growing suite of global climate models, most of which provide simulations for multiple future scenarios. This collection of models contains ranges of variability within and across models; the uncertainty that arises from different model constructs, from different scenarios of future climate drivers (such as emissions, aerosols, land use, and land cover), and from various forms of climate variability. Additionally, many GCMs provide an ensemble of model simulations for a given scenario, which is useful for disentangling the role of unpredictable and chaotic natural climate variations from trends produced by anthropogenic greenhouse gases and aerosols. Investigation of the range of regional climate changes and impacts contained in the growing set of climate projections requires regional downscaling techniques that are sophisticated enough to represent complex regional climate structure (including extreme events), yet sufficiently efficient that the computational load is not prohibitive.

This research developed downscaling techniques that exploited hybrid dynamical-statistical elements to provide improved resolution of California's highly variable (in space and time) meteorological conditions, including winds and coastal cloudiness. Also included in this research is exploratory modeling of selected hydrological systems, including surface and groundwater systems.

This report describes the development of downscaling and hydrologic modeling techniques as they apply to California weather, climate, and hydrologic phenomena. Several elements were included: statistical and dynamical downscaling of meteorological variables; hybrid techniques using both statistical and dynamical methods to obtain improved downscaling results; hydrological modeling, including both surface and groundwater components; and groundwater modeling of selected aquifers. Additional necessary and complementary elements are also presented, which either inform or stem from these downscaling and hydrologic modeling

approaches. These include observed datasets, which are needed to train some forms of downscaling techniques and evaluate results from all downscaling techniques.

CHAPTER 2:
Project Approach

This chapter describes the techniques and development of statistical, dynamical, and combined statistical-dynamical hybrid downscaling of global climate and weather simulations for California. Additionally, it describes some hydrological model approaches that employ meteorological variables from downscaled weather and climate modeling.

Some important components involved in statistical and dynamical methods to obtain improved downscaling results include improvements in gridded observational datasets; hourly statistical downscaling; consideration of vector wind variables; evaluation of downslope wind model simulations; and possible improvements in physical processes in dynamical modeling of coastal clouds, including aerosol-aware techniques.

The Localized Constructed Analogs (LOCA) method is a statistical scheme that produces downscaled estimates suitable for hydrological simulations using a spatial matching scheme to pick appropriate analog days from an observational or model dataset. LOCA is designed specifically to produce better estimates of extreme days; it also provides a more realistic depiction of the spatial coherence of the downscaled field. Additionally, LOCA reduces the problem of producing too many light-precipitation days. It is computationally efficient and provides the capacity to downscale a selected set of climate variables including temperature, precipitation, and a few other variables for many global-climate model reanalyses or projections.

Dynamical downscaling involves running numerical models representing atmosphere and climate dynamics at high-resolution over a regional, as opposed to a global, domain. Regional dynamical models typically employ lower-resolution climate model outputs as the boundary conditions that guide their solutions. These models use physical principles to reproduce local climates, including the time-varying three-dimensional atmospheric structure. Because they are computationally intensive and computer-resource expensive, dynamical modeling typically simulates a limited number of global-climate scenarios.

The hydrological modeling component of this effort includes the development and exploration of two hydrological model systems, SHUD and ParFlow.CLM. The Simulator for Hydrologic Unstructured Domains (SHUD) is a multi-process model that represents major hydrologic processes capable of simulating a broad range of spatial and temporal scales. ParFlow.CLM is a groundwater/land surface model that provides a more detailed simulation of surface hydrology and variably saturated subsurface is applied to specific aquifers.

2.1 Localized Constructed Analogs Downscaling

Most downscaling approaches fall into either dynamical or statistical methodologies for translating global and regional climate model outputs to finer-scale structures over complex landscapes such as in California. Of the statistical techniques, LOCA (Pierce et al., 2014; Pierce and Cayan, 2015) uses larger-scale climate patterns along with finer-scale historical weather to develop realistic estimates of fine-scale climate and weather that occur with modeled large-

scale patterns. Scripps Institution of Oceanography at the University of California, San Diego, (UCSD) developed and used LOCA to downscale 32 GCMs from the Coupled Model Intercomparison Project, Phase 5 (CMIP5) archive at a 1/16th-degree spatial resolution (http://loca.ucsd.edu/, and Pierce et al., 2018). LOCA downscaling was implemented over various spatial domains, contingent on available historical training data for given variables of interest, ranging from California to most of North America, from central Mexico through Southern Canada. For California's Fourth Assessment generation of LOCA, the historical period was 1950-2005, along with two future greenhouse gas emissions scenarios: Representative Concentration Pathway (RCP) 4.5 and RCP 8.5 over the period 2006-2100 (although some models stop in 2099). Variables produced for the Fourth Assessment were daily values of minimum and maximum temperature; precipitation; humidity; wind speed; and downward, short-wave radiation.

The LOCA method is a statistical scheme that produces downscaled estimates suitable for hydrological simulations, using a multi-scale spatial matching scheme to pick appropriate analog days from observations. First, a pool of candidate-observed analog days is chosen by matching the model field to be downscaled to observed days over the region that is positively correlated with the point being downscaled; this leads to a natural independence of the down-scaling results to the extent of the domain being downscaled. Then the one candidate analog day that best matches in the local area around the grid cell being downscaled is the single analog day used in that area. Most grid cells are downscaled using only the single locally selected analog day, but locations whose neighboring cells identify a different analog day use a weighted combination of the center and adjacent analog days to reduce edge discontinuities. By contrast, existing constructed analog methods typically use a weighted average of the same 30 analog days for the entire domain. By greatly reducing this averaging across analog cases, LOCA produces better estimates of extreme days, constructs a more realistic depiction of the spatial coherence of the downscaled field, and reduces the problem of producing too many light-precipitation days. The methods, algorithms, and validations of LOCA are available in a series of publications (Pierce et al., 2014, Pierce et al., 2015, Pierce and Cayan 2015, Pierce et al., 2018). Interested readers should consult those works for details of how the method works, which will not be repeated here.

In this research, increased spatial and temporal resolution of LOCA downscaling were developed and tested as an advance to previous work. LOCA hourly temporal resolution downscaling applications were produced using observed hourly temperature records at individual weather stations, and another using 3 km x 3 km gridded hourly vector wind and relative humidity produced by a dynamically downscaled weather analysis dataset. Addi-tionally, dynamical downscaling was applied to temperature, humidity, and wind at increased spatial resolution to the 3 km x 3 km grid, resulting in four times as many grid cells within a given area compared to previous downscaling efforts in California at 6 km x 6 km.

Although the LOCA method is more computationally expensive than existing constructed analog techniques, LOCA is still practical for downscaling numerous climate model simulations with limited computational resources. LOCA downscaling can afford to be conducted over many GCMs, including outliers. (Note: Because of its high cost, Weather Research and Forecasting (WRF) dynamical downscaling should be limited to the minimum expected to

faithfully reproduce a range of expected climate variability.) Analysis shows that six downscaled members should be considered, at a minimum, to downscale for regional modeling purposes (Pierce et al., 2009), ideally selected from different GCMs to reduce the multi-model averaged error. Beyond this minimum, the research team considered that 10 downscaled members will create an ensemble with mean and standard deviations expected to reasonably estimate the full suite of projections, if GCM projections are chosen carefully.

2.2 Dynamical Model Downscaling

Dynamical downscaling involves running high-resolution climate models on regional domains (usually a limited subdomain). Regional dynamical models typically employ low-resolution climate model output as boundary conditions. These models use physical principles to reproduce local climates but are computationally intensive model structures and physical parameterizations.

Regional dynamical models such as global and regional reanalyses are employed as drivers of fine-scale dynamical or statistical downscaling models. Historical reanalysis using a dynamical model offers a way to develop a more complete, dynamically consistent set of observed records to investigate mechanisms controlling various forms of variability, including extreme events. Global and regional reanalyses results, which capture the larger-scale atmospheric environment, are used as input to finer-scale (downscaled) dynamical and statistical models, or, as stated on the European Center Copernicus website, (https://climate.copernicus.eu/climate-reanalysis), "Climate reanalyses combine past observations with models to generate consistent time series of multiple-climate variables. Reanalyses are among the most-used datasets in the geophysical sciences. They provide a comprehensive description of the observed climate as it has evolved during recent decades, on 3D grids at sub-daily intervals."

Recent reanalyses (such as ERA5 global - hourly, ~31 km spatial resolution, 1979-present) from the European Center for Medium Range Forecasting (Hersbach, et al., 2020), Modern-Era Retrospective analysis for Research and Applications, Version 2 (MERRA-2) global (hourly, 0.5° × 0.625° grid, 1980-present) from the National Aeronautics and Space Administration (NASA) Goddard Space Flight Center (Molod, et al., 2015; Hinkelman, et al., 2019) and the North American Regional Reanalysis (NARR) (Mesinger, et al., 2006) over the continental United States (CONUS) (3-hourly, 32 km, 1979-present), from National Oceanic and Atmospheric Administration National Centers for Environmental Prediction (NOAA/NCEP) are available over the relatively modern satellite era. Although spatial resolution provided by the two global reanalyses (ERA5 and MERRA-2) has become finer than it was just a few years ago, their 30 to 50 km gridding is still too coarse to capture important structures over California's complex coastal and interior landscapes. In this research, dynamical downscaling experiments were conducted to replicate historical climate conditions aimed at simulating coastal low clouds (CLC), including marine stratocumulus clouds (MSc), stratus and fog, along and over the California coast, along with wind and humidity over the California region.

Regional dynamical models are often customized to better replicate certain physical variables (for example, coastal stratus clouds) by tailoring model structure and physical parameterza-tions. Like all methods, dynamical model output contains biases, which are often more than minor incremental offsets. Spatial resolution can be refined by nesting successively smaller

domains inside larger coarser domain simulations. Regional dynamical models are generally more computationally expensive than statistical methods but produce a full set of atmospheric variables—including those for which observational data may be sparse—that are dynamically consistent and can be sampled over high temporal resolution. Dynamical models generate a high-volume dataset and are usually confined to a limited set of climate model scenarios and sometimes over a restricted time period.

Regional dynamical downscaling resulting from a one-size-fits-all model configuration may have limitations. Although the WRF mesoscale numerical weather model (Skamarock, et al., 2008) has become a common dynamical downscaling tool, each WRF application must use a tailored configuration to reproduce target processes with the best possible accuracy. There are well-documented WRF configurations for hurricanes, severe convection, fire weather, air pollution meteorology, wind-resource forecasting, and atmospheric rivers. Each application requires trade-offs in model parameters that reduce biases in targeted variables but can increase biases in others.

2.3 WRF Aerosol Sensitivity Simulations

For this research, dynamical downscaling experiments were conducted to replicate historical climate conditions using a configuration of WRF that simulates MSc along and over the California coast. Coastal Low Clouds (CLC), including stratocumulus, stratus, and fog, are a persistent, seasonal feature of the region's climate. The presence and variability of CLC has numerous effects. Most pertinent here is that CLC attenuate incoming solar radiation, determine available energy for solar photovoltaic cells, and modify energy demand by modulating coastal temperatures. Accounting for these clouds improves solar energy forecasting (Mathiesen et al., 2012). Iacobellis and Cayan (2013) demonstrated that summertime CLC is strongly associated with surface temperature variations along the coast.

Atmospheric aerosols can modulate cloud reflectivity, and therefore, their impacts on incoming solar radiation through indirect aerosol effects (Twomey et al., 1977; Albrecht et al., 1989). A well-known form of this indirect effect may occur in the shallow, relatively warm MSc clouds that frequently form in the eastern North Pacific, off and along, the California coast. An increase in the concentration of aerosols creates more condensation nuclei, causing an increase in water droplets and greater cloud reflectivity. Aerosol indirect effects and other feedbacks caused by the interaction between clouds and aerosols are the largest source of uncertainty in the effort to estimate climate sensitivity to greenhouse gases (IPCC, 2013, Chapter 7, page 573).

Most configurations of WRF, including the configuration chosen to perform the primary dynamical downscaling task in this project, assume a fixed global background number of aerosols available to participate in cloud nucleation. In the real atmosphere, aerosol concentrations exhibit great spatiotemporal variability. Concentrations are also expected to change with population and economic activity in future climates. Therefore, simulations are needed to estimate the sensitivity of CLC reflectivity to aerosol concentration.

The change in cloud albedo in response to the change in cloud droplet concentration (N_c) is known as susceptibility. Broadly, it is expected that CLC albedo will be most susceptible when

cloud water amount is robust, free atmosphere humidity is high, drizzle rate is low, and baseline aerosol concentration is low. The research team developed new WRF model code to vary N_c and to couple changes in simulated cloud top effective radius, to simulated cloud albedo,[2] thus allowing WRF to simulate CLC susceptibility. New WRF code was added to the final WRF-CA-CLC configuration (Section 3.2.2), and sensitivity tests were performed by simulating warm seasons (May to Sept) for 2011 and 2015, with N_c = 150 (clean) and 600 (polluted) cubic centimeter (cm^{-3}) to estimate susceptibility and its effects on seasonal and diurnal cycles of CLC albedo.

2.4 Hybrid Dynamical-Statistical Downscaling

Hybrid downscaling exploits the ability and output of dynamical downscaling in capturing fine-scale atmospheric features by combining a dynamical model's high spatial and temporal resolution datasets, which are used for training the statistical model, with the bias corrections and computational savings of a statistical model. This technique can be applied to downscaling multiple GCMs and also to "backcast" historical climate data using a global atmospheric model reanalysis. Importantly, the efficiency of the hybrid technique allowed the team to downscale multiple emission scenarios and multiple time periods. For example, the ~40-yr, 3-km spatial resolution vector wind dataset, constructed via hybrid downscaling techniques, was generated using a 15-year high-resolution WRF model run as training data. Simply extending the WRF model run to 40 years rather than using the hybrid approach would have been prohibitively expensive.

LOCA was used to perform sub-daily downscaling of vector winds and humidity, at hourly resolution. Previously, wind speed (but not wind direction) was downscaled using the LOCA technique. Vector wind downscaling required an extension of LOCA downscaling to consider vector fields along with an auxiliary variable, sea level pressure (SLP), used because of SLP's key role in representing regional circulation patterns and in generating pressure gradients that drive wind. Specifically, U and V (the zonal and meridional components of the vector wind), and SLP are jointly downscaled by LOCA; then the wind speed from the downscaled U and V fields is computed and bias-corrected to the training data's wind-speed field. This approach helps preserve the correct relationships between U and V in the downscaled data, while retaining wind-speed distributions that agree with the training data.

The LOCA technique was extended to hourly time resolution by virtue of the availability of hourly gridded training data from the dynamical model as well as the global reanalysis being downscaled. Surface and near-surface winds are only sparsely measured, and those locations where winds are measured usually provide only limited time histories, which are often contaminated with spurious measurement errors, reinforcing the need for regionally modeled wind products (Guzman-Morales et al., 2016). The understanding of wind structure over California and surrounding regions is muddied by both lack of quality surface observations and differences presented by different model results. For example, the climatology of annual mean wind speed from several reanalyses and observational datasets (Figure 1) indicates that the

[2] This change to WRF code was novel at the time research was being performed. In parallel, WRF code developers added a similar capability and released it with WRF version 4.3 on May 10, 2021.

broad range of magnitudes and disparate spatial patterns exist between different products. In this research, for a training dataset for the LOCA statistical downscaling scheme, a regional high-spatial-resolution wind record from a fine-scale atmospheric model was employed, making this a hybrid downscaling approach. The numerical model wind dataset from a WRF regional atmospheric model run by the Desert Research Institute (DRI) was employed; this model strongly corresponds to topographic features (Figure 1), and the model is used by the wildfire prevention and management community (Brown et al., 2016; Sapsis et al., 2016). The DRI-WRF product was analyzed onto a 3-km spatial grid and provided hourly temporal resolution. The DRI-WRF training data was bias corrected by DRI-WRF providers to available Remote Automated Weather Stations (RAWS) observations by computing errors between the observed and model winds at grid cells containing RAWS stations, then interpolating the errors between station locations, using an inverse-distance weighting approach. Errors were computed separately for each season and hour of the day to account for the seasonal and diurnal variability of wind and its possible misrepresentation in the WRF model output.

Figure 1. Climatology of Annual Mean Wind Speed from Several Reanalyses and Observational Datasets

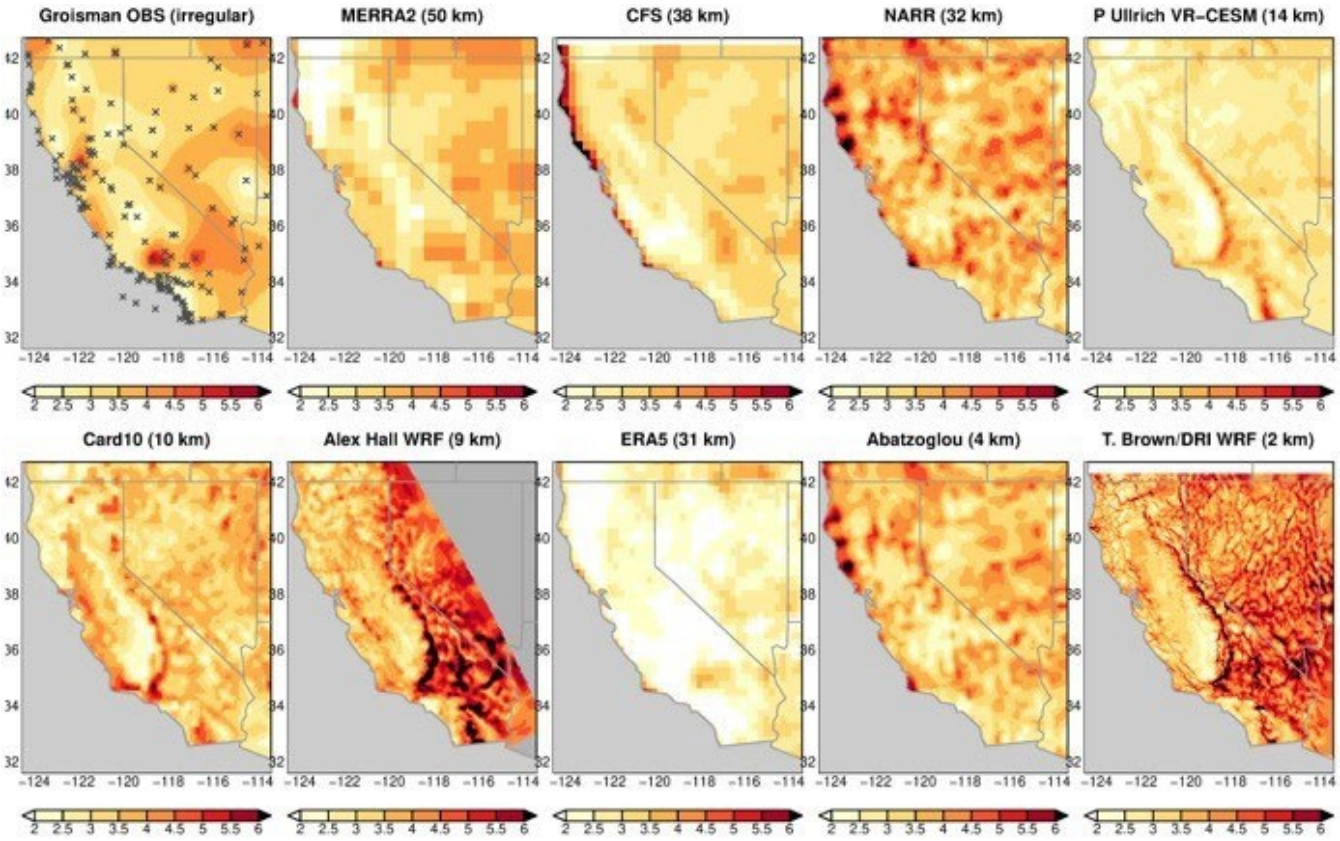

The images indicate that a broad range of magnitudes and disparate spatial patterns exists between different products.

Sources: Groisman: observations from meteorological stations. MERRA2: A NASA reanalysis. Climate Forecast System: NOAA/NCEP Climate Forecast System. NARR: NOAA/NCEP North American Regional Reanalysis. VR-CESM: Variable resolution Community Earth System Model (from the National Center for Atmospheric Research in Boulder, CO), courtesy of Paul Ullrich. Card10: California Reanalysis at 10 km, produced by M. Kanamitsu and H. Kanamaru. Alex Hall WRF: WRF model courtesy of Alex Hall at University of California, Los Angeles. ERA5:

European Center for Medium Range Weather Forecasting (ECMWF) Reanalysis version 5. Abatzoglou: GRIDMET data from J. Abatzoglou at the University of Idaho, based on NARR and station observations. DRI WRF: WRF run from the Desert Research Institute, courtesy of Tim Brown.

A necessity in evaluating downscaled winds and other variables is the availability of observational data over time periods with sufficient representation of variability from daily extremes to interannual fluctuations. An observational dataset with increasing usefulness is weather data collected by state utilities. The IOU San Diego Gas & Electric (SDG&E) initiated installation of a meteorological station network in 2010, bringing a total of 174 stations by 2019 in the San Diego County region. The SDG&E network follows RAWS procedures and variable operational definitions but logs observations every 10 minutes instead of every hour (Cao & Fovell, 2016). Although less extensive in time and spatial coverage relative to the RAWS network, SDG&E finer time and spatial resolution observations allowed closer examination of WRF performance, at a scale relevant to wildfire weather. The produced WRF wind fields were evaluated with special attention to seasonal Santa Ana wind conditions.

2.5 Hydrological Modeling

Modelers, policymakers, and stakeholders have a growing need for high-resolution and detailed information about streamflow and the temporal-spatial distribution of hydrologic fluxes in watersheds. This need reflects the growing importance of matching climate and hydrologic research for detailed long-term predictions and projections of future water resources for ecological systems and the environment, agricultural development, and food security. While projected changes in precipitation are inconsistent among different GCMs depending on the radiative forcings and model physics (Chang et al., 2016), these differences are further influenced by the climate downscaling and hydrologic modeling methods. For the hydrologic modeling methods, the question arises of how future climate variability will propagate through a hydrologic system where surface water and groundwater resources are coupled (Sulis et al., 2012). Since developed water and energy systems are interdependent (IAEA, 2012), it is expected that projected changes in water supply will impact on production (e.g., hydropower) and energy use (e.g., groundwater pumping) in the future. In this project, representations of hydrologic phenomena were developed and explored using two hydrological model systems: SHUD and ParFlow.CLM. Major characteristics are compared in Table 1.

SHUD is a multi-process, multiscale, and multitemporal model that integrates major hydrologic processes and solves physical equations with the finite volume method (Shu et al., 2020). Governing equations are solved within an unstructured mesh domain consisting of triangular cells. The variables used for the surface, vadose layer, groundwater, and river routing are fully coupled together with a fine-time step. The SHUD uses 1D unsaturated flow and 2D groundwater flow. River channels connect with hillslope via both overland flow and baseflow. The model, while using distributed terrestrial characteristics (from climate, land use, soil, and geology) and preserving heterogeneity, supports efficient performance through parallel computation.

As an intellectual descendant of the Pennsylvania State Integrated Hydrologic Model (PIHM), the SHUD model is a continuation of 16 years of PIHM model development in hydrology and related fields since release of the first PIHM version (Qu, 2004). The conceptual structure of

the two-state integral-balance model for soil moisture and groundwater dynamics was originally developed by Duffy (1996); the partial volumes occupied by unsaturated and saturated moisture storage were integrated directly into a local conservation equation. This two-state integral-balance structure simplified the hydrologic dynamics, while preserving the natural spatial and temporal scales that contribute to runoff response.

SHUD's many fundamental ideas and its conceptual structure from PIHM, including the solution of hydrologic variables using CVODE[3]. The code has been completely rewritten in a new programming language, with corresponding improvements to the underlying algorithms that have adapted new mathematical schemes and flexible input and output data formats. Although SHUD is forked (derived) from PIHM, it still uses CVODE for solving the ordinary differential equation system but modernizes and extends PIHM's technical and scientific capabilities.

SHUD is a robust integrated modeling system with the potential to provide scientists with new insights into their domains of interest, which will benefit development of coupling approaches and architectures that incorporate scientific principles. The SHUD modeling system can be used for applications in: hydrologic studies from hillslope scale to regional scale; model domain ranges from 1 m^2 to 106 km^2; water resource and stormwater management; coupling research with related fields such as limnology, agriculture, geochemistry, geomorphology, water quality, and ecology; climate change; and land-use change. In summary, SHUD is a valuable scientific tool for any modeling task associated with hydrologic responses.

ParFlow.CLM is an integrated groundwater/land-surface model that simulates variably saturated subsurface flow by solving the 3D Richards equation using a cell-centered finite difference scheme (Ashby and Falgout, 1996; Jones and Woodward, 2001; Kollet and Maxwell, 2008). ParFlow has a fully integrated overland flow simulator that solves the kinematic wave equation of shallow water for runoff routing (Kollet and Maxwell, 2006), and is coupled to the Common Land Model (CLM 3.0) (Dai et al., 2003) to solve water and energy budgets at the land surface, at an hourly time step. Pre-defined river networks are not used in ParFlow, and streamflow is generated by the uniform application of kinematic-wave approximations. In ParFlow.CLM, surface and subsurface flow equations are solved simultaneously, and saturated and unsaturated zones are not explicitly defined by compartments of fixed size. As a result, unsaturated zone water content is controlled by infiltration and water-table dynamics.

ParFlow.CLM model inputs are hourly meteorological forcings (precipitation, air temperature, atmospheric pressure, wind speed, specific humidity, and downward shortwave and longwave radiations), topography, subsurface hydraulic parameters (porosity, van Genuchten parameters, specific storage) and vegetation parameters. Model outputs are: soil moisture, depth to water table, pressure head and relative saturation in the subsurface, evaporation, transpiration, snow-water equivalent, infiltration, and streamflow. The computational grid has a uniform horizontal spatial discretization with any desired grid size, and vertical discretization is variable with finer-resolution grids near the land surface to capture root-zone dynamics and coarser resolution grids at depth. ParFlow.CLM is designed for massively parallel computer systems

[3] CVODE is a solver for stiff and non-stiff ordinary differential equation systems.

using distributed forcing and land-cover types, with the capability to simulate the impacts of groundwater pumping and irrigation on surface water/groundwater exchange.

ParFlow has been successfully implemented to simulate hydrologic processes at one kilometer scale across the entire CONUS (Maxwell et al., 2015). However, such applications are computationally intensive and require access to sufficient computational resources. Water-management options such as reservoir operations have not been incorporated into the latest version of the model. Feasible applications are assessing the impacts of climate variability, irrigation and groundwater pumping on surface water-groundwater exchange, snowmelt, groundwater recharge and evapotranspiration processes, and understanding feedback processes between groundwater and land-surface hydrologic systems. ParFlow is also coupled with the WRF model (Williams and Maxwell, 2011), and provides a compatible platform for regional climate downscaling, while embedding detailed hydrological processes in the modeling framework. However, a fully integrated climate-groundwater framework is computationally expensive.

Table 1. Description of SHUD and ParFlow.CLM Hydrologic Models

Specifics	SHUD	ParFlow.CLM
Subsurface flow processes	Two layers: unsaturated and saturated zone. The two layers are split by water content (groundwater table).	3D subsurface flow as a continuum (no fixed size compartments for saturated and unsaturated zones)
Subsurface physics	1D and 2D Richard equation are applied in unsaturated and saturated layers respectively.	3D Richards equation
Land surface processes	Interception, evaporation, transpiration, snow melt.	Common Land Model (CLM) to solve water and energy budgets
Overland flow	2D kinematic or diffusive wave approximation of the shallow water equations	2D Kinematic wave approximation of the shallow water equations
Stream network	Pre-defined river, detailed geometry of river is required; kinematic or diffusive wave approximation.	No pre-defined river networks. Streamflow develops as a result of uniform application of the kinematic wave approximation on a terrain.
Numerical scheme	Unstructured domain; Finite volume method	Cell-centered finite difference
Horizontal discretization	Flexible domain discretization	Uniform grids of any size
Vertical discretization	Two layers split by water content	Variable spacing
Temporal resolution	Self-adaptive time step based on convergence criteria. Second to hourly.	Hourly

Specifics	SHUD	ParFlow.CLM
Model inputs	**Spatial**: elevation, soil, geology, land use, hydrology, and weather station. **Attribute**: parameters for soil, geology, and land use. **Time-series**: precipitation, air temperature, wind speed, specific humidity, and downward shortwave radiation.	Precipitation, air temperature, atmospheric pressure, wind speed, specific humidity, and downward shortwave and longwave radiations, topography, subsurface hydraulic parameters (porosity, van Genuchten parameters, specific storage), and vegetation parameters
Model outputs	**State variables of hillslope**: snowpack, surface ponding water, soil moisture, groundwater storage. **Fluxes of hillslope**: Evapotranspiration (ET), infiltration, groundwater percolation, overland flow, groundwater flow. State variable of river: river stage. **Fluxes of river**: flow from upstream, flow to the downstream, surface runoff, baseflow.	Soil moisture, depth to water table, pressure head and relative saturation in the subsurface, evaporation, transpiration, snow water equivalent, infiltration, and stream flow
Water management options	Natural water system only. Extra coupling is necessary for water management.	Pumping and irrigation, no reservoir option
Parallel implementation	Yes, OpenMP	Yes
Applications	Laboratory, watershed, and continental scale applications.	Watershed and continental scale applications

Sources: from analyses herein, see text for details.

2.5.1 SHUD Simulation of the Sacramento River Watershed

In the present study, SHUD was configured and employed for modeling of surface and groundwater in several domains of various sizes: in the Wagon Creek and the Catchments Attributes and Meteorology for Large-Sample Studies watersheds, over the Sacramento River watershed (from the highlands to the delta) and over the entire state of California. With the ability to work across scales, SHUD allows hydrology to be studied in many possible contexts. Those contexts include the behavior of water in regions of rough topography, in light of water resource and stormwater management, and in conjunction with related fields such as limnology, agriculture, geochemistry, geomorphology, water quality, and ecology, climatic and land-use change. Whereas many existing hydrologic modeling systems are unable to deal with California's rough topography and significant topographic variation, SHUD has been designed with this relatively extreme regime in mind.

The calibration of the SHUD model adopted the Covariance Matrix Adaptation Evolution Strategy (CMA-ES) (Hansen 2006, Auger and Hansen 2005). The automatic CMA-ES calibration is robust and able to converge to global optimization, at low computing cost.

2.5.2 Integrated Surface Water-Groundwater Modeling Using ParFlow.CLM

Several physically based integrated hydrologic models have been developed that couple surface water and groundwater processes (Maxwell et al., 2014; Paniconi and Putti, 2015). The research team configured an integrated groundwater/land surface model, ParFlow.CLM version 3.2.0, to simulate terrestrial hydrologic processes (Ashby and Falgout, 1996; Jones and Woodward, 2001; Kollet and Maxwell, 2008). ParFlow.CLM simulates variably saturated sub-surface flow using the 3D Richards equation and is coupled to the Common Land Model (CLM 3.0) (Dai et al., 2003) to solve water and energy budgets at the land surface at an hourly time step. Model inputs were hourly meteorological forcings (precipitation, air temperature, atmospheric pressure, wind speed, specific humidity, and downward shortwave and longwave radiation), topography, subsurface hydraulic parameters, and vegetation parameters.

The ParFlow.CLM modeling approach provides multiple benefits compared to other existing coupled or integrated hydrologic models. The ParFlow.CLM model simulates the entire terrestrial hydrologic cycle from the top of the mountains to the deepest part of the aquifer system using a 3D discretization. Furthermore, the ParFlow.CLM is coupled to the WRF model. Such an integrated atmospheric-hydrologic modeling system (called ParFlow.WRF) can provide an ideal platform for regional climate downscaling while embedding detailed hydrological processes in the modeling framework. However, a fully integrated climate-groundwater framework is computationally expensive at this moment. The research team used the ParFlow.CLM model to simulate hydrologic processes at watershed scale because this model has the potential to simulate the impacts of groundwater pumping and irrigation on surface water-groundwater exchange. Improved understanding of these processes has potential impacts on energy needed for pumping and irrigation.

CHAPTER 3:
Project Results

3.1 LOCA Downscaling at Sub-Daily Resolution

Some applications require sub-daily information, such as hourly temperatures for energy applications, hourly winds for wildfire analyses, and hourly solar insolation for photovoltaic analyses. Until now California's climate change assessments have focused on daily data. This project's analysis was pushed to more detailed sub-daily time resolutions.

Two distinct approaches to sub-daily downscaling are addressed here. For some historical reanalyses, such as MERRA-2 (Molod et al., 2015; Hinkelman 2019) and ERA5 (Hersbach et al., 2020), hourly data is already available, albeit on a coarse spatial grid (~30 to 50 km). Likewise, some meteorological station observations are available at hourly resolution. When available, this hourly data can be used directly. For example, in historical hourly wind down-scaling, each hour of the day was downscaled using hourly reanalyses and hourly training (described in more detail below). In other situations, primarily in future model projections, climate models saved only daily data; observed hourly data had to be combined with daily model projections to produce projections of hourly temperature. This methodology, which estimates hourly temperature for projected climate situations, was employed in producing hourly temperatures at selected meteorological stations of relevance to California energy applications.

3.1.1 LOCA Hourly Temperature

The first component of sub-daily downscaling was hourly time resolution temperature, which enabled investigation of energy-related temperature extremes. Existing techniques to disaggregate daily temperature minimums (Tmin) and daily temperature maximums (Tmax) to hourly values have important limitations. For example, a common approach is to fit a climatologically determined diurnal cycle to the Tmin and Tmax values and take the hourly values from this fitted curve. (For some applications, such as agricultural-degree days, a triangle is often fitted instead of a sinusoid.) The drawback of this approach is that it discards important aspects of sub-daily variability. In other words, two days can have very different progressions of hourly temperature even when they have the same Tmin and Tmax. This research devised a better method of disaggregating daily Tmin and Tmax to hourly values that retains realistic sub-daily variability, which can be important to energy-industry stakeholders.

To retain realistic sub-daily variability, future model projections of daily Tmin and Tmax were disaggregated to an hourly time step at 29 meteorological stations using an analog-day matching technique similar to what the LOCA downscaling approach uses. (See Pierce and Cayan, 2019.) The hourly weather observations originate from the NOAA Integrated Surface Dataset database. The weather stations were chosen by the California Energy Commission's (CEC's) Electrical Demand Forecast group to provide weather data for California's electricity-demand forecasting zones. Those zones are representative of both California's electricity balancing authority areas and transmission zones.

Besides having application to demand forecasts and other energy utility concerns, this exercise provided the opportunity to devise and test an hourly disaggregation technique that translates to other applications (such as hourly wind and humidity downscaling) described in Section 3.1.2.

The approach to generating hourly temperatures (given that day's Tmin and Tmax) follows. First, the three-day sequence of model Tmin and Tmax was constructed from the day before, the day of, and the day after the model day being disaggregated to hourly values. The best matching observed three-day sequence of Tmin and Tmax in the training data set, was then identified, subject to the constraint that the central matching analog day must be in a +/- 45 day-of-year window around the day-of-year being disaggregated.

There are two reasons for using a three-day sequence of Tmin-Tmax rather than matching only the day being disaggregated. Matching six values provides a more accurate constraint than matching on two values, and the point of the exercise is to generate days with realistic transitions from one day to the next, which is better addressed by matching the days before and after the day being disaggregated. A weighted root mean square error (RMSE) was used to evaluate the quality of the match between the model Tmin/Tmax series and the historical observations. The weights are one for the central day, and 0.5 for the preceding and subsequent days. This emphasized the match in the day being disaggregated, while still taking into consideration information from both the previous and subsequent days.

The research team's analog day approach was compared to the more traditional method of using climatological diurnal cycles as described previously, which is called the *climatological curve* approach. The climatological diurnal cycles for this more traditional method were chosen based on station, month, and quartile of the diurnal temperature range for the day being disaggregated. The intent was to examine whether the analog-day approach captures observed sub-daily variabilities that the traditional climatological curve approach discards.

Example hourly sequences produced by the analog-day method and the climatological-curve method appear in Figure 2(A). By construction, the climatological curve approach (dotted red line) generates a smooth solution with very little variability in the afternoon and nighttime hours, which is unlike what is seen in the observations (solid black line). The analog matching approach (broken blue line) captures realistic variability at all hours of the day.

A comparison between the original hourly observations and cross-validated disaggregations from the analog-matching technique and climatological-curve techniques is shown in Figure 2(B). As expected from the way the methods were constructed, an analog approach captures the observed variability extremely well. Histograms of the fraction of time that each hour is the warmest (red) or coldest (blue) hour of the day are shown, in winter (Dec-Jan-Feb), for the observations (top), analog-day disaggregation (middle), and climatological-diurnal cycle (bottom) methods. In comparison to the analogue approach, the climatological curve approach severely underestimates variability on time scales shorter than a day, reaching a deficit in variance spectral power of nearly two orders of magnitude at the highest frequencies. Based on these and other analyses (Pierce and Cayan, 2019) on hourly temperature downscaling, it was concluded that the analog-day matching approach to disaggregating daily Tmin/Tmax to hourly values does a much better job of capturing sub-daily variability than more traditional

approaches. Application of the analogue method to projected climate scenarios is shown in Figure 2(C), which illustrates the multi-model ensemble average projected change. This is the projected change in the number of hours either above (red and orange lines) or below (blue and green lines) the indicated temperature threshold in degrees Fahrenheit. The red and blue lines are for RCP 8.5; the orange and green lines are for RCP 4.5. The purple dot and whisker show the observed mean value and 95-percent confidence interval from the year 2000 to 2018. These plots clearly indicate the simulated rise in frequency of hot hours, the decrease in the frequency of cold hours, and the marked divergence, in about 2040, of the upward (hot hour) trajectory or downward (cold hour) trajectory of the RCP 8.5 scenario relative to that of the RCP 4.5 scenario. Overall, the hourly disaggregation technique developed in this research achieves its goals of generating hourly future projected temperature values that match observations over the historical period, correctly replicate the global climate model projected trends, and preserve realistic variability on sub-daily time scales.

Figure 2. Hourly Temperatures Obtained by a Statistical Scheme vs. Those From Airport Station Observations at Bakersfield, California (KBFL)

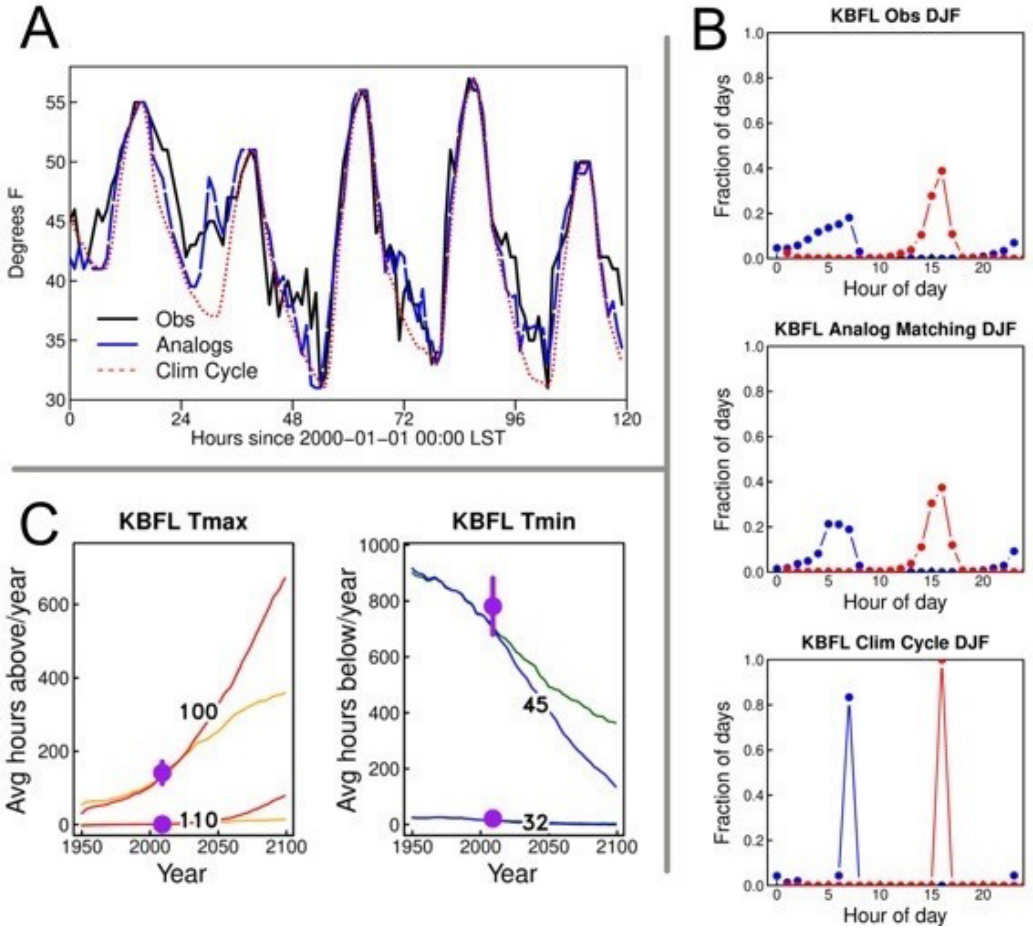

A: Time series of the original observed hourly temperature values (black), the analog day disaggregation (blue), and the disaggregation based on fitting climatological diurnal cycles (dotted red).

B: Histograms of the fraction of time that each hour is the warmest (red) or coldest (blue) hour of the day, in winter (Dec-Jan-Feb), for the observations (top), analog day disaggregation (middle), and climatological diurnal cycle (bottom) methods.

C: Multi-model ensemble average projected change in the number of hours either above (red and orange lines) or below (blue and green lines) the indicated temperature threshold in degrees F. The red and blue lines are for RCP 8.5; the orange and green lines are for RCP 4.5. The purple dot and whiskers show the observed mean value and 95 percent confidence interval from 2000 to 2018.

Sources: See text for details and NOAA surface data.

3.1.2 LOCA Hourly Vector Wind and Relative Humidity

In downscaling the vector winds with LOCA it was found that a full multivariate downscaling process including vector winds, SLP, and relative humidity simultaneously in the analog selection process did not represent the relative humidity fields as well as when relative humidity was independently downscaled without including winds and humidity. Adding more predictor fields to the LOCA process makes it progressively harder to find closely matching analog days, so there is a tradeoff between how many predictor fields are selected and the quality of the final downscaled field. While the gain in skill achieved by independently downscaling relative humidity was reckoned to outweigh any benefit of improved presentation of covariation between certain variables, the performance in modeling SLP and winds was relatively strong. Downscaling SLP and vector wind is dynamically compelling because of the important role of pressure gradients in determining wind fields. Thus, SLP and winds were downscaled together, but as explained above, relative humidity was downscaled separately. Note that the fields are all still connected through the physics of the driving GCM (both MERRA-2 and ERA5 were downscaled over their available time periods beginning 1980 and 1979, respectively). The temporal consistency of different downscaled variables was vital for capturing phenomena that inflict compound impacts.

Figure 3 shows a comparison of historical modeled winds (used as a surrogate for direct observations and taken from the LOCA training data, which is DRI-WRF here) to LOCA downscaled vector wind and humidity from ERA5. The data being downscaled (ERA5) has a native spatial resolution of 31 km x 31 km and is downscaled to 3 km x 3 km. LOCA captures the structure of the Santa Ana events reasonably well over land, though less so over the oceans, a deficiency the research team traced back to the original ERA5 data being downscaled. The strong winds in the three illustrated events are captured well, along with the dry relative humidity, with the exception of a band of extreme low relative humidity immediately adjacent to the coast that is seen in the observations but not in the LOCA downscaled fields. Neither the observations nor the downscaled data show signs of being steered by topographic gaps and hills in the region, in accordance with the current understanding of the meteorology of Santa Ana winds.

It is important that any downscaled wind field realistically capture the magnitude of observed winds. Figure 4 shows the mean and 99.9th percentile of 4:00 p.m. local time wind speeds from winter (Dec-Jan-Feb) and summer (Jun-Jul-Aug). LOCA captures the magnitudes and spatial details of the observed wind distribution extremely well, not only in California but also over the adjacent ocean regions (including the somewhat complicated structure offshore in summer), and over Nevada. Although the Santa Ana wind events are critical to wildfire incidence in the populous regions of Southern California, they are not the only wind phenomena of importance in the state.

Figure 3. A Comparison of LOCA Downscaled Winds and Relative Humidity vs. Those From the DRI High-Resolution Modeled Dataset Used as a Surrogate from Observations During Three Individual Strong Santa Ana Events

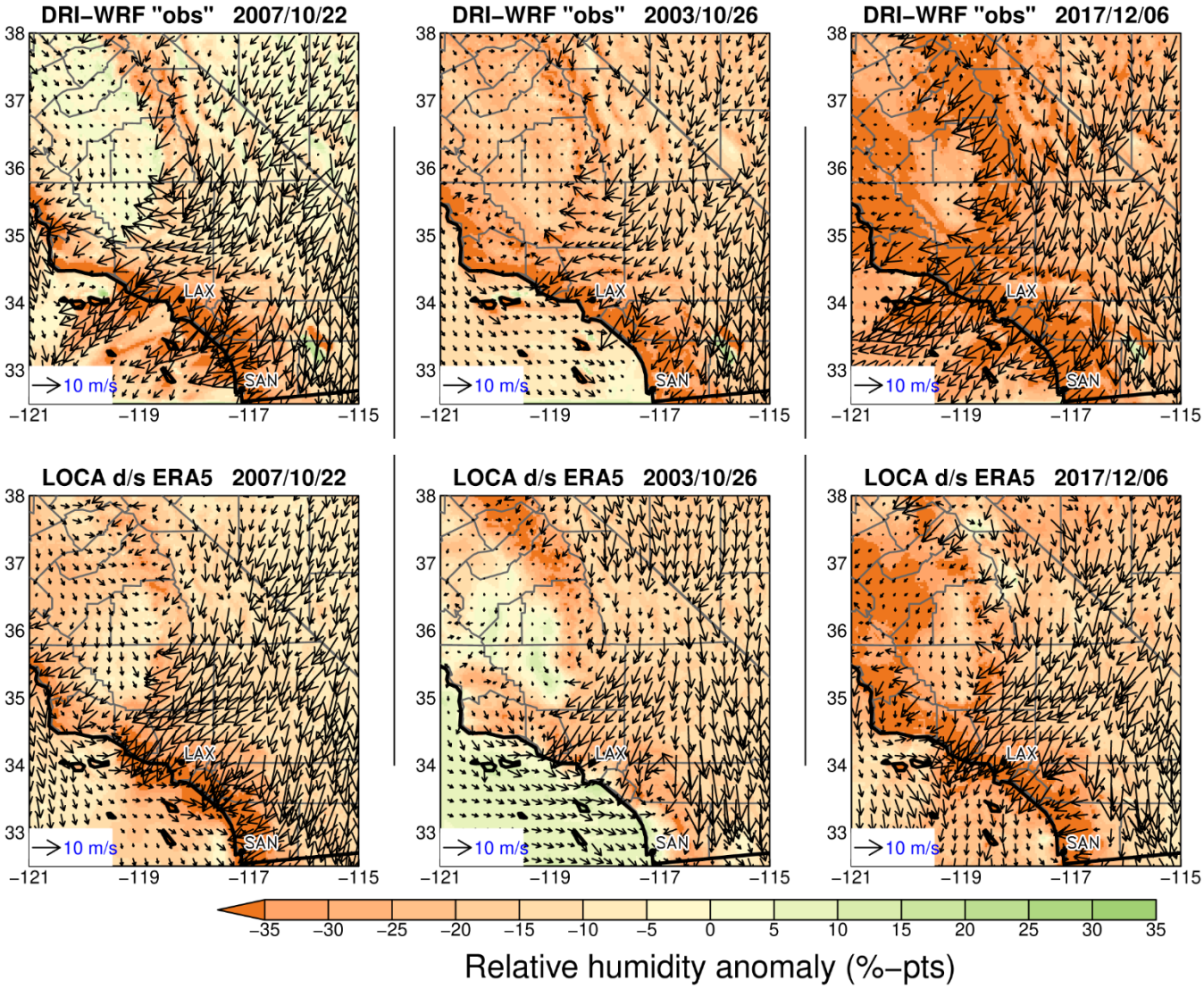

These images show strong Santa Ana wind events in 10/22/2007, 10/26/2003, and 12/06/2017 at 0Z universal time produced by LOCA downscaled ERA5 reanalysis with that from DRI-WRF. Downscaled results were determined from portions of training dataset that do not include these cases. Colors show relative humidity anomaly (%) from long term average, while arrows show the vector wind speed (m/s) and direction. Observed and LOCA-downscaled wind vectors are subsampled for greater clarity; the native resolution is 3 km.

Sources: See text for details.

Figure 4. A Comparison of Seasonal Wind Speeds in the Training Data and LOCA Downscaled Data Set

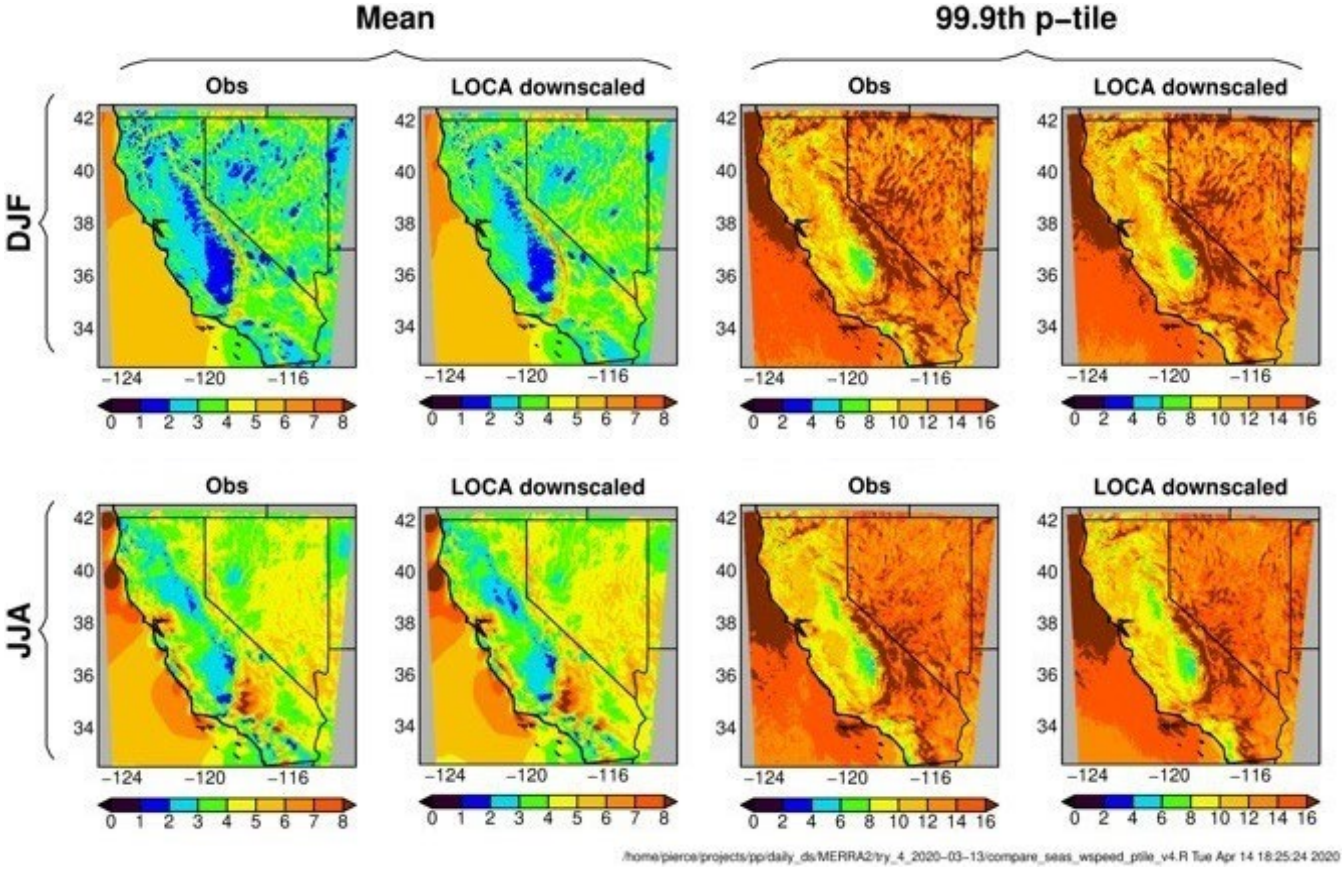

The training data is marked as "Obs" – observations- here. Top row is winter (Dec-Jan-Feb [DJF]), lower row is summer (Jun-Jul-Aug [JJA]). In each row, the left two columns show the mean wind speed (m/s), while the right two columns show extreme (99.9th percentile) values. All analyzed data is hourly taken at 4:00 p.m. local standard time.

Sources: See text for details.

Another key pattern is the delta breeze, a strong onshore flow in the Bay Area during spring and summer that ventilates the Central Valley and modifies both electrical demand (through a drop in air-conditioning use when the delta breeze is strong) and local air pollution. Figure 5 (upper) shows a strong delta breeze event in the observations (left), reanalysis (middle), and LOCA downscaled fields (right). Wind vectors are at the native resolution in ERA5 (31 km) but subsampled from the LOCA native resolution of 3 km for greater clarity. LOCA wind speeds and directions are much more consistent with the observations than seen in ERA5, with a strong branch of the delta breeze flowing northeast in the Central Valley and another branch flowing south inshore of the coastal hills. Although ERA5 has a spatial resolution too coarse to capture these important local details, they are realistically reproduced in the LOCA downscaled field.

The lower panel of Figure 5 shows a similar comparison for a Sundowner wind event in the Santa Barbara area of Southern California. These are gusty downslope winds often observed on the southern slopes of the Santa Ynez Mountains. Again, LOCA downscaling captures many

important local details of the Sundowner wind that the ERA5 analysis cannot due to its significantly coarser resolution. For example, wind speed (color shading) is strongly influenced by the local topography. The observed and LOCA patterns of wind speed show many similarities, especially over inland topography, that ERA5 cannot capture.

Figure 5. Comparison of an Individual Strong Delta Breeze Event and Sundowner Wind Event in the DRI-WRF Training Data from the ERA5 Reanalysis, and the ERA5 Reanalysis Downscaled With LOCA

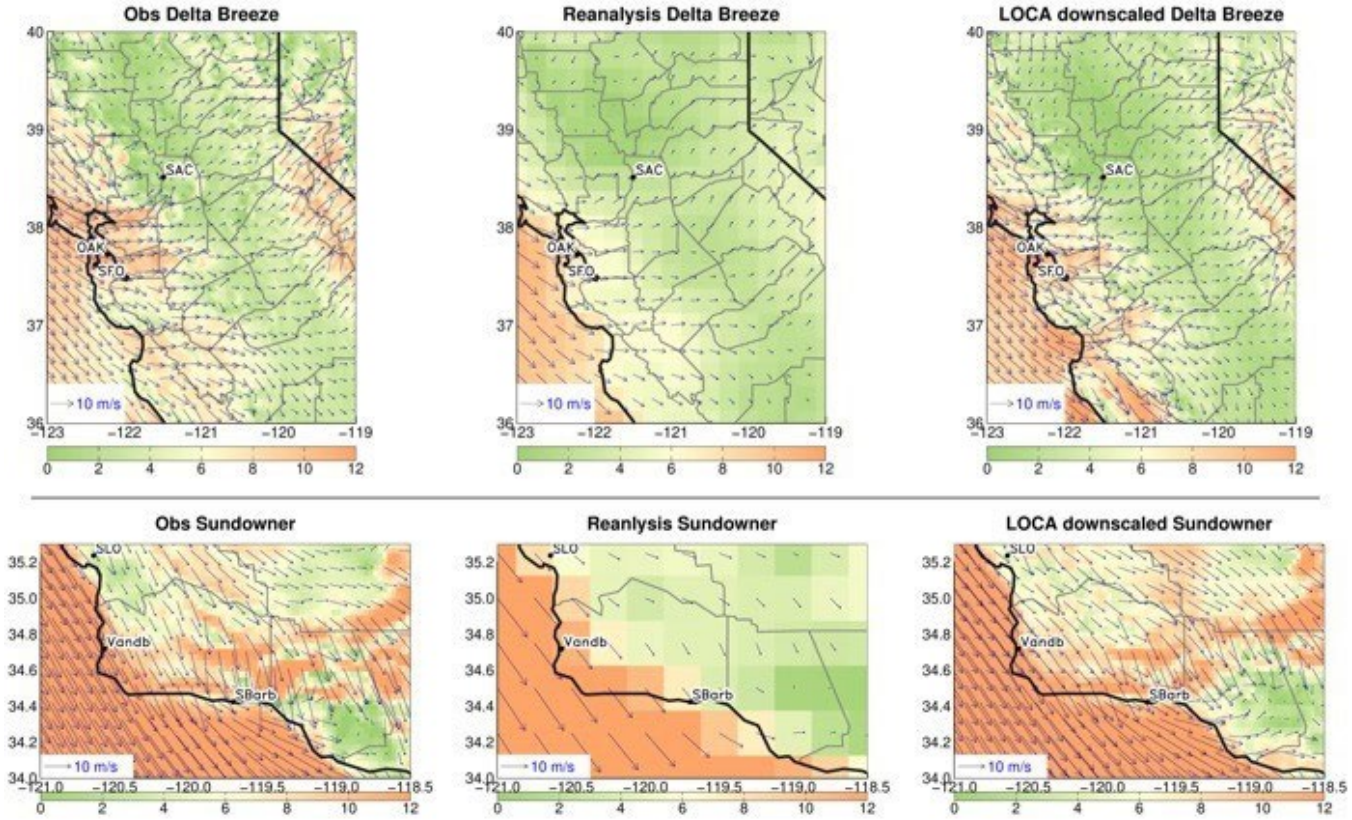

The individual strong Delta Breeze event is shown in the top row, 2017/06/11 at 1:00 p.m. local standard time. The Sundowner wind event is shown on the bottom row, 2009/04/15 at 9:00 p.m. local standard time. The DRI-WRF training data is marked as "Obs" (Observations). LOCA downscaled winds and humidity was obtained from training dataset that did not include these cases. Colors show wind speed in m/s, while arrows show the vector wind speed and direction. Observed and LOCA-downscaled wind vectors are subsampled for greater clarity; the native resolution is 3 km.

Sources: See text for details.

3.1.3 The Crucial Role of Observations: A New Precipitation Training Dataset

One example of the critical role played by historical observational datasets was instigated by the precipitation training dataset consisting of gridded observations from the Livneh 2015 dataset used in the Fourth Assessment, which in some cases suggested that daily extreme precipitation might be too low. Work done as part of this research (Pierce, et al., 2021) demonstrated that using the standard Livneh (et al., 2015) daily precipitation dataset, the

method of time-adjusting daily precipitation called the "split" precipitation observations, which have a range of observation times (but most commonly 7:00 a.m.), produces substantially lower values than those from the non-split data. The new unadjusted gridded daily precipitation generally produces a better match to daily station precipitation values. Furthermore, comparing the split and new (Pierce, at al., 2021) non-split precipitation, resulted in a 27 percent reduction in annually averaged one-day maximum precipitation averaged over the continental U.S. This split precipitation could affect a hydrologic model's representation of local flooding. When applied to the Variable Infiltration Capacity (VIC) land surface model, which was also used in Pierce et al.'s (2018) work for the Fourth Assessment to provide projections of land surface variables, the split precipitation results in annually averaged one-day maximum runoff that is 38 percent lower than that from the new non-split precipitation (Pierce, et al., 2021). This difference is greater than the 27 percent increase in annually averaged one-day maximum precipitation because of non-linearities in the physics of runoff. Interestingly, the new version of the dataset that avoids the time adjustment also results in a 17 percent annual mean runoff increase over the continental U.S. This is because the prior split version of the precipitation data spreads extremes over two days and thus reduced the runoff efficiency of the surface. However, the effect is less pronounced in California than elsewhere in the continental U.S. (Pierce et al., 2021). The increase in runoff with a fixed precipitation obtained from the non-split precipitation mandates a decrease in evapotranspiration, which under a VIC land surface hydrological model comparison between non-split and split precipitation input, declines 2.3 percent, and is associated with a decline in latent heat flux of 2.2 percent. Finally, the original split precipitation time-adjusted gridded precipitation increased the number of wet days beyond that in the underlying station data, which affects the parameterization of surface shortwave radiation. With more realistic wet day fraction provided in the revised non-split version of the Livneh dataset (Pierce, et al., 2021), the land surface model exercise indicates that annual average surface solar averaged over the continental U.S. increases 3.3 percent. Larger increases occurred over regions in the eastern half of the U.S. where daily precipitation frequency is higher, and smaller increases occurred in the western U.S., especially California and Nevada, where daily precipitation frequency is low. In general, the difference in the occurrence of daily precipitation could affect solar energy production and ecological simulations.

3.1.4 Bias Correction

In both dynamical and statistical models, the ideal bias correction procedure would jointly adjust multiple variables using a full multivariate approach. For example, a model may not produce uniform biases in T and P in simulating warm and cool precipitation events. The existing LOCA bias correction scheme (Pierce et al., 2015) addresses this using conditional bias correction; for example, the bias correction of temperature is conditional upon the presence or absence of precipitation so that the differing impacts of snow and rain are better captured in the final result. In addition, when selecting the analog days to use in the downscaling process the LOCA spatial downscaling process can jointly downscale multiple variables simultaneously by evaluating the match between observed days and the model day being downscaled across multiple variables. As part of this project, the research team evaluated different approaches to downscaling near-surface vector winds and relative humidity by jointly downscaling those fields with each other and sea level pressure. Optimal results were found when jointly

downscaling sea level pressure along with the meridional and zonal component of near-surface winds. It was found that adding relative humidity to this joint process degraded the results, likely because imposing too many simultaneous constraints when comparing the model fields to observed days resulted in too few matching analog days. This process was used for producing the downscaled surface vector winds. As part of the project, two fully multivariate bias correction techniques that have been developed and published (Cannon 2018; Guo et al., 2019) were also examined. These methods come at a price in increased computational demand, up to a factor of 30. For the next generation of climate projections, it will have to be evaluated whether the up to 30-fold increase in time needed to do this form of multivariate bias correction is worthwhile and acceptable, given the need to process all of California for multiple models, ensemble members, and scenarios. This might largely be determined by how many models, ensemble members, and emissions scenarios are desired in forthcoming CMIP6 downscaling effort.

3.2 WRF Dynamical Modeling Results

A regional model dynamically downscaled historical reanalysis dataset was produced using the WRF-CA-CLC version of the WRF model. The WRF downscaling was previously applied to a coarser (9km) WRF downscaled version of the NARR. This 9km WRF reanalysis was provided by Professor Alex Hall's group at University of California, Los Angeles (UCLA). For this research, the 3km spatial resolution WRF-CA-CLC was run for a rectangular domain approximately enclosing California (Figure 6) through a period spanning April 2008 to February 2019. The resulting full atmospheric dataset generated by WRF for this research is quite large (over 30 terabytes [TB] for 11 years), which has been saved for the intermediate term, and access during this period will be considered upon request to the project investigators. Additionally, a post-processed subset of the WRF-CA-CLC dataset was extracted to provide variables that are relevant for low cloud processes, fire weather, and basic climate dynamics (for example, sea-level pressure and 500 hPa geopotential height). The post-processed files, which in total amount to about 1TB, contain 80, 2-D variables, including temperature, precipitation, hub height wind, albedo, wind gust estimates, and inversion layer fields. The full list is shown in Table 2. The post-processed files are available every hour from April 1, 2008, to February 28, 2019, on the 3-km WRF-CA-CLC grid. Grid coordinates and other supporting metadata are also provided in the post-processed files. Access to the post-processed files can be arranged upon request to the project investigators.

3.2.1 Marine Stratocumulus in WRF

Marine Stratocumulus clouds cover large areas of the North Pacific Ocean offshore California during the summer months, but the extent of their inland migration is both not-well-characterized and critical for understanding energy supply and demand. Figure 7 shows the intra-seasonal extent of albedo by Geostationary Operational Environmental Satellite (GOES) satellite observations and an early test version of WRF-CA-CLC. Albedo is a measure of the reflection of sunlight by the combined effects of the atmosphere and the earth’s surface. For the region and season studied here, albedo is driven primarily by the presence of bright MSc over dark surfaces. Figure 7 shows the mean coverage of clouds, but also displays the daily variability of cloud coverage extent through the coefficient of variability. While WRF-CA-CLC is

able to simulate inland-penetrating clouds, this analysis indicates fine grain improvements needed to target in further model development. Such improvements may be critical for understanding fluctuating patterns in energy demand and anticipating solar energy resources on a regional scale.

Figure 6. WRF Domains for Multi-Decade Dynamical Downscaling

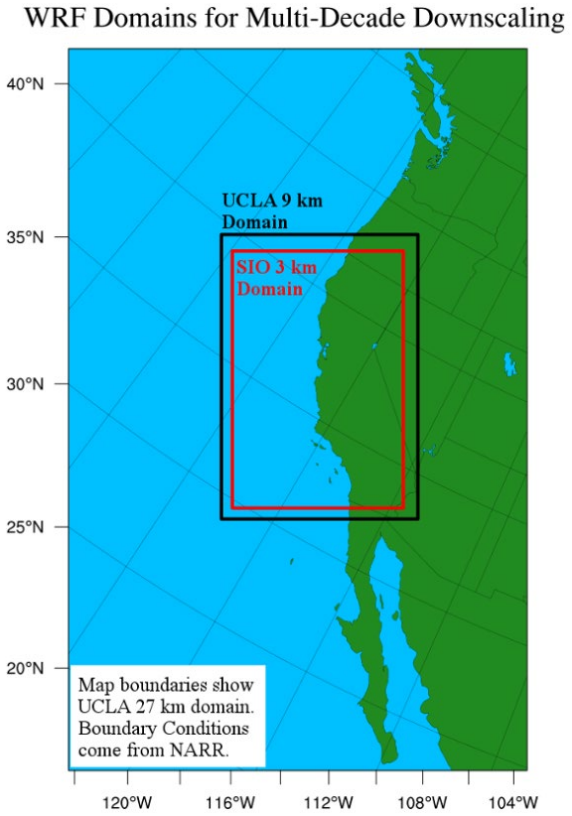

9 km and 3km domains shown by black and red outlines, respectively.

Source: From project analyses and Professor Alex Hall's research team at UCLA

Figure 7. Mean Daily Summer Season (May – September) Albedo (%)

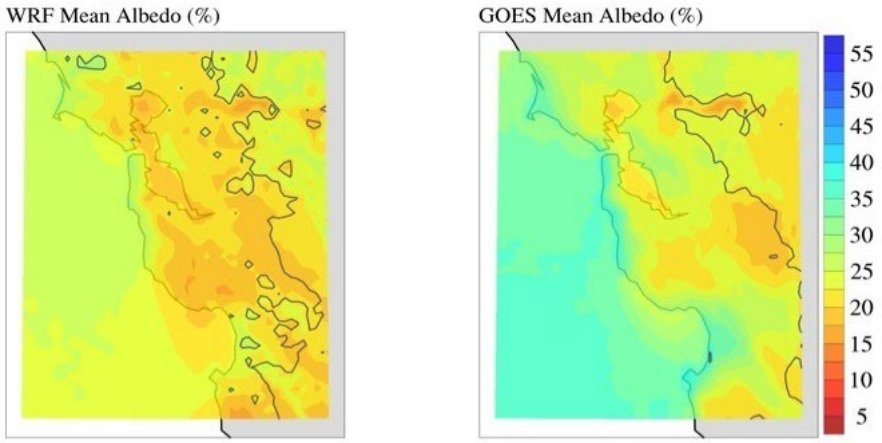

On the Left: WRF-CACLC v0 and Right: GOES. The black line indicates where coefficient of variability (σ/μ) exceeds 1.0.

Sources: See text for details. GOES-West satellite data provided by NOAA.

Table 2. Post-Processed WRF-CA-CLC Output Variables

Variable Name (in output file)	Variable long name	Levels	Description / Notes
T2	2m temperature	2m above ground level (AGL)	Temperature at 2m AGL (degrees kelvin)
THETA1000, etc.	potential temperature	1000, 925, 850, 700, 500, 300hPa	
Z1000, etc.	geopotential height	1000, 925, 850, 700, 500, 300hPa	Geopotential Height, in meters, mean seal level (m MSL)
PREC	precipitation	surface	1-hr accumulated precipitation
TPW	total precipitable water	column	
Q2, Q1000, etc.	water vapor mixing ratio	2m, 1000, 925, 850, 700, 500, 300 hPa	Daily mean can be estimated from hourly output.
U1000, V1000, etc.	vector winds on pressure levels	1000, 925, 850, 700, 500, 300 hPa	Vector Wind Components Rotated to Earth-Relative (Zonal and Meridional)
U10, V10	vector winds at 10m	10 m	
Uhub, Vhub	vector winds at 80m	80 m	Diagnosed from standard WRF 3-D output
Gust10min	maximum wind speed last 10 minutes	10 m	Maximum wind gust over last 10 minutes of the hour. Only available for 2008, 2009 and 2018
Gust1hr	maximum wind speed during last hour	10 m	Maximum wind gust over last hour
GUST_UST	wind gust estimate		Friction velocity estimate of wind gust
GUST_TKE	wind gust estimate		Brasseur estimate of wind gust
Wind1hr	average wind speed	10m	Average wind speed in last hour
Wind10min	average wind speed	10m	Average wind speed in last 10 minutes (only in 2008, 2009 & 2018)

Variable Name (in output file)	Variable long name	Levels	Description / Notes
HainesLow, HainesMid, HainesHigh	Haines index		Lower Atmosphere Stability Index
AET	actual evapotranspiration (AET)	surface	
CAPE	convective available potential energy		Moist unstable convective available potential energy
CIN	convective inhibition		Maximum convective inhibition experienced by any parcel
Z0C	atmospheric freezing level		Altitude of first encountered temperature less than 0°C
PSFC	surface pressure	surface	Units: Pa
ALBEDO_ALL	ALBEDO	column	Total Albedo at top of atmosphere (TOA)
ALBEDO_SFC	ALBEDO_SFC	surface	Albedo of Land Surface
ALBEDO_BCK	ALBEDO_BCK	surface	Expected surface albedo from MODIS climatology
CLDFRA_LOW	cloud fraction low	500m AGL	Fractional sky coverage by clouds near 500m AGL
CLDFRA_MID	cloud fraction mid	2000m AGL	Fractional sky coverage by clouds near 2000m AGL
CLDFRA_HIGH	cloud fraction high	6000m AGL	Fractional sky coverage by clouds near 6000m AGL
PBLH	boundary layer height		Depth of Boundary Layer (m AGL)
QCLOUD_925	cloud water mixing ratio at 925 hPa	925 hPa	
QCLOUD_700	cloud water mixing ratio at 700 hPa	700 hPa	
QCLOUD_500	cloud water mixing ratio at 500 hPa	500 hPa	
CWP / CWP700	cloud water path	column / column below 700hPa	

Variable Name (in output file)	Variable long name	Levels	Description / Notes
LWCLD_TKE	low cloud turbulent kinetic energy (TKE)		Mean TKE in low cloud layer
LWUP	longwave up	surface	Upwelling Longwave irradiance at the surface
SWDOWN	shortwave down	surface	Downwelling Solar irradiance at the surface
SWTOA	shortwave top of atmosphere	top of atmosphere	Downwelling Solar irradiance at the top of atmosphere
SST	sea surface temperature	surface	Sea-Surface Temperature (Bulk)
SOLZEN	solar zenith angle	column	Cosine of Solar Zenith Angle
LCL	lifting condensation level		Lifting Condensation Level Height (m MSL)
IBH	inversion base height		Altitude of Base of Lowest Inversion
ISTR	inversion strength		Temperature Change through Lowest Inversion
ITH	inversion top height		Altitude of top of lowest temperature inversion
IBP	inversion base pressure		Pressure at top of lowest temperature inversion
LHF	latent heat flux	surface	Upward-directed Latent Heat Flux at Surface
SHF	sensible heat flux	surface	Upward-directed Sensible Heat Flux at Surface
CTT	cloud top temperature	column	Temperature at Top of Highest Cloud
SLP	sea level pressure	column	Pressure reduced to mean sea-level
SNOW	snow water equivalent	surface	1-hr Accumulated Snow-water-equivalent
SMOIS	soil moisture	surface	Soil moisture at 5 cm depth
XLAT	latitude		
XLONG	longitude		
XTIME	time		Minutes since April 1 0z of given year

Variable Name (in output file)	Variable long name	Levels	Description / Notes
XLAND	land mask		1 for land, 2 for water
HGT	terrain height		Height (m)

Sources: From analyses herein, see text for details.

3.2.2 Configuring WRF-CA-CLC

At project start, it was not known how WRF should be configured to best capture important modes of climate variability in CLC. Hence, the project team proposed a series of configurations, differing in their sub-grid scale physical process models and vertical resolution. The proposed configurations are depicted in Table 3. A baseline configuration (v0) was proposed based on team experience with WRF simulations of California weather and climate phenomena. Figure 7 shows the performance of v0 compared to observations. The other configurations in Table 2 focus on the treatment of the atmospheric boundary layer, including the method and degree of numerical closure for simulating turbulence ("BL Variables" column), and whether mixing and advection of cloud water ("Mix/Advect" column), or shallow convection were empirically included. Sensitivity analyses were performed by running each configuration in Table 3 during a typical MSc season: May to September 2010. Model bias, variability and temporal evolution of CLC were compared to upper-air and satellite observations. These analyses were used to choose the best configuration for simulating CLC without negatively impacting the accuracy of simulated vector winds. Based on the above measures, configuration v4 was chosen to simulate the full 2008 to 2019 timeseries. An additional configuration, not shown in the Table, tested the sensitivity of adding model vertical layers to the v4 test. It was found that additional vertical levels did not materially improve the above metrics. In the following two sections, select analyses are depicted to help the reader visualize the process of sensitivity experiments and ultimate WRF-CA-CLC configuration selection.

3.2.3 Intra-Seasonal Variability of Saturation Simulated in the Coastal Boundary Layer

The mechanisms responsible for moistening the subtropical marine boundary layer during extensive MSc episodes are well-documented (Wood 2012; Clemesha et al., 2017). Less well-documented is the vertically resolved intra-seasonal variability in boundary layer, moisture and clouds. Figure 8 shows an analysis emerging from the active period created by comparing WRF-CA-CLC simulations to daily balloon-borne soundings, collected by National Weather Service observers and obtained from the University of Wyoming at: http://weather.uwyo.edu/upperair/sounding.html. Both simulations and sounding observations are valid for cloudy mornings near 00 Universal Coordinated Time (UTC) and drawn from three California locations near the coast: Oakland, Miramar, and Vandenburg Air Force Base. Three configurations of WRF-CA-CLC from Table 3 are shown, to investigate effects of different model boundary layer parameterizations on clouds. The center panel in Figure 8 shows that all WRF-CA-CLC versions overestimate the daily variability of saturation in the lowest atmospheric layers but underestimate saturation near the surface at pressures below 950 hPa. Crucially, these model disparities occur near the average top of the cloud layer, meaning all configurations regularly

produce much too dry boundary layers below the marine stratocumulus cloud deck. The far-right panel shows that in these critical layers with pressure greater than 950 hPa, the total water mixing ratio is biased low in all versions of the model. In the far-left panel, the cloud water mixing ratio variability shows that model configurations with the Total Energy – Mass Flux (TEMF) boundary layer often produce much more cloud in lower atmospheric layers, despite the low bias in total water content.

Figure 8. Profiles of Observed and WRF-CA-CLC Simulated Cloud Properties Morning (12 UTC) Lower Tropospheric Profiles During Summer 2010 Simulations

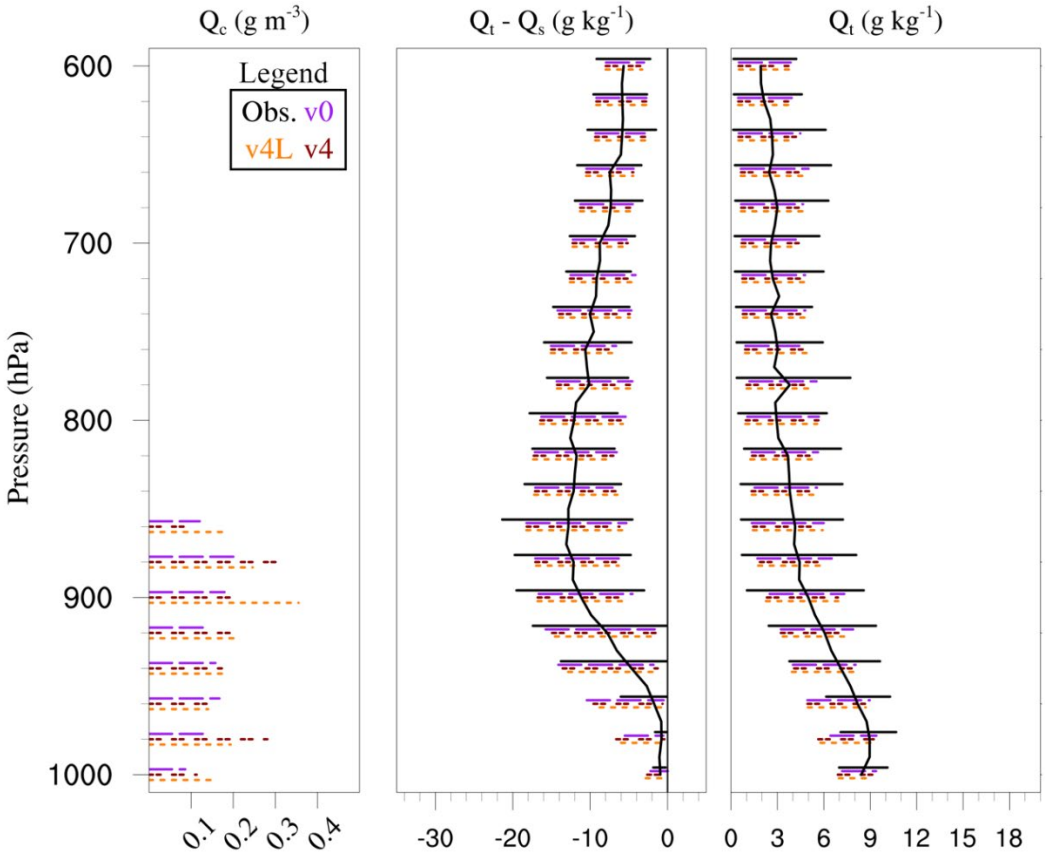

On Left: cloud liquid water (g/m^3) from WRF-CA-CLC versions v0, v4, v4L for all coastal national weather service sounding sites (NKX, VBG, OAK) where GOES albedo at 15 UTC indicated cloudy conditions. Horizontal lines drawn between lower/upper 10% values.

In Center: As in the left panel, except profiles of saturation deficit: Qt – Qs (g/kg). Observed values calculated from National Weather Service sounding temperature and dewpoint. Bold black line indicates observational mean profile. The thin black vertical line indicates saturation. Where the quantity approaches saturation, there is water available to condense clouds.

On Right: As in the center panel, but for total water mixing ratio (Qt – g/kg). A threshold albedo equal 0.3 was used to detect cloudy conditions. Approximately 220 observations is the maximum number in any vertical layer.

Sources: from analyses herein, see text for details, and GOES-West satellite and observed sounding data provided by NOAA.

Table 3. WRF-CA-CLC Sensitivity Tests

Perturbation	BL Variables	Mix/Advect	Shallow Convection
Test name			
v0 (Baseline)	TKE	Off	Off
v1	TKE	Off	On
v2	TKE	On	Off
v3	TKE	On	On
v4	TEMF	Off	Off
v5	TEMF	On	Off

These are the WRF versions considered for dynamical downscaling. Columns refer to parameterized processes a, b, c where the prognostic BL Variables TKE and TEMF are used, Mixing and advection (Mix/Advect) of cloud hydrometeors in the boundary layer, and shallow convection and turned on or off. Green highlighting shows tests that were performed for May to November 2010.

Sources: from analyses herein, see text for details.

In the versions considered for dynamical downscaling, as shown in Table 3, version v2 was proposed but not run. It is included in the table because it is part of the natural perturbations of BL Variables, Mix-Advect, Shallow Cumulus that one would arrive at. The Final configuration (WRF-CA-CLC) was chosen as v4 based on coastal low cloud accuracy during 2010 test period. Version 4 was the version that we employed in the multiyear reanalysis simulation because v4 performed best in replicating stratocumulus clouds over the eastern North Pacific and along the California coast, and also produced reasonable simulation of Santa Ana winds in Southern California.

3.2.4 Simulated MSc Are Limited by Boundary Layer Turbulent Mass Fluxes and Boundary Conditions

Figure 9 shows the accuracy of MSc presence by two configurations (v0, v4, see Table 2) of WRF-CA-CLC by comparison to GOES satellite observations of albedo. In the mean, v4, a version of WRF-CA-CLC including the TEMF boundary layer model, is far more accurate than v0, the WRF-CA-CLC baseline version. This is true for all configurations using the TEMF boundary layer model (v4, v4L, v5) compared to all other versions. The TEMF model allows more vigorous development of turbulent mass fluxes, especially near boundary layer top where the other boundary layer models tested do not allow prognostic treatment of turbulent mass fluxes. Combined with the above result, this indicates that MSc in WRF-CA-CLC simulations are limited by turbulent mass fluxes in marginal saturation environments; for example, the amount of moisture that is transferred upward from the ocean surface to the level at which condensation occurs and clouds form. This result, along with the intra-seasonal variability result, is being developed for a peer-reviewed manuscript (Martin et al., *in-prep*.).

These different parameterizations had significant influence on marine cloudiness, and ultimately the model version v4 (in this research's tests, see Table 3) was selected by the research team because it produced greater marine cloudiness than the other versions, which were strongly biased toward unrealistically clear conditions.

A crucial factor in the degree of fidelity of the dynamical downscaled historical results is the choice of the large-scale model used as boundary conditions for the fine-scale WRF simulation.

A comparison between downwelling solar radiation from different atmospheric reanalyses (Figure 10) makes this point; the ERA5 reanalysis produces patterns of marine and coastal cloud that are far superior to those from the NARR and MERRA-2 Reanalyses (as gauged by their comparison to observed cloud albedo from GOES data). It should be noted that ERA5 is a very new (~mid-2019) dataset, and dynamical downscaling using ERA5 as WRF boundary conditions is still nascent, both to the community and to this project. Future dynamical downscaling of MSc over coastal regions of California may benefit from using ERA5 as boundary conditions instead of the current NARR.

Figure 9. July 2010 Mean Albedo At 15Z (7 a.m. PST) From WRF V0, and WRF V4 vs. GOES Observations

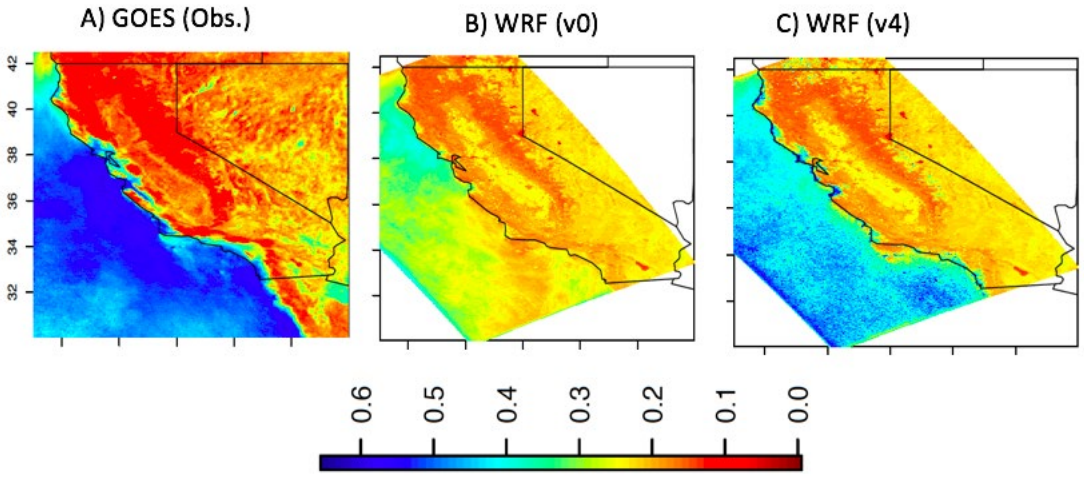

Sources: See text for details; GOES-West satellite data provided by NOAA.

Figure 10. Daily Averaged Surface Downwelling Solar Radiation (W/M2) Over the West Coast of the United States

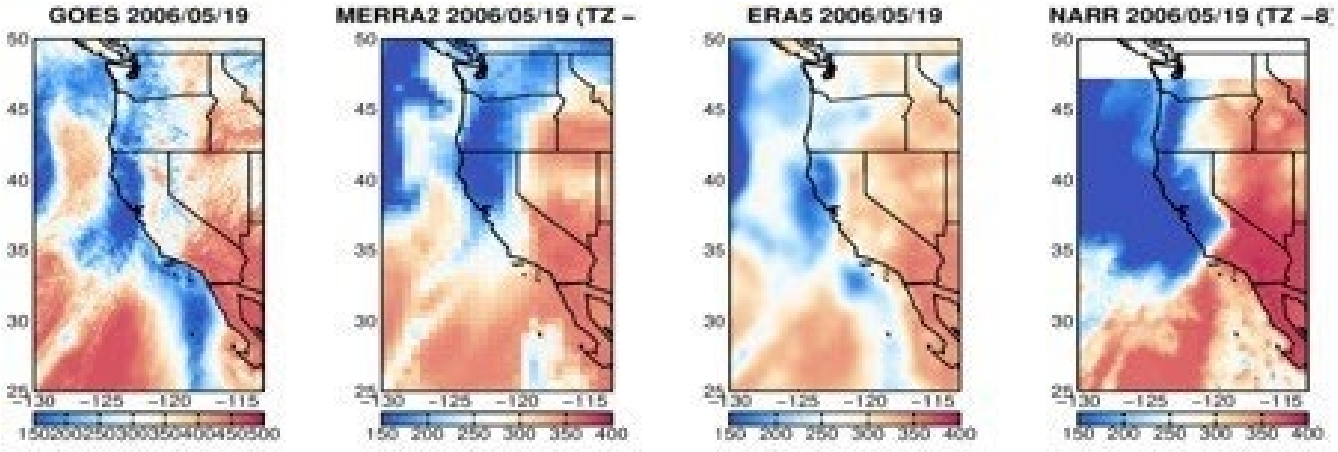

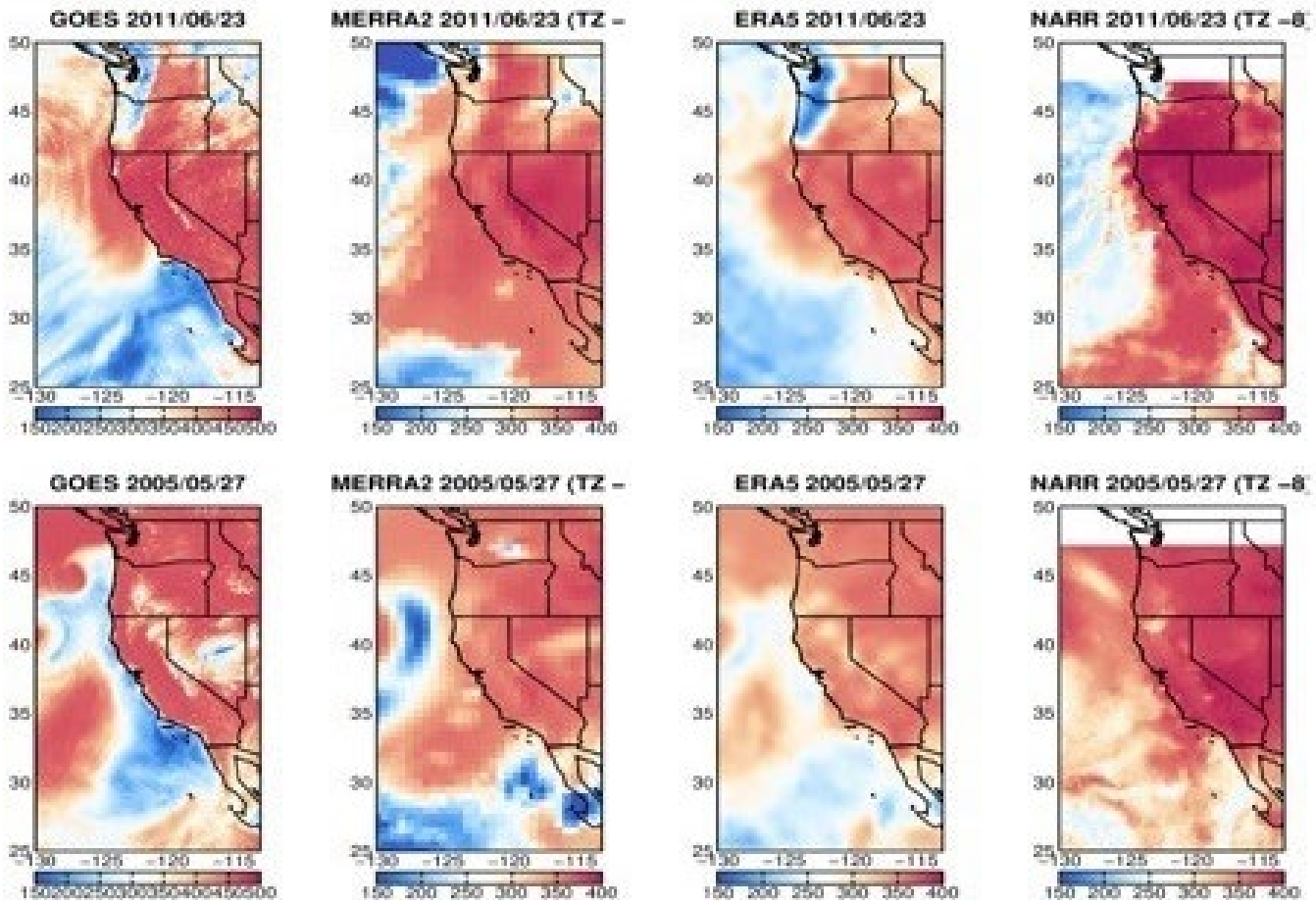

From left to right: GOES satellite observations, MERRA2 reanalysis, ERA5 reanalysis, and the NARR reanalysis. Each row shows one day, as per the panel title. Days are selected based upon having a strong land/sea contrast in values along the coast of Southern California. So, for instance, blue areas indicate heavy marine stratus clouds (low surface solar radiation), red colors indicate clear conditions (high surface solar radiation).

Sources: GOES-West satellite data provided by NOAA. MERRA2: A NASA reanalysis. NARR: NOAA/NCEP North American Regional Reanalysis. ERA5: ECMWF Reanalysis version 5.

3.2.5 Interannual Variability in Modeled MSc

Year-to-year variability in MSc and other coastal low-cloud types along the Western United States has been linked to fluctuations in eastern North Pacific sea-surface temperatures associated with the Pacific Decadal Oscillation (Schwartz et al., 2014). A multi-year WRF simulation affords the unique opportunity to examine the fidelity of interannual variability in modeled MSc.

A disproportionate fraction of California's population lives within the coastal zone, and a growing amount of rooftop solar generation is correspondingly sited there. Skill in modeling CLC along and near the coast is therefore vital to understanding the processes that drive CLC and to plan for future variability and possible change. Morning albedo averaged over May to September for eight years is shown for locations along a transect in northern and southern California (Figure 11). From this examination, model skill at capturing interannual variability in cloudiness is mixed (and lowest) at the immediate coast. The model more skillfully tracks

observed interannual variability in albedo approximately 40 km inland from the coast, which represents the typical edge of inland penetration of CLC, although the model overestimates cloud presence. When the seasonal cycle over the warm season is preserved as shown by monthly (May to September) albedo from 2010 to 2018 (n = 40, Figure 12) the simulation of CLC at Oakland outperforms that at Vandenberg and San Diego. At the Oakland location the month-to-month changes in albedo are well captured, especially from 2013 to 2016 (r = 0.81, n = 20).

Figure 11. Time Series of Observed (GOES) and Modeled (WRF) Albedo

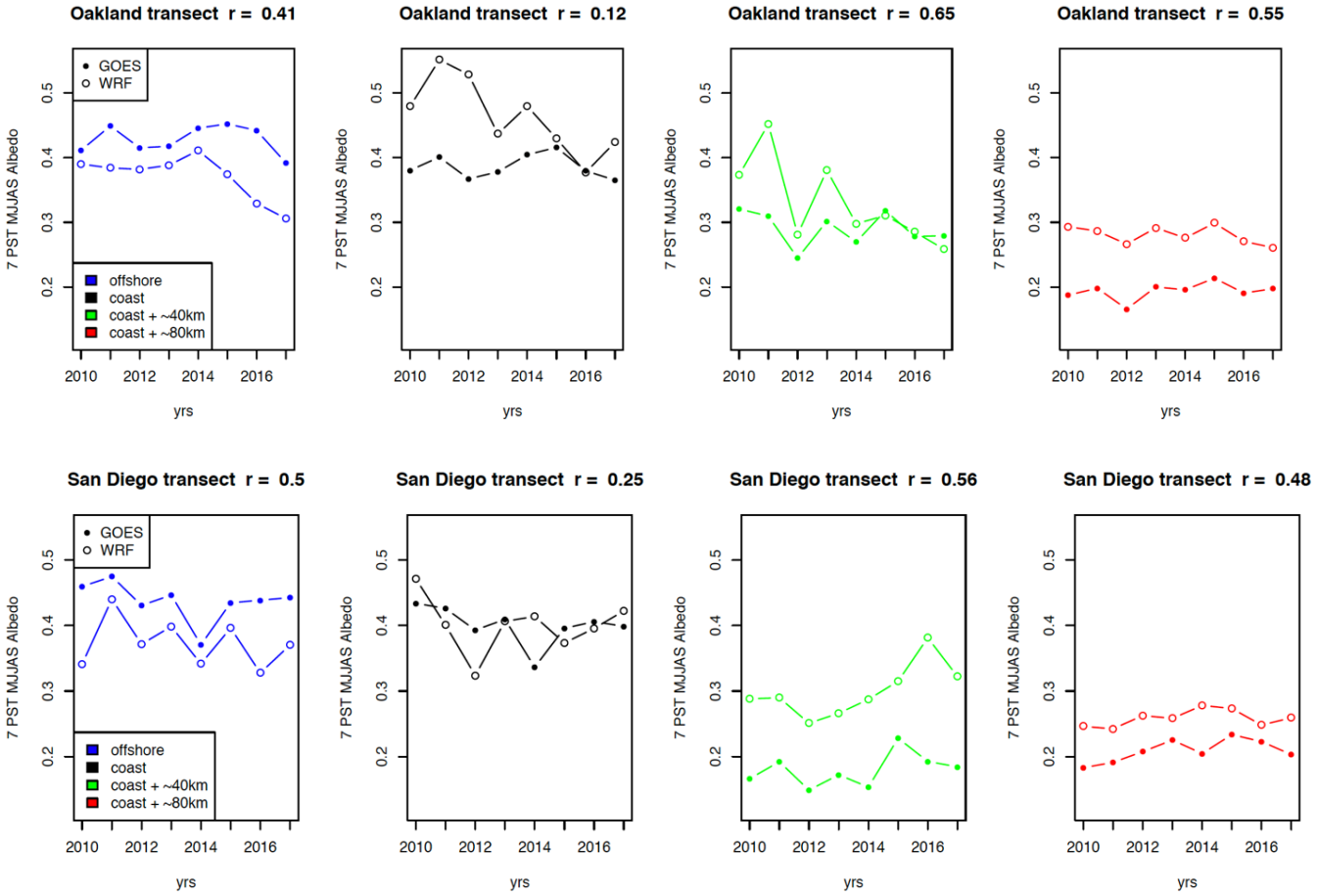

This figure shows the timeseries of observed (GOES) and modeled (WRF) albedo at 15Z (7 PST) averaged over May through September for 2010 to 2017 for a transect through Oakland (top) and through San Diego (bottom).

Sources: See text for details; GOES-West satellite data provided by NOAA

Figure 12: Time Series of Monthly Albedo for Each Warm-Season Month

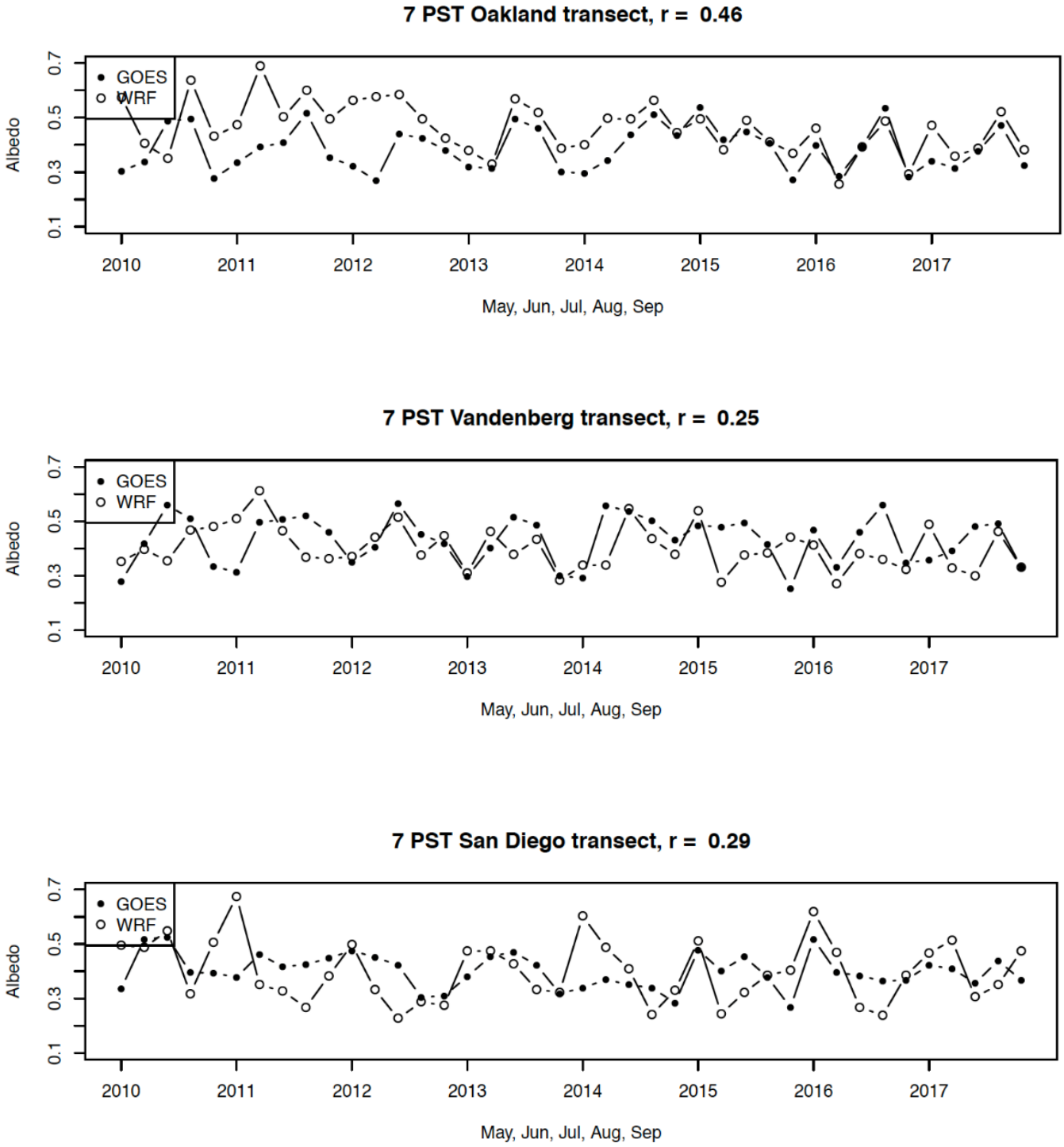

This figure shows the time series of monthly albedo for each warm season month (May through September) from 2010 to 2017 for grid cells at Oakland (top), Vandenberg (middle) and San Diego (bottom).

Sources: See text for details and GOES-West satellite data provided by NOAA.

3.2.6 Validation of WRF Sea-Level Pressure and Temperature Fields

As a means of checking the reasonableness of WRF-CA-CLC output, the research team compared SLP and 500 hPa geopotential height to MERRA2 reanalysis. MERRA2 is a state-of-the-art reanalysis product at approximately 50-km resolution. As an example of this test, Figure 13 shows the RMSE and bias computed for July for the years 2011 through 2018. The small values of each (<20 hPa) indicate that there are no large-scale problems with the WRF-CA-CLC runs. Alignment of the RMSE and bias with topography show the expected relationship for SLP between models of different resolutions, again confirming the validity of the WRF-CA-CLC, at a basic level.

Having hourly temperature data from both the WRF run and hourly stations across California allows comparison between the two and to determine how well WRF reproduces this aspect of weather and climate. Hourly temperatures are important because they affect energy demand, human health through heat stress, and agriculture. The 29 stations used are the same as those used in Pierce and Cayan (2019) and described in Section 3.1.1 and were selected for their importance to California's electric utilities. The period used for the comparison is mid-2013 through the end of 2014, which was the entirety of the data available when this report was generated. Although relatively short, it includes many days so that model estimates are still useful. This enables accurately removing the seasonal cycle, which was done on the basis of removing the best-fitting annual and semi-annual harmonics using a fast Fourier transform-based technique.

Figure 13. Root Mean Square Error and Bias from Daily Sea-Level Pressure (Hpa) of WRF-CA-CLC Compared to MERRA2 Reanalysis

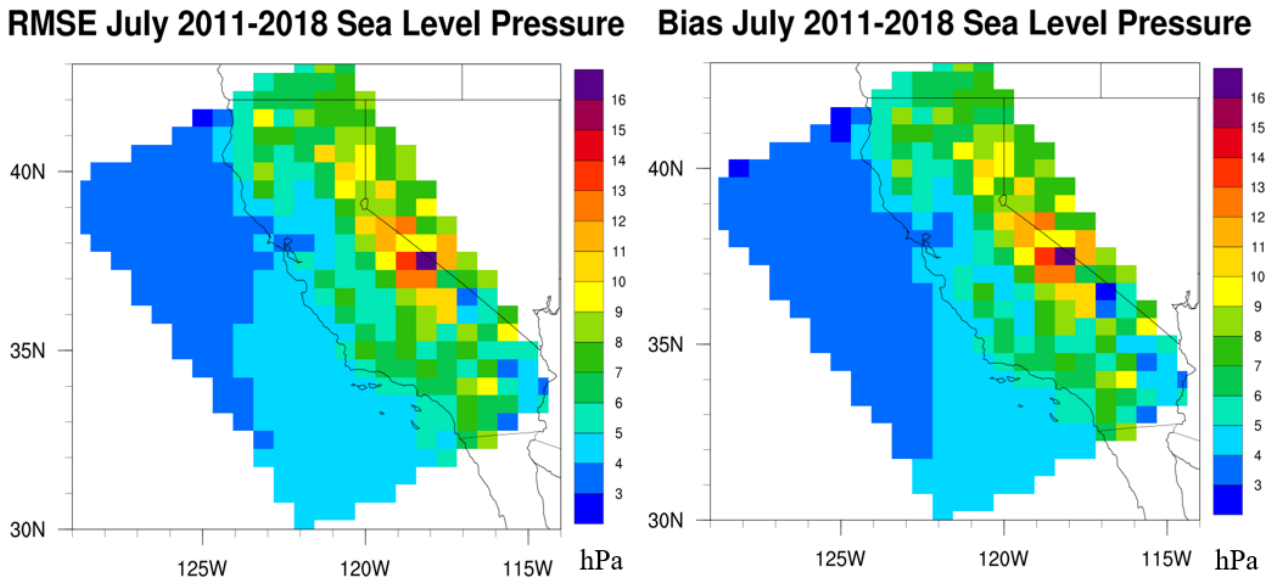

Sources: See text for details, and MERRA2: A NASA reanalysis.

Results comparing WRF to the observations for one of the stations (KBFL, Bakersfield Meadows Field, which is located centrally and provides a full set of data) are shown in Figure 14. The scatterplots show both actual values (panel a) and anomalies (panel c); R2 values are

0.93 and 0.72, respectively, showing that WRF captures the time evolution of the hourly values well. The power spectra (panel d) show an interesting divergence, however; at high frequencies (periods less than 12 hours) WRF has systematically less spectral power than the observations, culminating at near an order of magnitude less power at the Nyquist frequency (0.5 cycles/hour). Panels e) through h) were chosen to display the eight-day sequence of temperature anomalies for the hottest period in the record (panel e), coldest (panel f), most variable (panel g), and least variable (panel h). Overall, WRF does reasonably well, capturing most of the time evolution seen in the observations. Two exceptions can be seen: 1) the strong warming seen in panel g) after January 22, 2014, is not captured at this particular station (but is not a systematic problem across different stations, not shown); 2) as noted from the power spectra, the observations have more high-frequency variability than seen in the observations.

Figure 14. A Comparison of Hourly Temperatures (Degrees Centigrade) at Bakersfield Between WRF, and the Hourly Observations

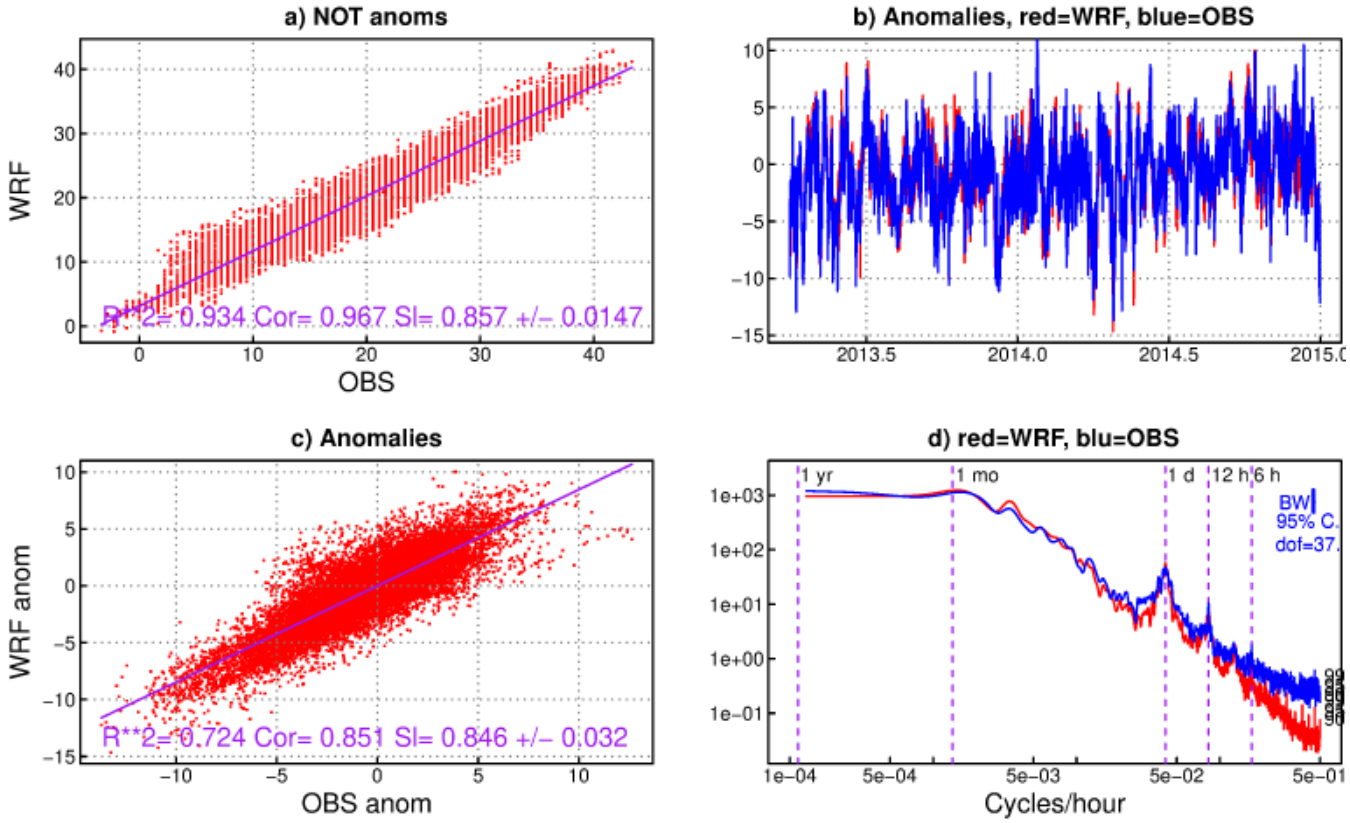

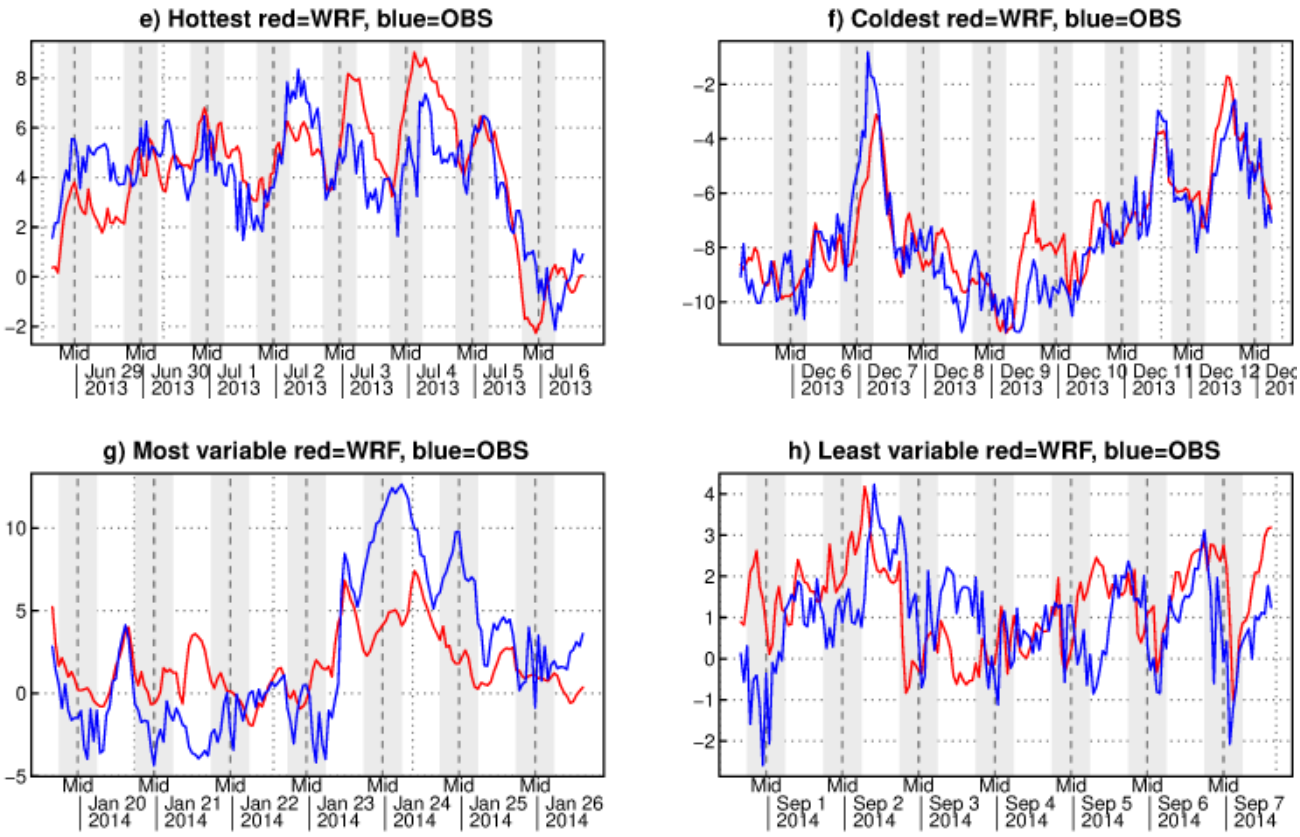

The hourly temperatures (degrees C) at Bakersfield in WRF are in red, and the hourly observations in blue. Sections of the figure show: a) scatterplot of actual hourly values (not anomalies) between the two data sets; B) time series over the period analyzed; C) scatterplot of anomalous values; D) power spectra; E) eight-day time series of hottest period; F) time series of coldest period; G) time series of most variable period; and h) time series of least variable period.

Sources: See text for details.

Correlations between the observed and WRF-generated hourly temperatures at all stations are shown in Figure 15, for both the original temperatures including the seasonal and diurnal cycles (left panel), and the anomalies (right panel). Unsurprisingly, correlation values are higher (> 0.75 typically) when the seasonal and diurnal cycles are included but are still reasonable in the anomalies fields (> 0.65 typically). In both cases, values are highest in the Central Valley and inland areas, and lowest along the coast. Weather Station KSBA (Santa Barbara) is particularly poorly reproduced in both.

Figure 15. Correlation of Hourly Temperature Values Between WRF and the Observations

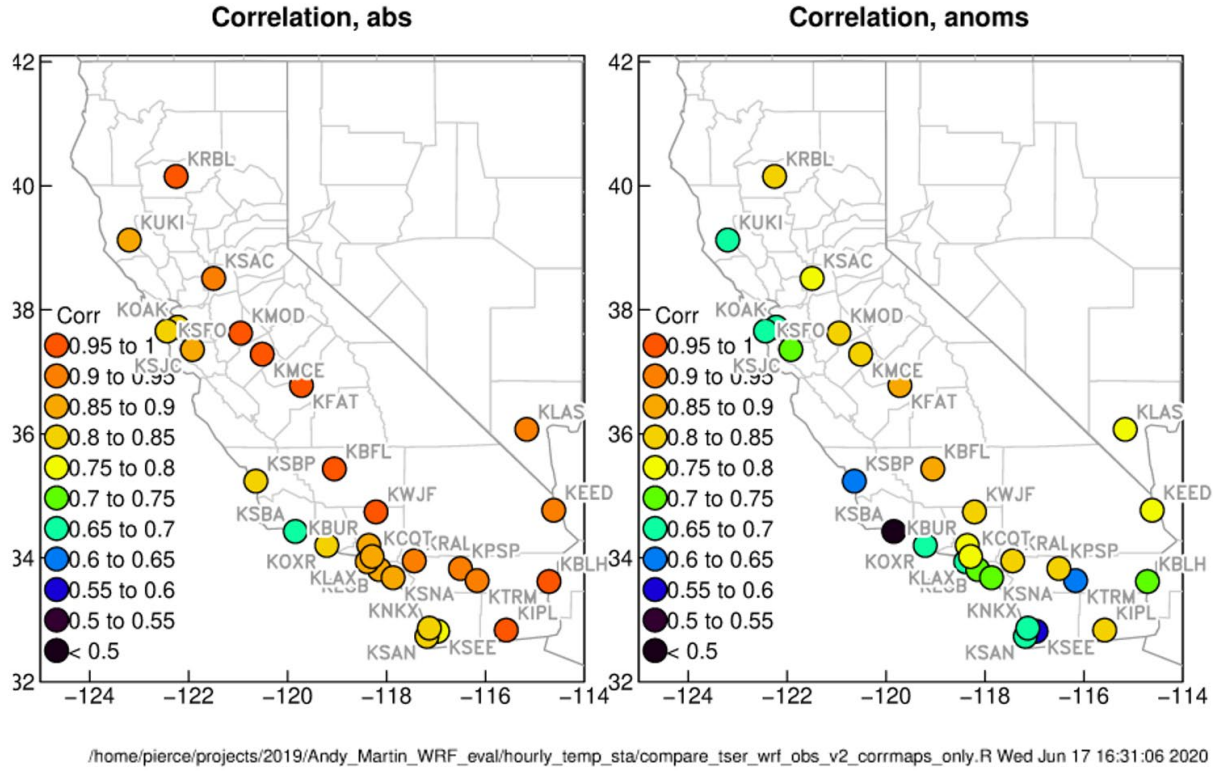

The correlation of hourly temperature values between WRF and observations is shown from the actual temperatures (left) and anomalies (right). Values are plotted at 29 stations; each station is labeled by its call sign.

Sources: See text for details.

Although a deficiency in spectral power is seen in the WRF results at all stations, it is not evenly distributed across the domain (Figure 16). The model's reproduction of hourly variability is weakest in the Bay Area and at some inland locations in Southern California, and highest in the Central Valley. The deficiency also raises the question of whether WRF has too little variability because it simulates an overly viscous boundary layer, which could both damp high-frequency variability and perhaps increase the spatial coherence of the WRF temperature patterns. This is tested in Figure 17, which shows the correlation between every station and its closest neighbor, for both the observations (left column) and WRF, illustrated as a function of high-pass frequency to see how the correlation structure varies at the highest frequencies. In the observations at the highest frequencies (top row), neighbor correlations are low, generally between 0.2 and 0.4, and highest in the Central Valley and Southern California. WRF does have unrealistically high values, but only in certain locations: Northern California, and an arc from Las Vegas through Needles, Blythe, Imperial, and Thermal (weather station labeled as KTRM). Yet, in other regions such as the Central Valley and Los Angeles regions, WRF simulates realistic values, while along the central coast from San Luis Obispo through Santa Barbara and Oxnard the modeled values are lower than observed. This geographical expression of differences persists at a high-frequency cutoff of 10 hours (middle row, Figure 17), and

the lower values from San Luis Obispo through Oxnard even persist at 24 hours. The research team concluded that there are some systematic geographical differences between observations and how WRF simulates spatial coherence. However, this is considerably more complicated than simply concluding that WRF is too spatially coherent, despite WRF's systematic deficiency in variability on hourly timescales.

Figure 16. Ratio of Hourly Temperature Spectral Power in WRF to That in the Observations

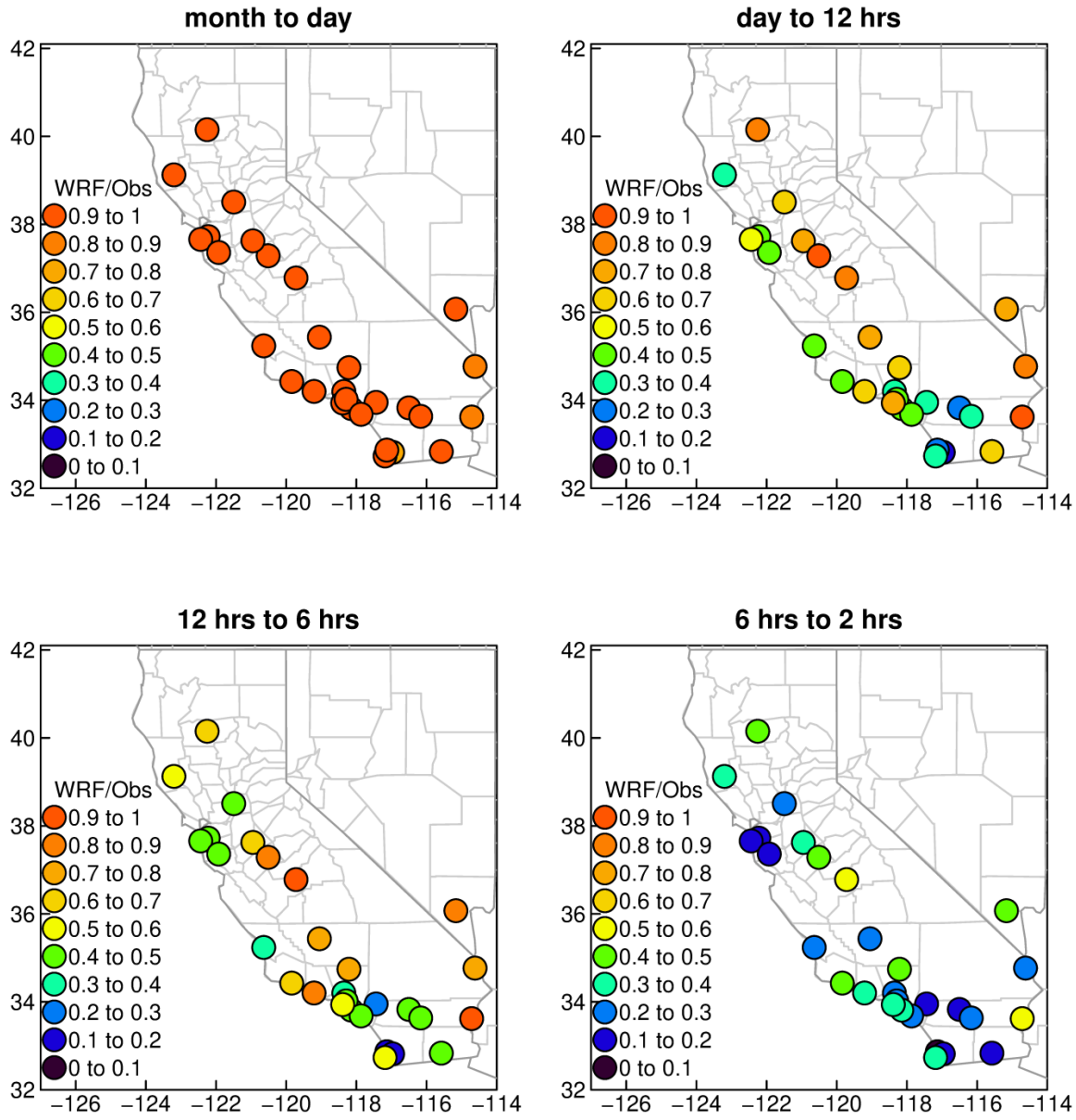

/home/pierce/projects/2019/Andy_Martin_WRF_eval/hourly_temp_sta/compare_spec_ratio_wrf_obs.R Wed Jun 17 14:49:09 2020

The ratio of hourly temperature spectral power in WRF to that in the observations in four frequency bands are shown, as indicated in the panel title, at 29 meteorological stations.

Sources: See text for details.

Figure 17. Correlation Between Temperature at Each Station and its Closest Neighbor

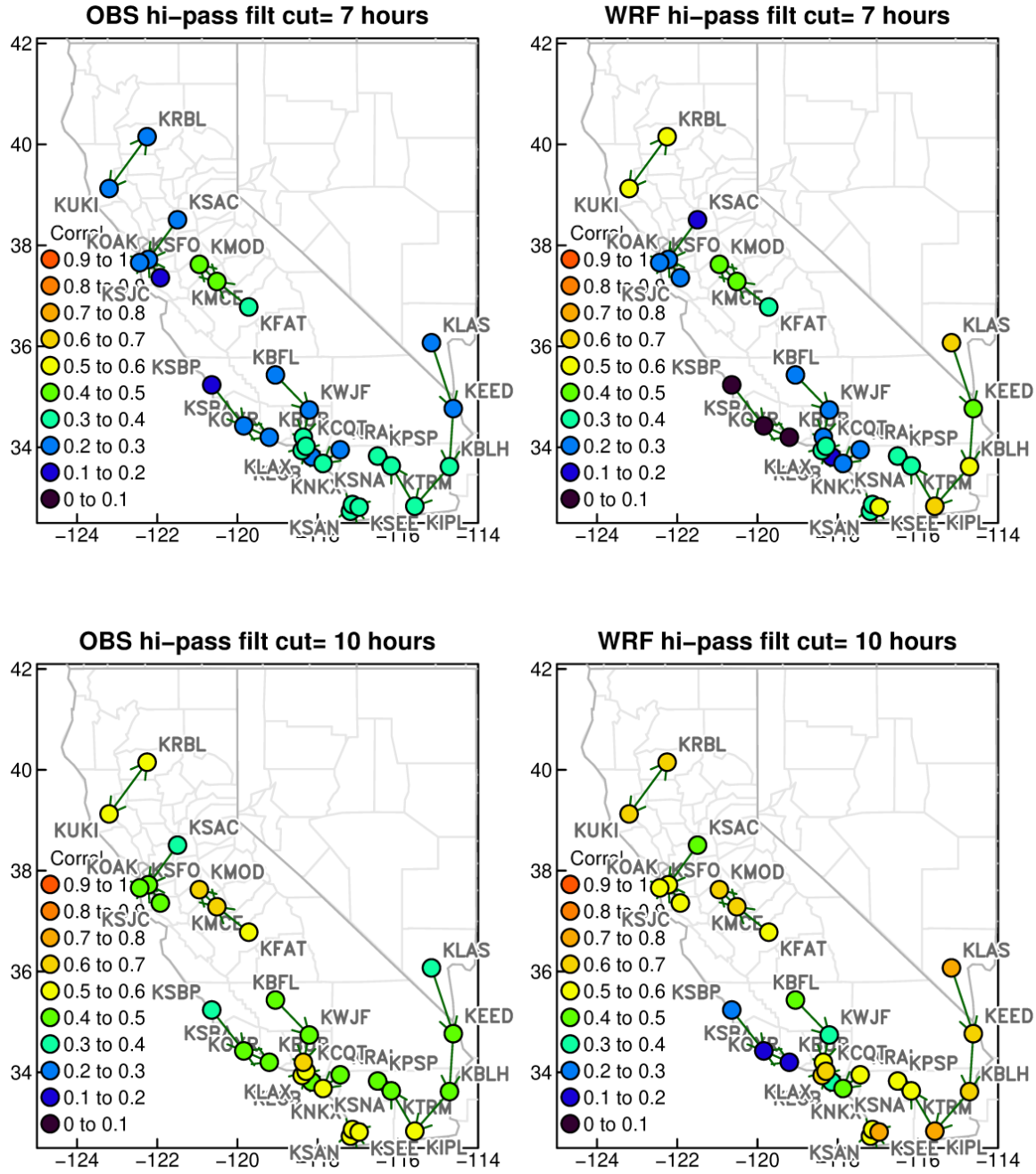

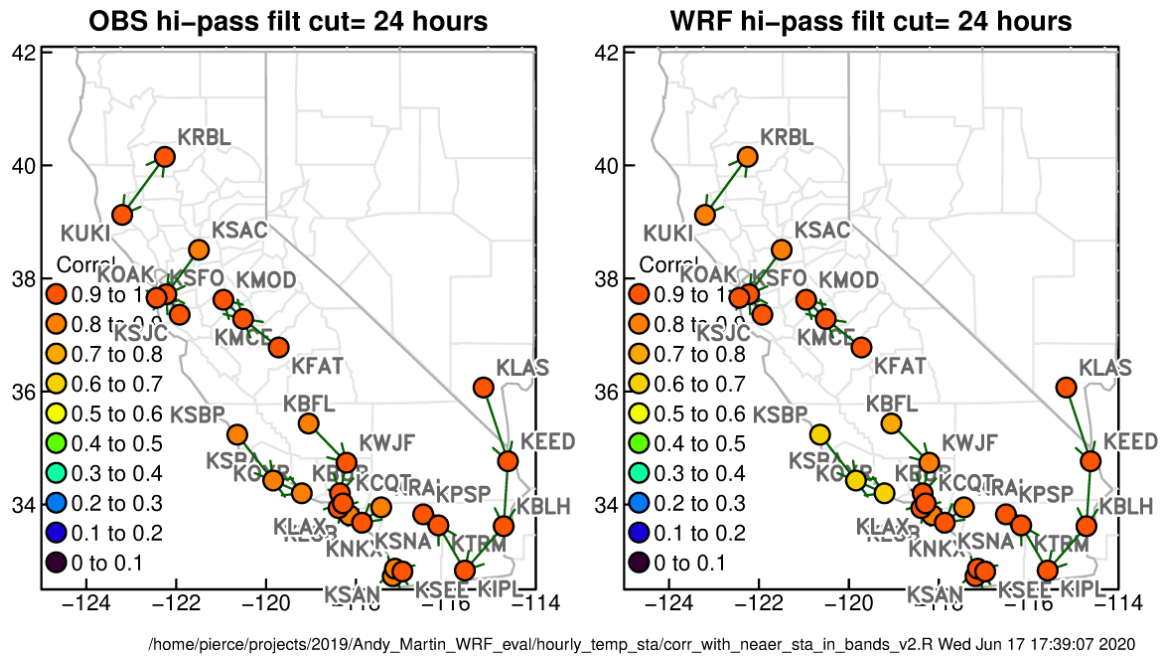

/home/pierce/projects/2019/Andy_Martin_WRF_eval/hourly_temp_sta/corr_with_neaer_sta_in_bands_v2.R Wed Jun 17 17:39:07 2020

The correlation between temperature at each station and its closest neighbor (indicated by arrows drawn from a station to its neighbor), in the observations (left column) and WRF (right column). Data in each row has been high pass filtered as indicated in the title; 7 hours in the top row, 10 hours in the middle row, and 24 hours in the bottom row.

Sources: See text for details.

3.2.7 Santa Ana Wind Evaluation

Comparison of the dynamical modeled winds from WRF-CA-CLC v4 against observed winds from the San Diego Gas and Electric (SDG&E) weather stations in the San Diego County region was performed for the overlapping period of August to November 2010. Figure 18 illustrates relatively good agreement over both longer and shorter periods during a Santa Ana wind event. Systematic bias in the modeled winds appears to exist. Biases are generally positive (modeled winds exceed observed SDG&E winds), and these overestimated speeds are largest in desert regions east of the local coastal mountains (Laguna Range) and to a lesser extent over the coastal regions. General agreement by month is best over the crest and on the western slopes of the coastal topography. For the Santa Ana wind event considered at a mountain crest location (Julian), the overestimation bias is strongest in the early afternoon and evening as well as in the longer temporal persistence of the modeled Santa Ana wind event. Results from the short modeling trials (Table 2) indicated that modeled winds are not exceedingly sensitive to the details of the chosen WRF physics package; these physical parameterization options had a greater effect in producing differing structures of coastal stratus clouds.

Figure 18. Wind Speed Mean Difference (WRF-v4-SDGE Obs) for Aug – Nov 2010

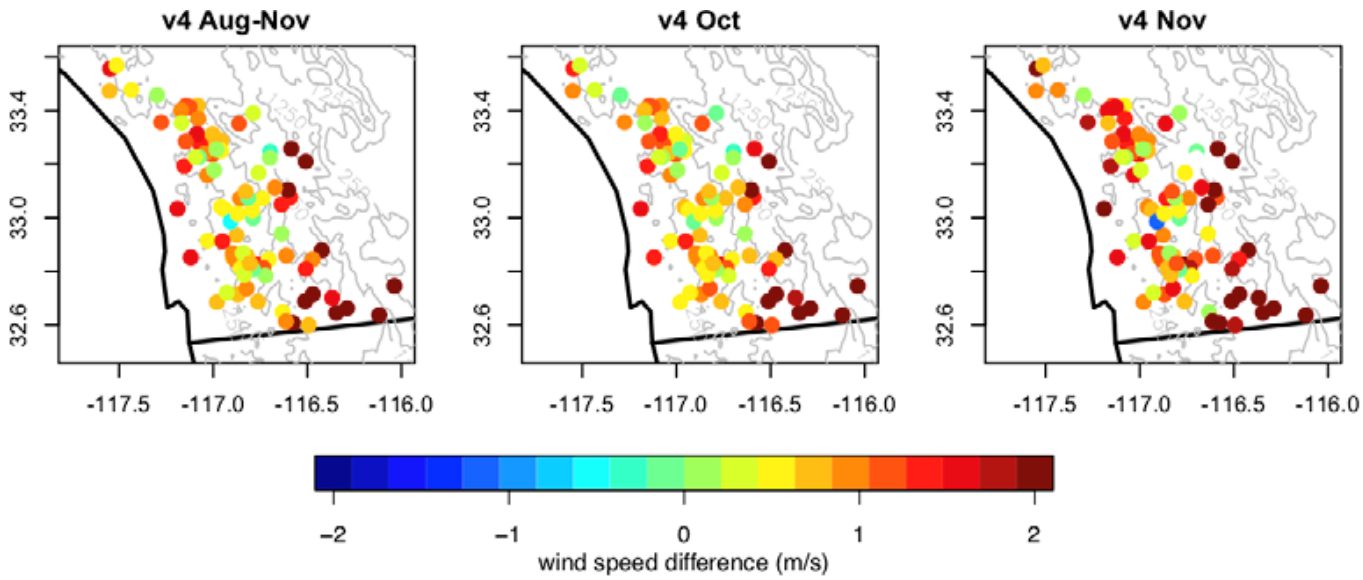

The figure shows the wind speed mean difference for WRF-v4-SDGE obs (Observations from SDG&E) for August to November 2010. The differences are shown for the complete period (most left column) and for October and November (subsequent two columns). SDG&E's 10 minute resolution observations are averaged to three hours to match WRF output resolution.

Sources: See text for details.

3.2.8 WRF CA-CLC Output

A regional model dynamically downscaled historical reanalysis dataset was produced using the WRF-CA-CLC version of Weather Research and Forecasting (WRF) model described in Section 3.2. The WRF downscaling was applied to a coarser (9 km x 9 km) WRF downscaled version of the NARR. This 9-km WRF reanalysis was provided by Professor Alex Hall's group at UCLA. The 3 km x 3 km spatial resolution WRF-CA-CLC was run for a rectangular domain approximately enclosing California (Figure 6) through a period spanning April 2008 to February 2019. The full atmospheric dataset generated by WRF is quite large (over 30 Tb for 11 years), which has been saved for the intermediate term. Additionally, a post-processed subset of the WRF-CA-CLC dataset was extracted to provide variables that are relevant for low-cloud processes, fire weather, and basic climate dynamics (such as sea-level pressure and 500 hPa geopotential height). The post-processed files amounted to about one TB and contained 80, 2-D variables including temperature, precipitation, hub-height wind, albedo, wind-gust estimates, and inversion-layer fields. The full list appears in Table 2.

The post-processed files are available every hour from April 1, 2008, to February 28, 2019, on the 3-km WRF-CA-CLC grid. Grid coordinates and other supporting metadata are also provided in the post-processed files. Access to the full dataset is arranged by request to project investigators, though more automated forms of access may be implemented in the future pending data-support funding.

3.3 WRF Aerosol Sensitivity Simulation Results

The dynamical downscaling model, WRF-CA-CLC, (Section 3.2) was used as the primary methodological tool to simulate both CLC and their brightening in response to increasing aerosol concentrations. Two simulations were run to represent clean and polluted particulate matter scenarios. The aerosol concentrations (150 cm^{-3}/ 600 cm^{-3}) representing each scenario were drawn from previously published observations at the California coast (Martin et al., 2017), and are, therefore, representative of both the current climate and current particulate matter regulatory structure in California. Aerosol susceptibility, defined as the relative change in albedo in response to an increase in aerosol concentration (see Methods, Appendix A) was the primary metric used to estimate the response in cloud brightness to particulate matter. The results obtained indicate that polluted conditions increase in the warm season (May to September) CLC albedo 15 to 20 percent along the California coast. This magnitude of increase is similar to the relative interannual variability in albedo found for the period 2009 to 2018, which was approximately 25 percent. The change in simulated albedo diurnal cycle in response to polluted conditions is small relative to its amplitude. CLC are most susceptible to polluted conditions in the month of July. Thinner clouds (by water path below 700 hPa) are more susceptible to pollutant aerosols than thick clouds (CWP_{700} > 0.1 millimeter [mm]) are, while the spatiotemporal variability in susceptibility is also greatest for thin clouds. The research team also demonstrated that the project's modeling methods allowed dynamically varying cloud-effective radius in response to changing aerosol concentrations produce more realistic relationships between cloud water amount and albedo, and that the default approach used before applying those methods produces clouds that are too bright, even for many polluted clouds. These results helped inform future regional downscaling efforts to investigate coastal low clouds and their impacts on surface insolation.

Figure 19: Clean vs. Polluted Cloud Simulation Results

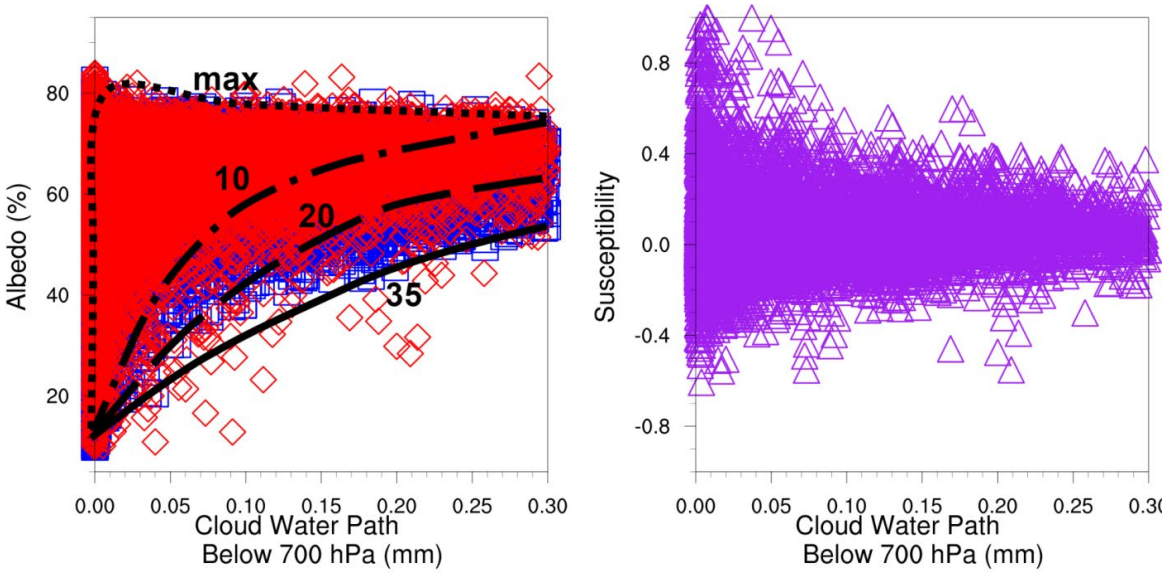

a) relationship between coastal albedo and CWP700 for Clean (blue) and Polluted (red) simulations. Black lines show theoretical model of Han et al., (1998) for re = 35, 20, 10 µm and for maximum albedo ("max"). b) As in a), except for susceptibility.

Sources: See text for additional details.

3.3.1 Relationship of Susceptibility to Cloud Water Amount

Figure 19 shows the relationship between CWP_{700} and albedo for WRF-CA-CLC warm season CLC in the California coastal zone, for both clean and polluted simulations. The California coastal zone was defined as the set of model grid points nearest the land/sea boundary, while retaining a land-surface type. This analysis serves as a validation of the model procedure and experimental method used. (See "model susceptibility process" discussion in Appendix A, page A-5.) Overlaid on Figure 19(a) are lines from the theoretical model of Han et al. (1998), whose authors explored the global relationship between liquid water path and albedo for liquid clouds. The approximate boundaries that albedo can take for a given value of liquid water path (equivalent to CWP_{700}) follow the line labelled "max" and the line for r_e = 35 micrometers (μm). Figure 19(a) shows that WRF-CA-CLC clouds closely follow these bounds. Figure 19(a) further shows that the effect of exchanging clean aerosol (blue) for polluted aerosol (red) conditions is to restrict the majority of clouds such that r_e does not exceed 20 μm. By contrast, clean conditions allow the albedo curve for clouds with r_e = 35 μm to be accessed in the model. Finally, both clean and polluted simulations produce clouds with albedo indicative of r_e > 10 μm for a given CWP_{700}. Recall from the model susceptibility process section that the Goddard radiative transfer model assumes r_e = 10 μm. Figure 19(a) demonstrates that allowing dynamic variation of r_e within a dynamical downscaling model allows a more realistic range of albedos for a given cloud-water amount and less bright clouds to develop, even for polluted aerosol conditions. Thus, projects attempting to dynamically downscale CLC should consider using a dynamically varying cloud-effective radius, used here to produce realistic cloud albedos. Figure 19(b) shows the relationship between susceptibility and CWP_{700}, essentially the fractional difference between the two populations in Figure 19(a). Thinner clouds experience a much higher range of susceptibility for a given value of CWP_{700} than for thicker clouds, as expected by varying r_e within the Han et al., (1998) theoretical curves. However, on average, susceptibility is greater for thinner clouds than for thicker clouds, as shown in Figure 19.

3.3.2 Mean Warm-Season Susceptibility

The illustrations in Figure 20 show the mean clean condition albedo and low cloud susceptibility for WRF-CA-CLC warm season (MJJAS) simulations, including cloudy (2011) and less cloudy (2015) years. During 2011 (Figure 20[a]), albedo is elevated (α >0.3) over nearly the entire coast, with pockets of very high (α >0.5) albedo. By contrast, elevated and very high albedo are confined primarily to the central and southern coasts in 2015 (Figure 20[c]). Low cloud susceptibility is higher in 2015, with a value of 0.21 compared to 0.16 in 2011. Han et al., (1998), discuss the relationship between cloud water path (CWP), $r_e$and α (see their Figure 1). Changes in r_e impact α more as CWP decreases. Thus, if coastal clouds were thinner on average during 2015, as suggested by Figure 20(c), then an increase in aerosol concentration from clean-to-polluted conditions would be expected to brighten clouds more, as shown in Figure 20(b, d). As seen in the main document, a susceptibility of 0.16 to 0.21 compares favorably to the relative interannual variability found in both WRF-CA-CLC and GOES (~0.25). Thus, the impact of polluted aerosol conditions on cloud brightening or reduction of solar insolation in the heavily populated California coastal zone may be approximately equivalent to the difference between a less cloudy warm season and a cloudier warm season.

Figure 20: Simulated 2011 and 2015 Cloud Results

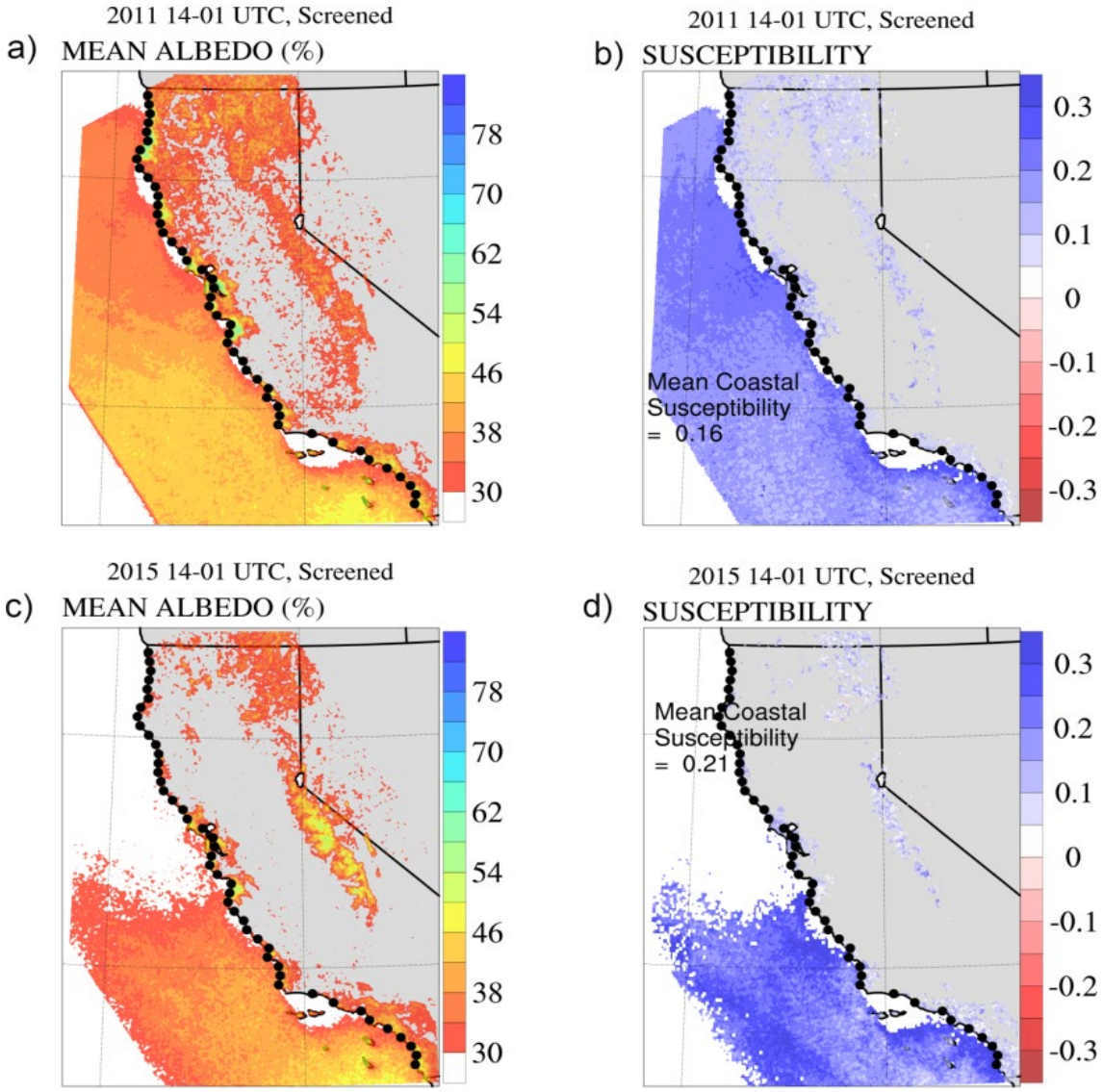

a) Mean warm season (May to September) albedo (%) from WRF-CA-CLC *Clean* simulation during 2011 (cloudy year) daylight hours (14 - 01 UTC). b) As in a, except aerosol susceptibility. Black dots show coastal grid points used to calculate mean coastal aerosol susceptibility = 0.16. c) As in a, except during 2015 (fewer clouds along California coast). d) as in b, except during 2015. Mean coastal aerosol susceptibility = 0.2.

Sources: See text for additional details.

3.3.3 Susceptibility by Month and Within the Day

Figure 21 depicts the mean clean condition albedo and low-cloud susceptibility, by month, for WRF-CA-CLC warm-season simulations, including both 2011 and 2015. A clear seasonal pattern in coastal and offshore albedo is visible, where clouds (and elevated albedo) are widespread during May, confined to the south coast largely south of Point Conception in June, begin moving northward along the coast in July, reach their northernmost coastal extent in August, and retreat southward along the coast again in September. The widespread elevated

(α >0.3) albedo in May, including over the Central Valley and inland desert regions, could be indicative of deep, precipitating clouds driven by synoptic weather systems identified by previous authors (e.g., Clemesha et al., 2016).

Figure 21: Mean Albedo (%) From WRF-CA-CLC Clean Simulation During Daylight Hours

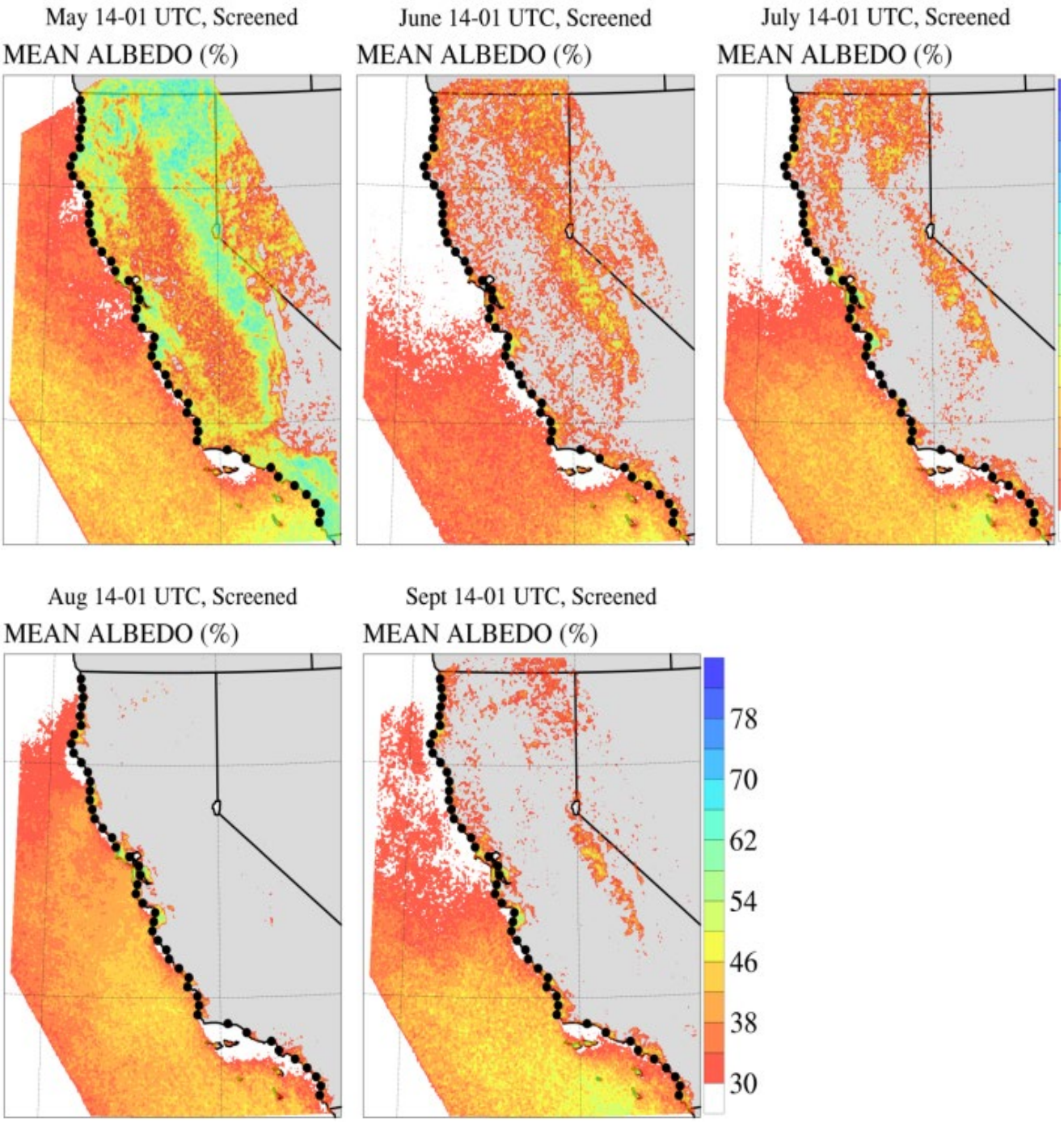

Daylight hours are 14 to 01 UTC (7AM to 6PM Pacific Daylight Time) for, top-left to bottom-center: May, June, July, August, September.

Sources: See text for additional details.

Figure 22: Mean Aerosol Susceptibility From WRF-CA-CLC Clean Simulation During Daylight Hours

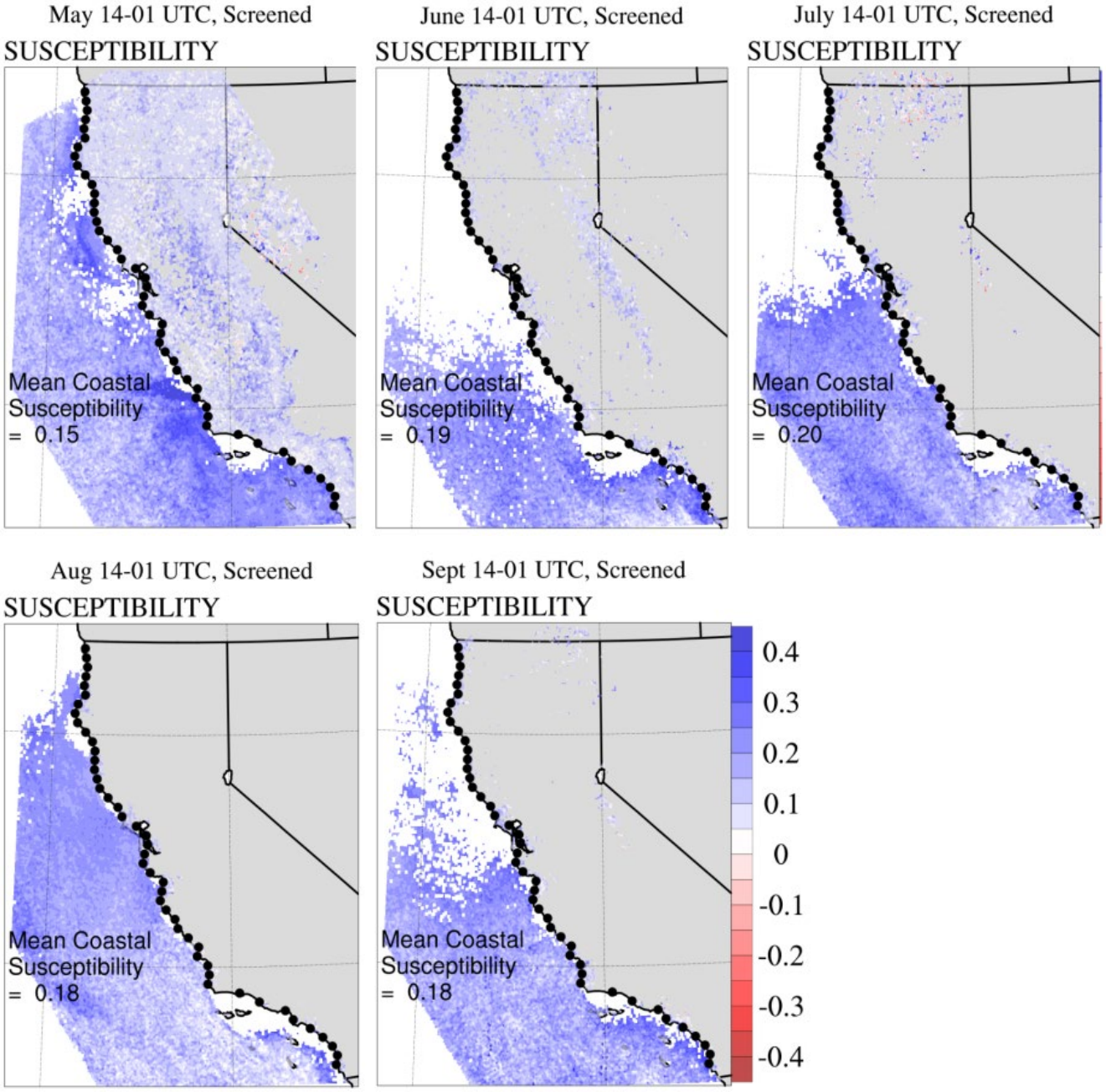

Daylight hours are 14 - 01 UTC for, top-left to bottom-center: May, June, July, August, September.

Sources: See text for additional details.

Albedo susceptibility (shown in Figure 22) follows the mean albedo seasonal cycle since it is only calculated in the presence of CLC. However, the value of coastal mean susceptibility, where defined, shows no such marked seasonality. The exception is for May, where mean susceptibility is relatively less at 0.15, compared to 0.19, 0.2, 0.18, and 0.18 for June to September.

As discussed, aerosol susceptibility is larger for thinner clouds (by cloud water path [CWP]), and the potential for deep precipitating clouds in May to contain much higher CWP may explain why the May susceptibility is lower than in late summer. Heat waves and clear skies are less common during May for most of the populated coastal zone; thus, the impact of particulate matter in reducing insolation through cloud brightening may be greater later in the summer when low clouds are thinner and more susceptible.

Similar mechanisms operate over the course of a day and there is also a diurnal cycle in aerosol susceptibility. Figure 23 shows the mean albedo diurnal cycle (daylight hours: 14 UTC to 01 UTC [7AM to 6PM Pacific Daylight Time]) for the 2011 warm season WRF-CA-CLC clean and polluted simulations, alongside the diurnal cycle from GOES observations of albedo in the California coastal zone (shown in Figures 20 to 22). Visually following the differences between the curves for clean and polluted simulations reveals that there is very little diurnal cycle in susceptibility except for that which may be caused by the variation in clean albedo (for example, the denominator of the susceptibility equation). In other words, polluted clouds show no systematic increase in reflectivity based on time of day. Also seen in Figure 23, the amplitude of the WRF-CA-CLC warm season diurnal cycle is significantly less than the GOES diurnal cycle (12 percent compared to 18 percent), and the model simulations prescribe a rebound of cloudiness in the evening, while the observational data does not show a systematic rebound. It should also be noted that the higher albedo level at all times of day (shown in Figure 23) is consistent with the high 2011 albedo shown in the interannual timeseries in Figures 11 and 12. Not shown in Figure 23 is the mean albedo diurnal cycle derived from 2015 warm season simulations, which are very similar in shape and amplitude, but differ somewhat in albedo absolute value. In particular, WRF-CA-CLC mean warm season albedo was less than GOES in 2015 (instead of more, as in 2011).

Figure 23: Mean Diurnal Cycle of CLC Albedo From WRF-CA-CLC Polluted, Clean, and GOES

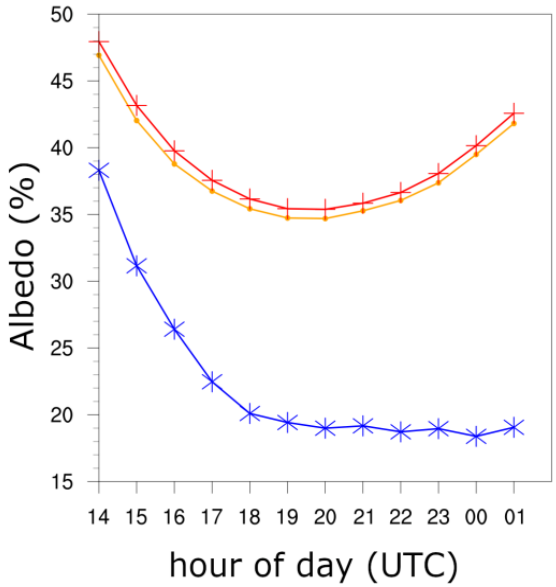

Mean diurnal cycle of CLC albedo (%) from WRF-CA-CLC Polluted (red), Clean (orange) and GOES (blue).

Sources: See text for additional details.

3.4 SHUD Model Results

The Sacramento River watershed (SW), shown in Figure 24, is the largest watershed in California and an invaluable source of fresh water for communities, agriculture, and ecosystems within the state. Nonetheless, this watershed is susceptible to dramatic shifts in water storage, which relate to changes in both snowpack and groundwater. Over the next century, groundwater withdrawals and precipitation variability are anticipated to put significant stress on this resource. Historical drought has also had a pronounced effect on groundwater tables in this watershed, and recovery following a drought tends to be slow. An accurate assessment of past water levels would be invaluable in preparing for the impacts of future drought.

The Sacramento River flows from Southern Oregon to San Francisco Bay. The total drainage area is about 72,000 km^2 while elevation ranges from 0 to 4,200 m. The climate in SW is a semi-arid hot Mediterranean. The spatial climatic characteristics are not only affected by latitude, terrain, and snow coverage but also by ocean wind and current; the climate varies spatially and temporally. Dramatic seasonal and annual climatic variations exist as well as substantial spatial heterogeneity. The eastern and northern mountains with greater rainfall and snow are significant contributors to groundwater for the entire watershed.

Figure 24. Location and Terrain of the Sacramento River Watershed

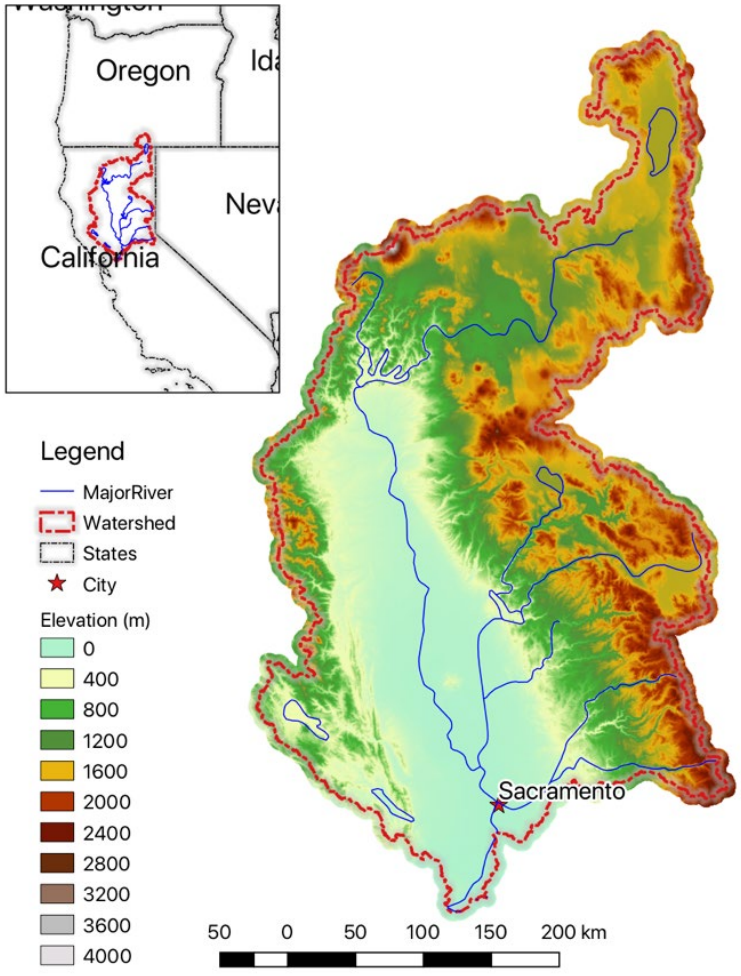

Sources: See text for details.

As shown in Figure 25, annual precipitation ranges from 400 mm/year to 1,500 mm/year; extreme annual precipitation was more than 4,000 mm/year in the northern mountainous area in 1983. In the severe drought of 2013, the mean precipitation was less than 270 mm/year, and maximum precipitation in the mountainous area was less than 650 mm/year.

The SHUD model was deployed for long-term hydroclimate simulations (1979-2018) in the Sacramento River watershed. The number of cells in the simulation domain is 6,841, with a mean area of ~10 km^2. Total length of the river network is ~13,550 km. The model ran with a single thread configuration, and it took about 70 hours to complete the 40-year simulation. The following paragraphs describe the results of that deployment for sub-catchments in- and for the entire Sacramento River watershed.

Figure 25: Annual Precipitation Variation From 1979 To 2017 and Monthly Mean and Variation (Bars and Whiskers) in Sacramento River Watershed

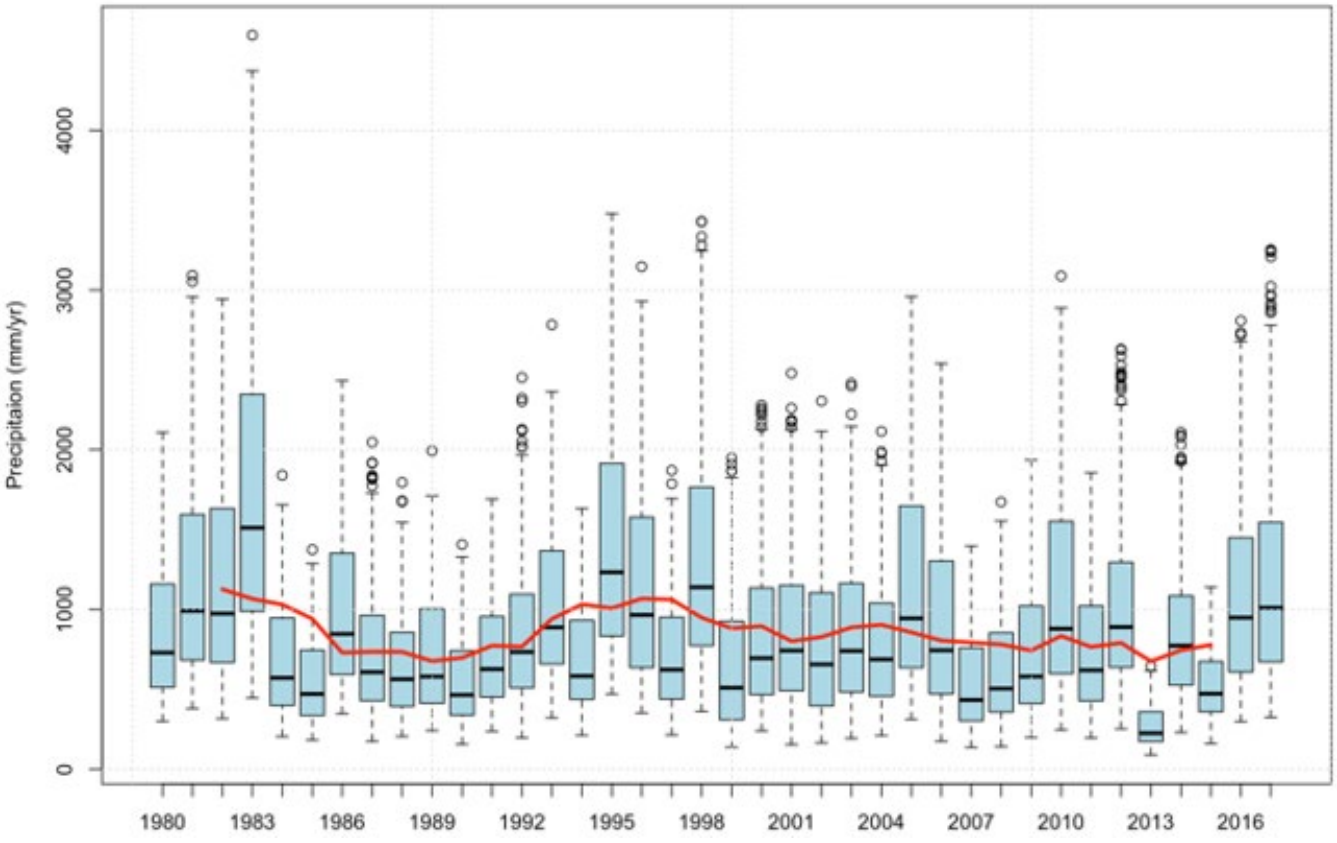

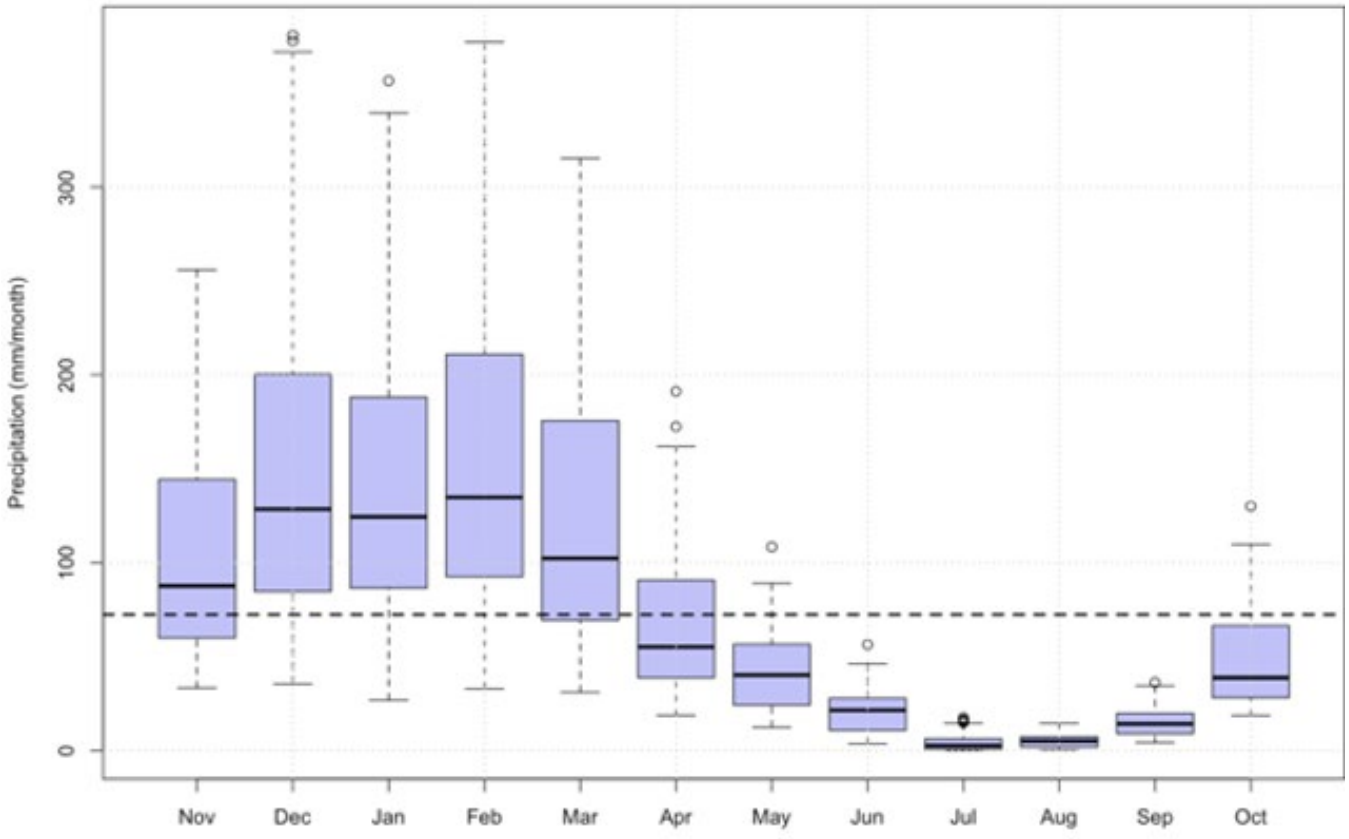

Sources: See text for details, based upon NLDAS data.

3.4.1 Sub-Catchments in Sacramento River Watershed

The heterogeneity of watershed characteristics is so dominant in spatial and temporal patterns that numeric solvers tend to be slow and unstable. This research, therefore, began with pre-experiments on sub-catchments. With the same input datasets, the calibration and analysis of 11 headwater sub-watersheds (Figure 26) were done where managed reservoirs are not present since modeling of these headwaters does not require knowledge of reservoir operations. From these results, calibrated parameters were applied to the entire Sacramento River watershed. Modeled discharge and groundwater depth for selected sub-catchments are shown in Figures 27 and 28 and show how the model produces the seasonal and episodic nature of discharge and the channelized groundwater structures observed in nature. The calibration of the model used the CMA-ES (Hansen, 2006; Auger and Hansen, 2005). The automatic CMA-ES calibration is robust and able to converge to global optimization with low computing cost.

At some sub-catchments in the Sacramento River watershed, the discharge data from the United States Geological Survey (USGS) gage stations were not highly associated with North American Land Data Assimilation System (NLDAS) precipitation data (Figure 29). This issue made it difficult for either the physically based SHUD model or statistical machine learning to capture the correct hydrograph; because of the poor physical relationship, calibration on those sub-catchments is not optimistic. The higher the correlation between appreciation and discharge, the better goodness-of-fitting that models can reach (such as sub-catchments 1, 3, 5,

7, 8, and 9), illustrating the general increase of discharge with increased precipitation, albeit in the midst of a complex non-linear relationship.

Figure 26: Eleven Sub-Catchments of Sacramento River Watershed Used for SHUD Model Calibration

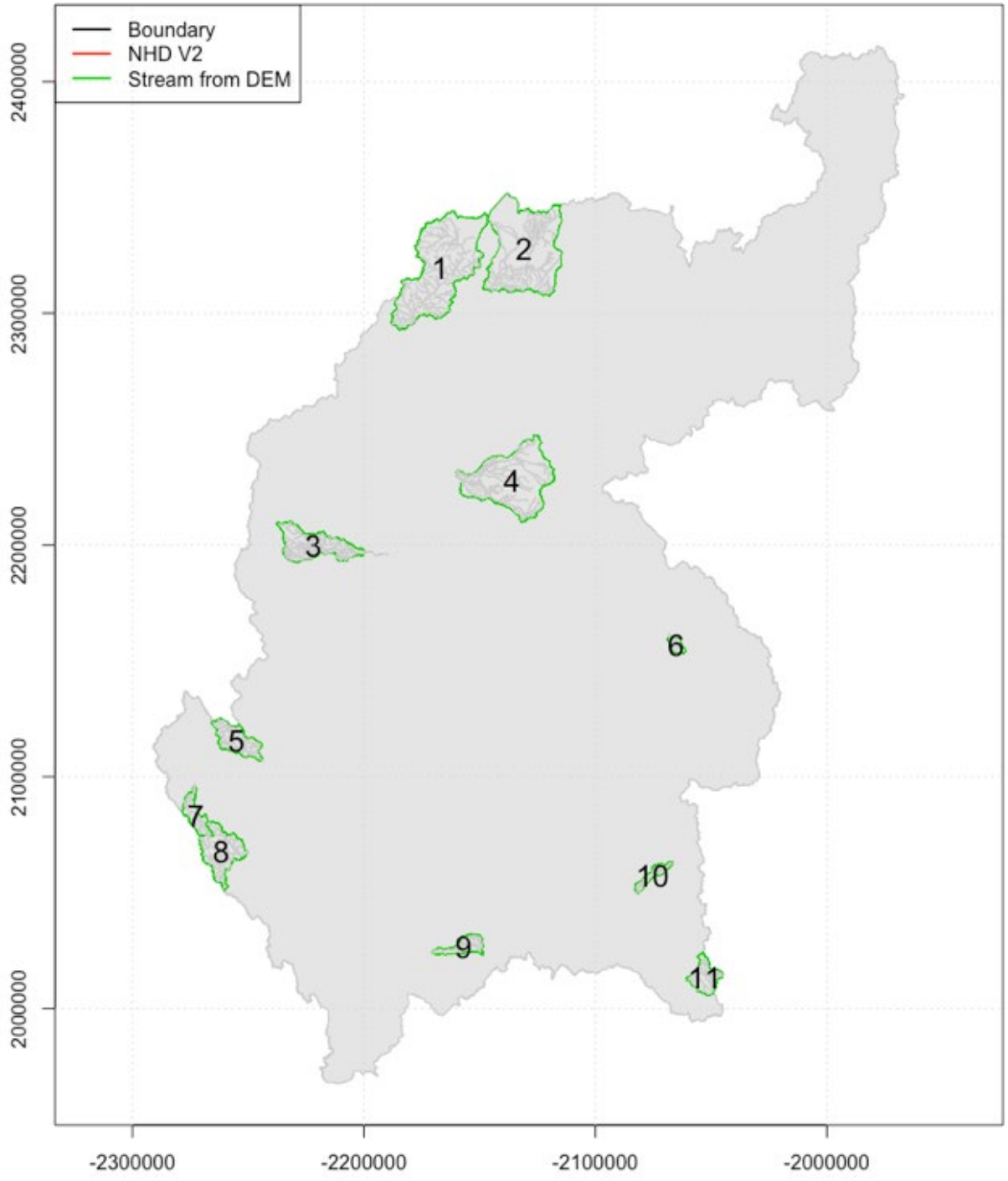

The 11 sub-catchments used for model calibration in the Sacramento River are headwater areas without any reservoirs.

Sources: See text for details.

Figure 27. SHUD Simulated and Observed Discharge at the Outlets of Sacramento River Watershed Sub-Catchments

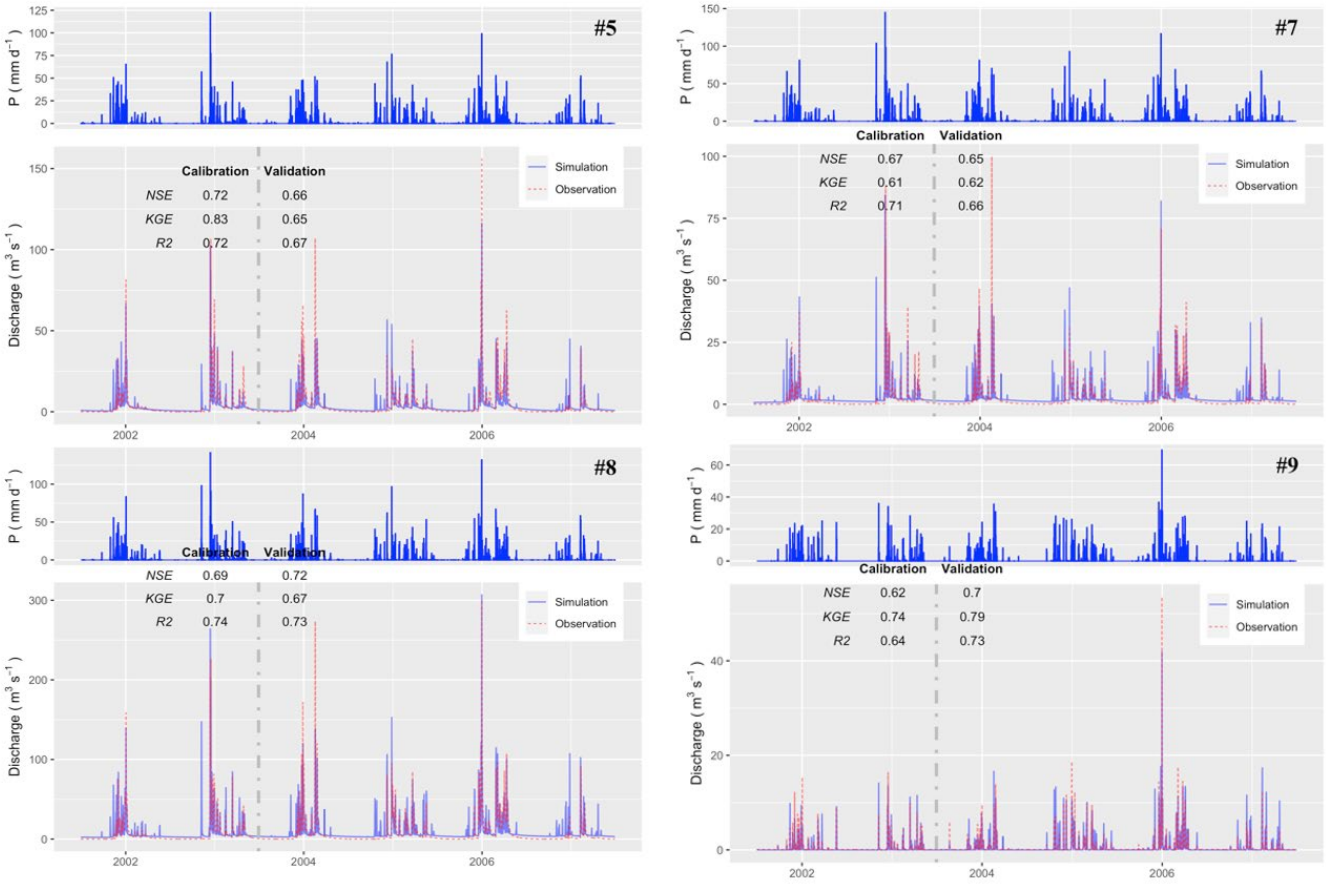

SHUD simulated and observed discharge at the outlets of Sacramento River watershed sub-catchments. #5 (top left), #7 (top right), #8 (bottom left), and #9 (bottom right).

Sources: See text for details.

Figure 28. Annual Mean Groundwater Depth Simulated by SHUD in Sacramento River Sub-Catchments

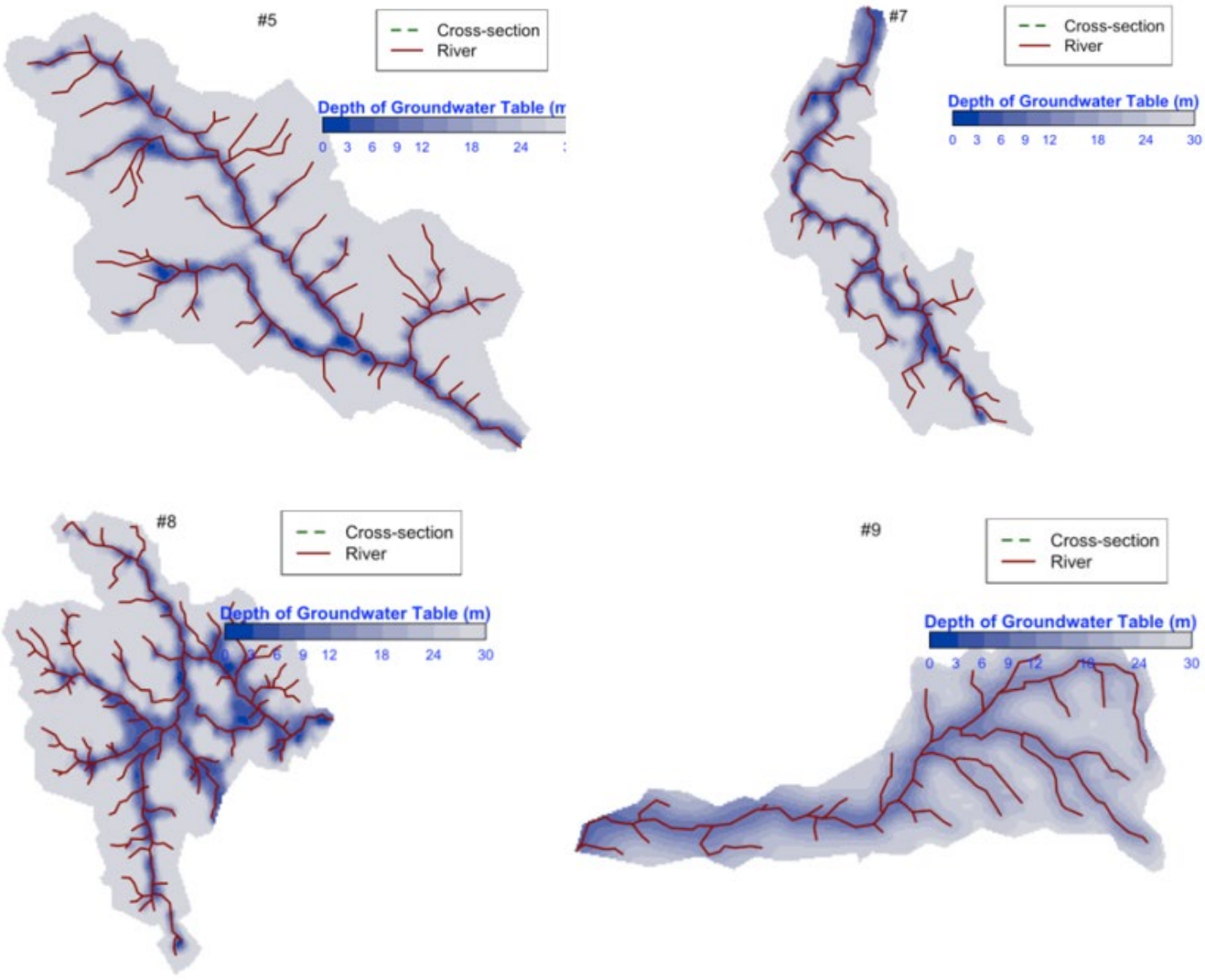

Annual mean groundwater depth simulated by SHUD in Sacramento River sub-catchments. #5 (top left), #7 (top right), #8 (bottom left) and #9 (bottom right).

Sources: See text for details.

Figure 29. Normalized Comparison of NLDAS Precipitation vs. Discharge of USGS Gage Station Data in 11 Sub-Catchments in the Sacramento River Watershed

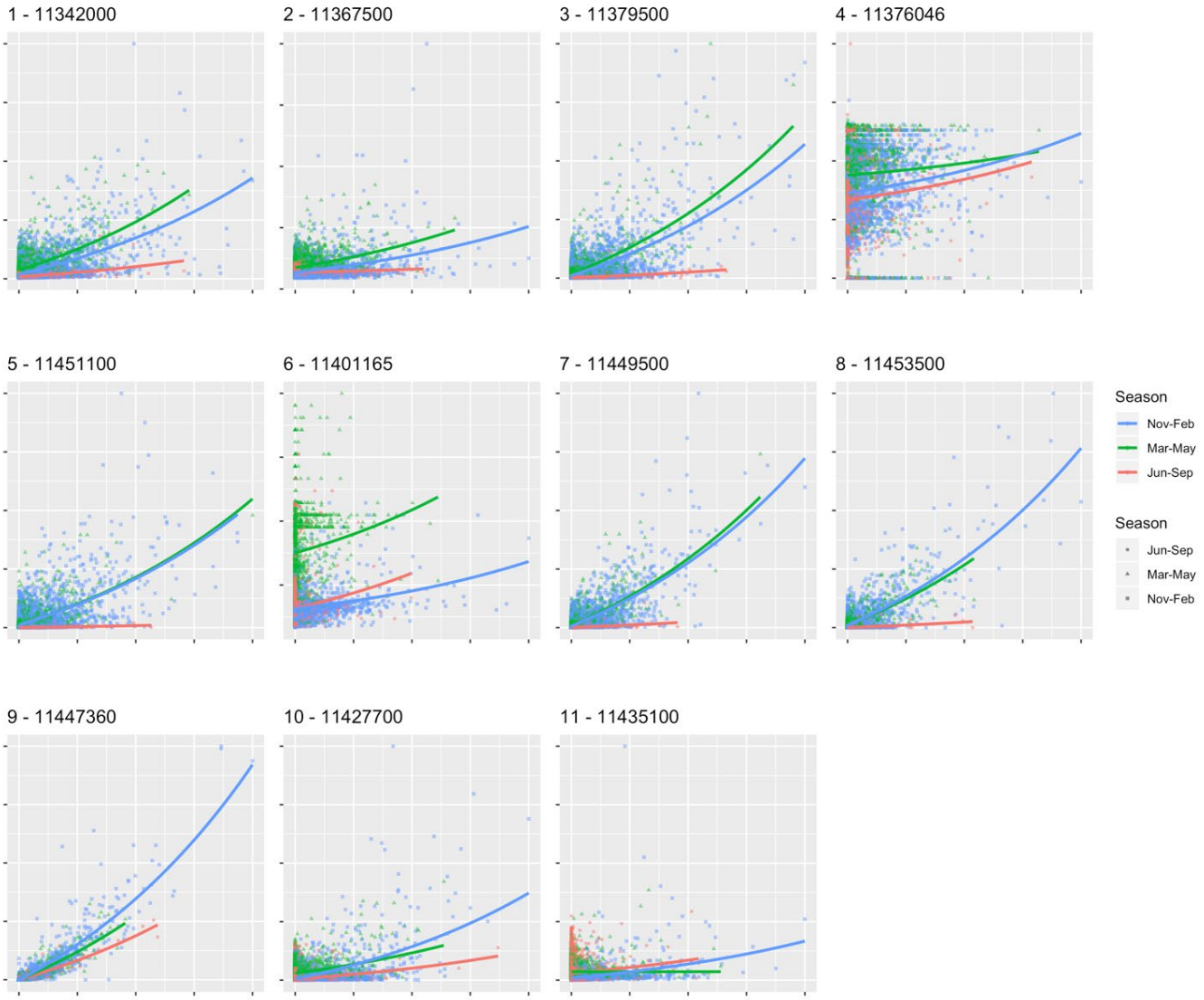

The seasonal categorization per sub catchment (nos. 1 to11) identifies the possible contribution from snow melt.

Sources: See text for details.

3.4.2 Simulation of Whole Sacramento River Watershed

In this research the SHUD model was deployed for long-term hydroclimate simulations (1979 to 2018) in the Sacramento River watershed. The number of cells in the simulation domain is 6,841, with a mean area of ~10 km^2. Total length of river network is ~13,550 km. The model ran with a single thread configuration; it took about 70 hours to finish the 40-year simulation.

The output discharge (Figure 30) and groundwater (Figure 31) appeared to have the correct magnitude and spatial patterns. The strong variation of precipitation determined the variation of streamflow. The streamflow in the watershed followed the seasonal variation of

precipitation. During drought, the base flow from groundwater depletion contributes to streamflow, and the excess infiltration replenishes groundwater in wet seasons.

The groundwater distribution follows the terrain and river network. Steep regions in the mountainous area tend to hold less groundwater, while the valleys have a built-up groundwater table.

Based on long-term groundwater-storage variations (Figure 32), groundwater has been decreasing since the 1980s. During the very dry 2013 to 2014 period, groundwater storage decreased by an average of 0.2 meters although the following years were relatively wet.

As an important natural reservoir for water storage, snowpack also influences water availability in the watershed. The variation of snowpack (Figure 33) follows the fluctuation of annual precipitation. Dry years show less snowpack storage, and the decline in snowpack over the period considered quite clearly contributed to the decline in groundwater storage.

Figure 30. Long-Term Hydrograph (Monthly) at the Outlet of the Sacramento River

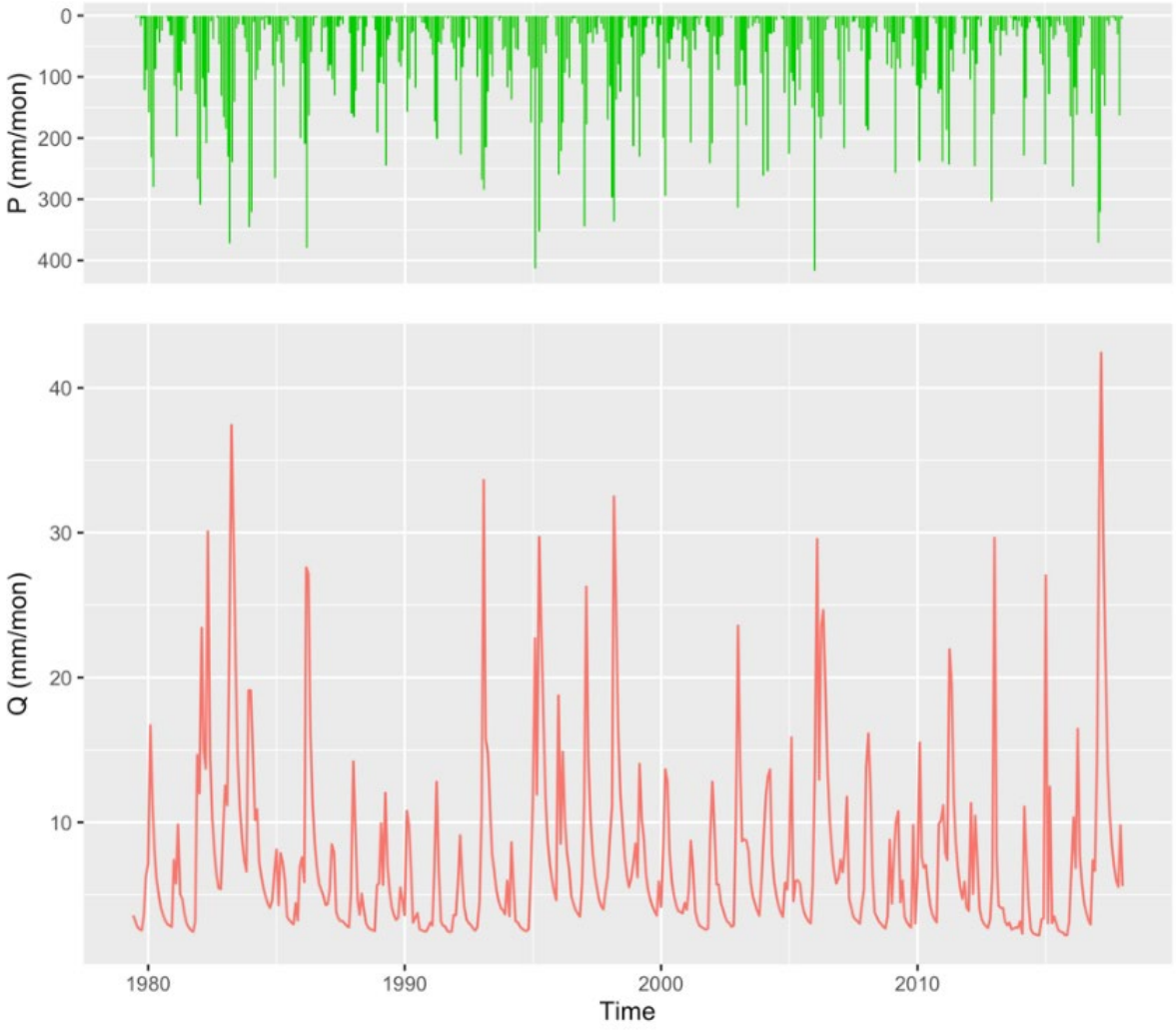

Sources: See text for details.

Figure 31. Average Groundwater Storage Within 30-Meter Aquifer, Integrated from SHUD Simulation

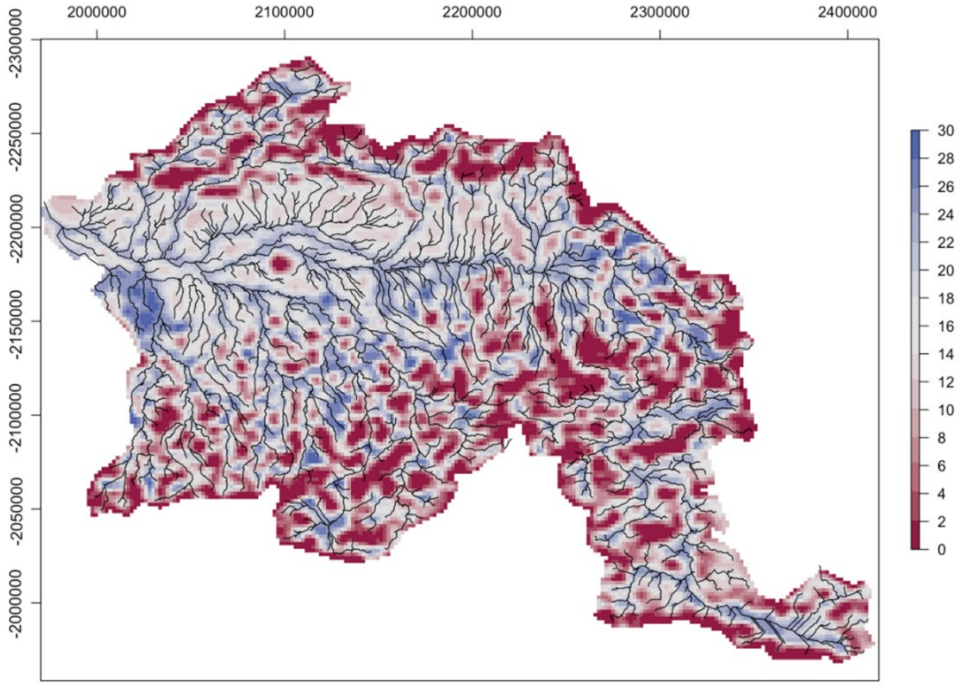

Figure 31 shows the Sacramento River watershed

Sources: See text for details.

Figure 32. Long-Term Trend of Average Groundwater Storage in the Sacramento River Watershed

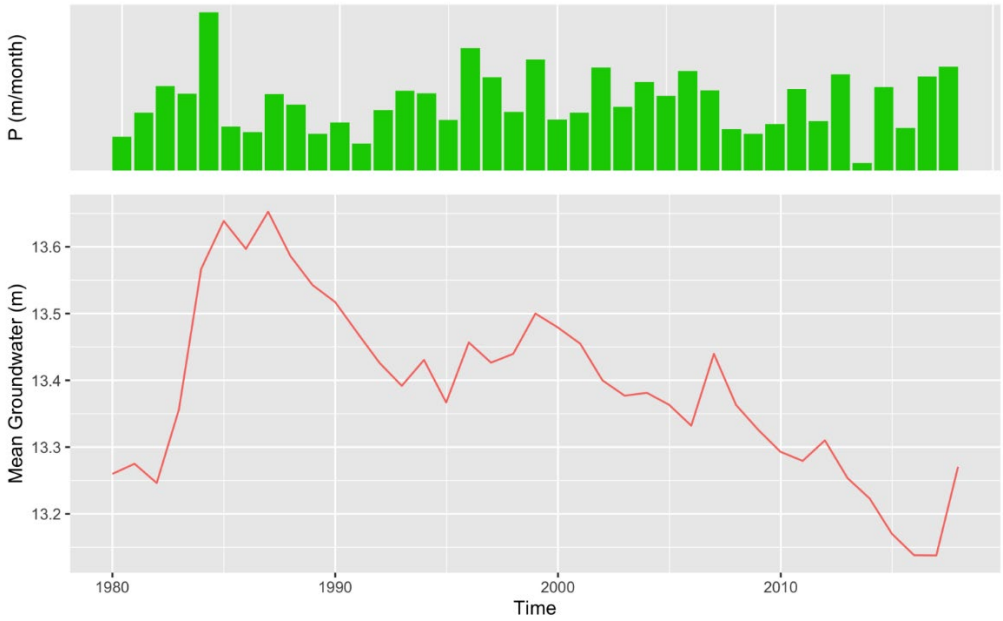

The difference in the mean groundwater level between the wet period in the early 1980s and the 2013 to 2014 dry period was 0.5 meter.

Sources: See text for details.

Figure 33. Snowpack in the Sacramento River Watershed, Simulated by SHUD

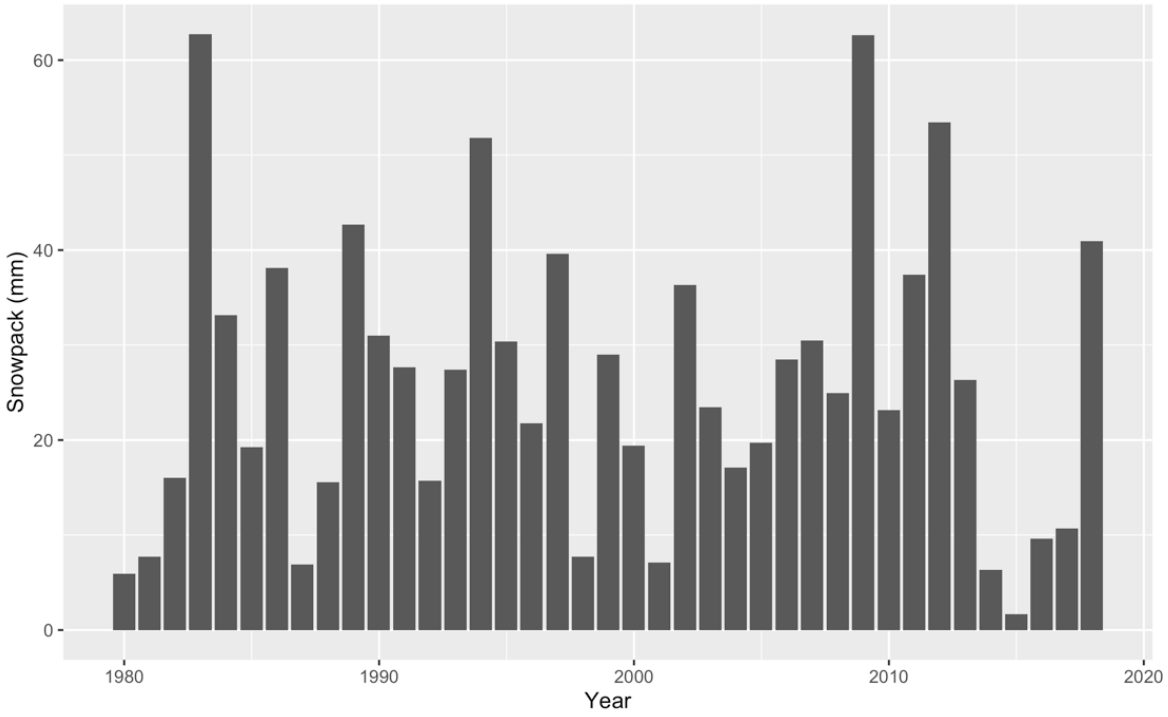

Sources: See text for details.

3.5 Parflow.CLM Results

The project examined how uncertainty in the precipitation datasets propagates through a process-based hydrologic model, resulting in uncertainty in the simulated hydrologic outputs. It was investigated how combined uncertainty in precipitation and air temperature forcings impacts simulated hydrologic fluxes and states in the Kaweah River watershed.

3.5.1 Assessing the Impacts of Precipitation and Temperature Uncertainty on Hydrologic Response in ParFlow.CLM

ParFlow.CLM was configured for the Kaweah River watershed in the Southern Sierra Nevada and Central Valley California (Figure 34). The study domain encompassed an area of 12,276 km^2 with highly variable terrain. The domain included the relatively humid Sierra Nevada mountain range and the semi-arid agricultural regions of California's Central Valley. Selecting a mountain catchment for this project was important for two primary reasons: 1) mountain catchments provide between 20 percent and 90 percent of streamflow worldwide (Viviroli and Weingartner, 2004), and 2) the Sierra Nevada watersheds are the main sources of streamflow and natural recharge to the Central Valley aquifer system. Furthermore, ground-water recharge and streamflow generation processes are poorly understood in high-elevation mountain ranges.

The Kaweah River watershed model has a horizontal grid resolution of 1-km^2 resulting in a computational grid with 124 columns and 99 rows. The total thickness of subsurface in the Kaweah River watershed model is set to 622 m. The subsurface consists of a 2-m-thick soil

layer (Chaney et al., 2016) overlaying weathered saprolite, fractured bedrock, with less fractured bedrock at depth. The thicknesses of these layers varies with depth, resulting in 15 layers with variable hydraulic properties.

Figure 34. (a) Location of The Parflow.CLM Study Domain Within the State of California. (b) Digital Elevation Model Used to Generate Slope Parameters for the Parflow.CLM Model

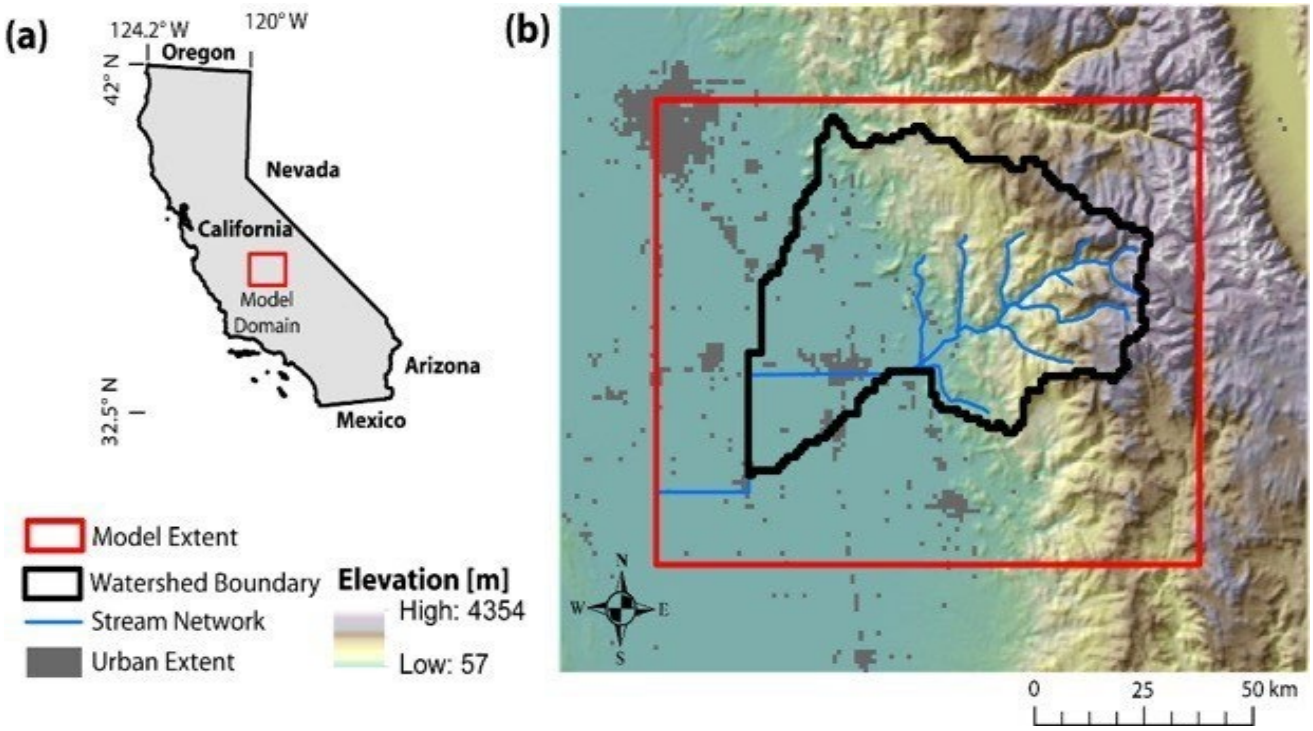

The watershed boundary and stream network derived from the four-directional routing scheme used within ParFlow.CLM are shown, as well as locations of urban development.

Sources: See text for details.

To reduce the impact of model initialization on simulated hydrologic fluxes, a two-step spin-up process was implemented until subsurface storage reached dynamic equilibrium with meteorologic forcings. In the first step, a constant net precipitation flux (P – ET) was applied to the initially dry ParFlow model to fill subsurface storage (Livneh et al., 2013). Next, the coupled ParFlow.CLM model ran recursively over a one-year period of hourly meteorological forcing for water year 2016, until the model reached dynamic equilibrium. Dynamic equilibrium is defined as when the absolute percentage change in subsurface storage becomes less than 0.1 percent in recursive simulations (Ajami et al., 2014). Water year 2016 is representative of average precipitation and air temperature conditions in the Kaweah River watershed.

The project focus was on the Kaweah River watershed while the team was learning how to implement this modeling approach and developing an approach with reasonable simulation times. The correct parameter sets that facilitated rapid simulation of the domain were determined. To simulate hydrologic processes of the Kaweah River watershed, 35 computational cores were used. The slowest simulations took 12 hours of simulation time (~420 CPU hours) per year of simulation.

After validating the model against a range of in situ (streamflow) and remotely sensed observations (evapotranspiration and snow water equivalent), the impact of uncertainty in model forcing datasets was assessed, focusing on precipitation and air temperature uncertainty. Gridded precipitation and air temperature datasets were used as historical records for downscaling climate projections but suffered from high levels of uncertainty. ParFlow.CLM simulations were performed for the Kaweah River watershed using precipitation and air temperature from four common gridded products: NLDAS-2, PRISM, Daymet, and Gridmet. An additional air-temperature dataset from the TopoWx product was used to represent topographically corrected air temperatures in the watershed.

As dense weather stations were not available in mountain catchments, it is not possible to quantify the accuracy of gridded meteorological products. To quantify the impact of uncertainty in meteorological forcings on the simulated water budget, the three-cornered hat method (Premoli & Tavella, 1993) was used to calculate the relative uncertainty of model-forcing data and simulated hydrologic fluxes and states. It was recognized that this was not a total measure of uncertainty, since it does not account for uncertainties created by the model structure and parameters.

First, uncertainty was calculated in basin averaged-time series of precipitation (*P*), streamflow (*Q*), *ET*, *SWE*, soil moisture (Θ), and potential groundwater recharge (*R*) for ParFlow.CLM simulations forced with different precipitation products was calculated, while keeping the rest of meteorological forcings the same (Figure 36). It was found that the datasets with the highest uncertainty in precipitation (*P*) did not result in the highest uncertainty for all output variables. It is particularly interesting to note that although the Gridmet forcing had the highest uncertainty in precipitation (*P*), it had the lowest uncertainty in streamflow (*Q*). Hydrologic models are typically calibrated and validated using only streamflow estimates. Project results suggest that this may not be an adequate approach if scientists are interested in the rest of the water budget, where the Gridmet dataset has greater uncertainty (*ET,* soil moisture, or potential groundwater recharge) than other products.

The spatially distributed uncertainty was calculated in each of the simulated water-balance components. It was demonstrated that although the greatest uncertainty in precipitation inputs is at the highest elevations of the Sierra Nevada, the highest uncertainty in simulated fluxes is found in the mid-elevation regions along the transition zone between the Sierra Nevada range and the Central Valley (Figure 36). This transformation of uncertainty was attributed to the impact of topography (Schreiner-McGraw and Ajami, 2020; 2022).

Figure 35. Uncertainty in Domain Average Time Series of Multiple Hydrologic Variables

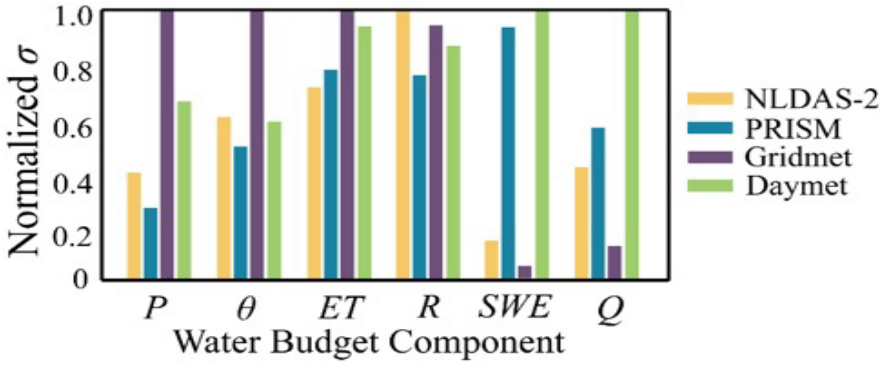

For each variable the uncertainty has been normalized by the dataset with the largest uncertainty to allow different variables to be displayed in the same chart. Precipitation (*P*), root zone soil moisture (*Θ*), evapotranspiration (*ET*), potential recharge (*R),* snow water equivalent (SWE), *and* streamflow (*Q*).

Sources: See text for details.

Figure 36. Root Error Variance (Σ) in Surface Water Budget Components, Averaged Across 100-Meter Elevation Intervals

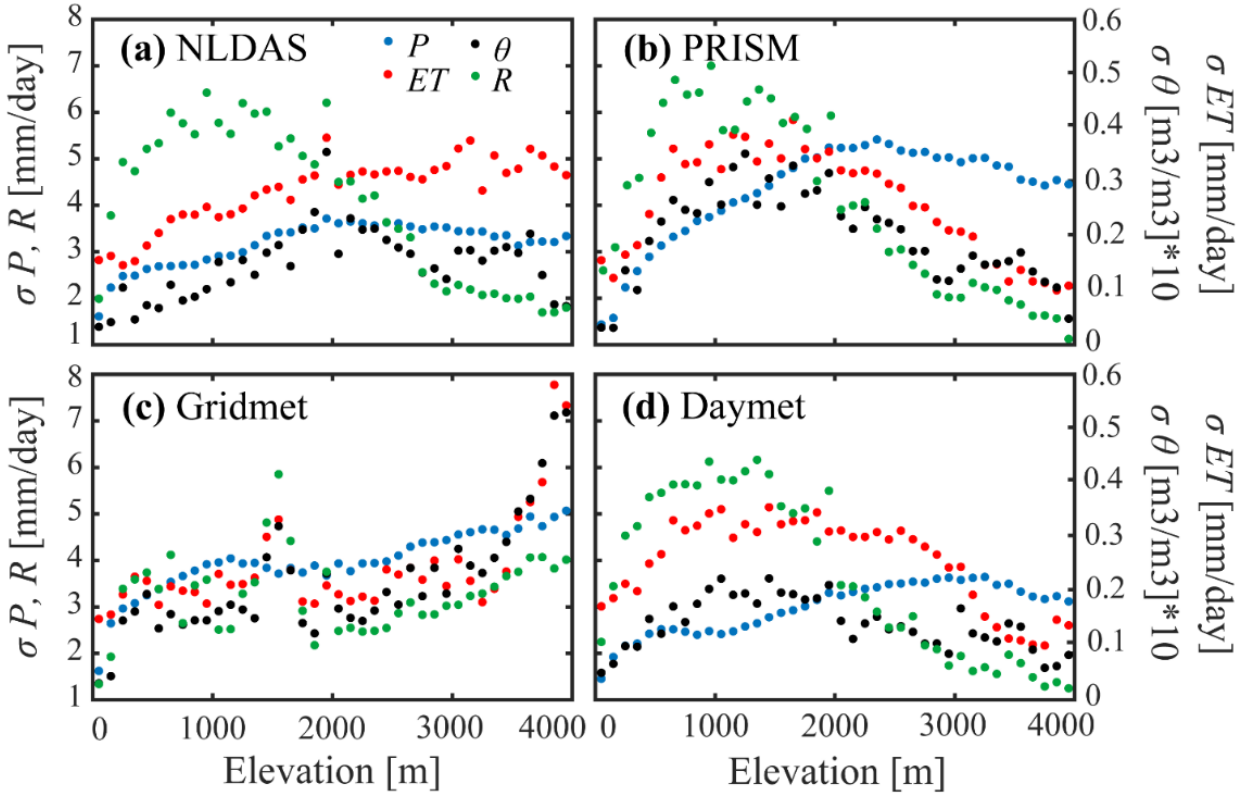

Precipitation (*P*), root zone soil moisture (*Θ*), evapotranspiration (*ET*), and potential recharge (*R*) are from models with variable precipitation using NLDAS-2 (a), PRISM (b), Gridmet (c), and Daymet (d) precipitation forcings.

Sources: See text for details.

Two additional numerical experiments were performed to assess impacts of uncertainty in air temperature as well as combined precipitation and temperature datasets on the water budget. Figure 37 shows the partitioning of the simulated annual water budget for the Kaweah River watershed upstream of the Terminus Dam. Uncertainty in the precipitation forcings created considerable uncertainty in the simulated water budget. For example, the simulated ground-water (GW) flux to the Central Valley aquifer ranges from 29 percent to 43 percent of annual precipitation in the Kaweah Terminus watershed. When the ParFlow.CLM model is forced with the mean of the multiple-precipitation datasets, but with variable air-temperature datasets, the groundwater flux ranges from 34 percent to 43 percent of precipitation. Combined variability in precipitation and air temperature forcings results in a higher range of simulated groundwater flux (27 percent to 50 percent of the water budget) to the Central Valley aquifer.

Figure 37. Water Balance Partitioning for Watershed Average Time Series of Multiple Hydrologic Variables

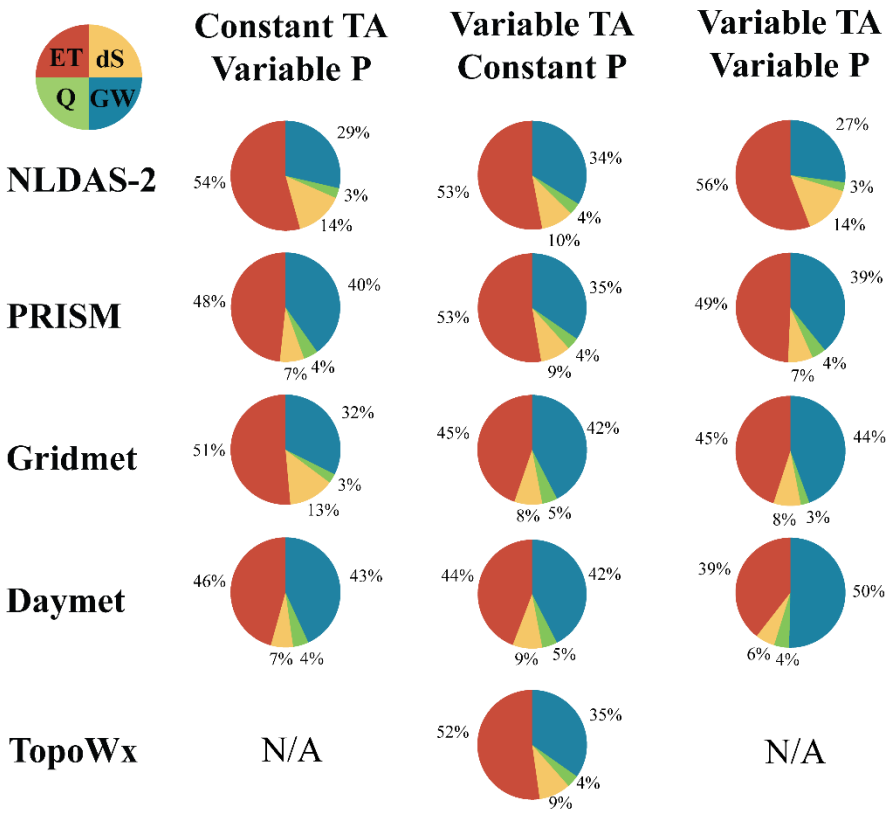

Simulation scenarios include variable precipitation (P) with NLDAS-2 air temperature (TA), variable air temperature from multiple datasets with mean of precipitation forcings (NLDAS-2, Daymet, Gridmet and PRISM), and variable temperature-precipitation simulations.

Sources: See text for details.

The combined impacts of uncertainty in precipitation and air temperature on hydrologic fluxes are not linearly additive, and a complex set of processes controls the watershed response to uncertainty in meteorological datasets. The primary factor that impacts water-budget partitioning is the total amount of snowfall predicted by each combination of forcing datasets

(Figure 38). These results highlight the need to develop gridded climate products that can accurately represent the hydrologic processes of mountain catchments.

Quantifying the uncertainty of simulated hydrologic fluxes caused by climate forcing is important because these gridded climate products are used to train or validate downscaled climate projections for climate-change impact studies.

Figure 38: Relation Between Total Annual Snowmelt and Water Budget Partitioning

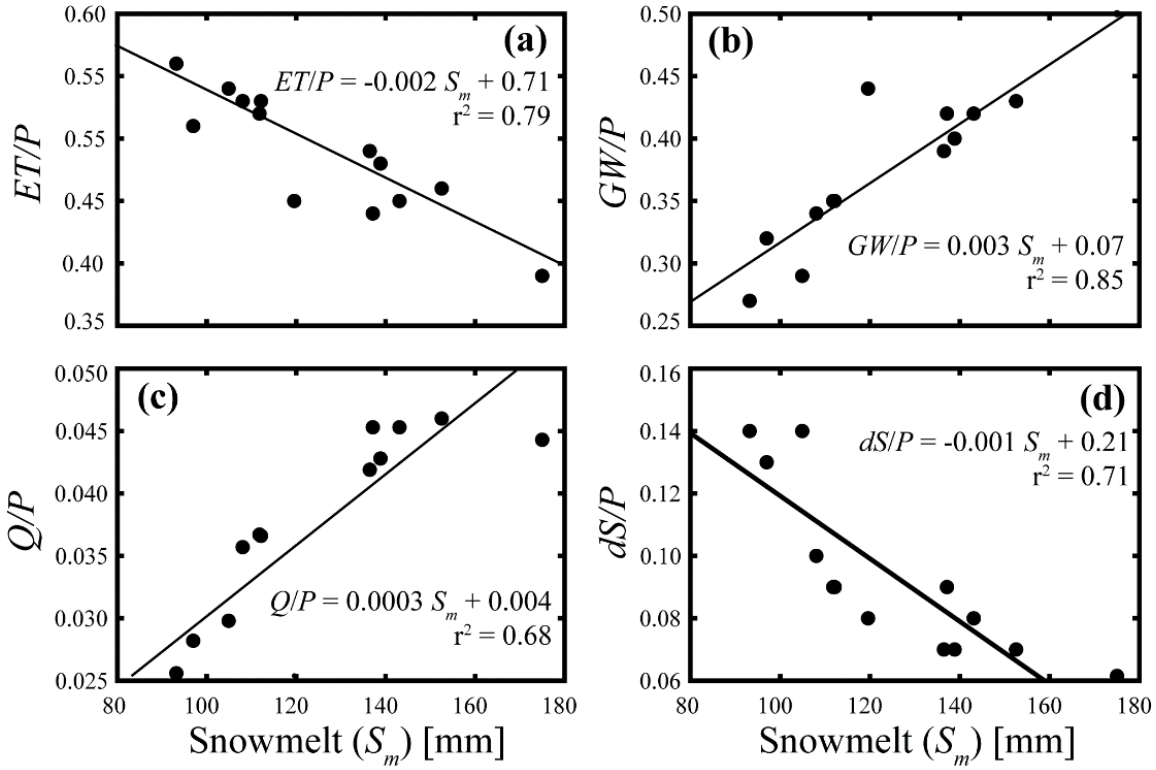

Snowmelt is calculated as the total negative changes in snow water equivalent (SWE) for each of 13 model scenarios.

Sources: See text for details.

3.5.2 Quantifying Groundwater Response Time to Droughts via Parflow.CLM

In addition to the observational study, synthetic numerical experiments were developed over a 9.3 km^2 watershed using ParFlow.CLM. The model was forced by two synthetic 30-year climate realizations to estimate groundwater lag and recovery times using a number of drought classification metrics in aquifers with a range of hydraulic conductivities. The model allowed the research team to precisely quantify changes in groundwater storage to ensure that drought classification metrics are reliable (Schreiner-McGraw et al., *in prep.*).

An important consideration for water management under drought conditions is how long it takes the meteorological droughts to propagate through the hydrologic system and cause groundwater drought. Results of this continental scale analysis indicate that average lag times

between precipitation drought and groundwater drought is about 15 months, and lag time can increase up to 15 years in some wells. On average, groundwater recovery time is about three years, and the groundwater recovery time increases with increasing drought severity. These results have important implications for sustainable groundwater management in California.

Quantifying groundwater response time and recovery to climate change and droughts is one of the main objectives of this CEC project and has important implications for groundwater management under the California Sustainable Groundwater Management Act and energy use for groundwater pumping. This focus is on using groundwater observations as well as idealized simulation domains to quantify these impacts while developing new metrics to quantify groundwater response time to droughts. To explore the groundwater response time to climate change, the research team used droughts as examples of meteorological changes imposed on the hydrologic system.

A key challenge in quantifying groundwater response time to droughts is associating observed changes in groundwater levels with corresponding observed changes in precipitation that caused the groundwater drought. Through this project, precipitation observations from the PRISM dataset and groundwater-level data from the Climate Response Network were used to test the efficacy of different drought classification methods on quantifying the groundwater response time to droughts. The research team found that the previously used lagged-correlation between the standardized precipitation index (SPI) and the standardized groundwater index (SGI) is a reliable method (Bloomfield and Marchant, 2013) to quantify the impacts of aquifer properties on the groundwater response time, while other metrics are required to understand the impact of precipitation properties on groundwater drought (Schreiner-McGraw and Ajami, 2021). The performance of these metrics was examined across 634 observation wells in unconfined aquifers that are not impacted by human activities.

CHAPTER 4:
Technology and Knowledge Activities

4.1 Technology and Knowledge Transfer Activities

The methods and results of various elements of this research have been transferred via numerous activities: Undergraduate, graduate, and postdoctoral scholars have been trained (partially) via funding of this research; scientific manuscripts have been published and are in review; presentations (oral and poster) have been held at conferences such as Fall Meetings of the American Geophysical Union; and teleconferences have been held with CEC staff on the project's data, methodology, and findings. These activities are described in the following sections.

Additionally, some of the project's results have been shared so that other researchers could benefit from its preliminary findings. For example, two interim reports to the CEC are publicly available—the first two listed in Section 4.3. The hourly vector-wind fields are currently used by Alex Syphard, chief scientist at Sage Insurance Holdings and adjunct professor in the Department of Geography at San Diego State University, and Jon Keeley, research scientist with the U.S. Geological Survey Western Ecological Research Center and adjunct professor in the Department of Ecology and Evolutionary Biology at the University of California, Los Angeles, to examine the role of wind in destructive California wildfires.

Access to the regional model dynamically downscaled historical reanalysis dataset can be arranged by request to the project team. This full atmospheric dataset, generated by WRF is quite large (over 30 Tb for 11 years), has been saved for the intermediate term. The WRF downscaling was applied to a coarser (9km x 9 km) WRF downscaled version of the NARR. This 9 km WRF reanalysis was provided by Professor Alex Hall's group at UCLA. The 3 km x 3 km spatial resolution WRF-CA-CLC was run for a rectangular domain that approximately enclosed California (Figure 6) from April 2008 to February 2019.

A post-processed subset of the WRF-CA-CLC dataset is also available. This subset was extracted to provide variables relevant to low-cloud processes, fire weather, and basic climate dynamics such as sea-level pressure and 500 hPa geopotential height. The post-processed files:

- Amount to about 1 TB.
- Contain 80, 2-D variables including temperature, precipitation, hub-height wind, albedo, wind-gust estimates, and inversion layer fields. The full list appears in Table 2.
- Are available every hour from April 1, 2008, to Feb 28, 2019, on the 3-km WRF-CA-CLC grid. Grid coordinates and other supporting metadata are also provided in the post-processed files.

4.2 Training Opportunities

This project provided partial support for advising undergraduate intern Alexis Harris (Portland State University's Center for Climate and Aerosol Research Experience for Undergraduates program) from June to August 2019. It also provided funding for one postdoctoral scholar at the University of California, Riverside. Partial support was provided to train one undergraduate and one master student in data analysis and integrated hydrologic modeling. This project also supported Shiheng Duan, graduate student researcher at the University of California, Davis, and provided funding for one postdoctoral scholar at the University of California, Riverside.

An undergraduate student was trained under the direction of Dr. Martin in climate-model evaluation methods using the WRF-CA-CLC dataset to evaluate the seasonal progression of lower tropospheric stability along the California coast against published works and existing model reanalyses. Ms. Harris participated through the National Science Foundation-funded Center for Climate and Aerosol Research at Portland State University, a research site for undergraduates.

Postdoctoral scholar Sweta Das was trained under the direction of Dr. Martin to verify WRF model cloudiness and albedo using satellite (GOES) data. Dr. Das is applying this training toward research contributions to CEC Project PIR-19-007.

4.3 Manuscripts Published

Cayan, Daniel, David Pierce, Laurel DeHaan, Janin Guzman-Morales, Alexander Gershunov, Rachel Clemesha, Andrew Martin, Paul Ullrich, Lele Shu, Hoori Ajami, Adam Schreiner-McGraw. 2020. "Downscaling Using Dynamical and Statistical Methods." White paper for the CEC, part of EPC-16-063, available at: https://efiling.energy.ca.gov/GetDocument.aspx?tn=232882

Note: These research results were made available so that all applicants for the CEC's Grant Funding Opportunity GFO-19-311: *Climate Scenarios and Analytics to Support Electricity Sector Vulnerability Assessment and Resilient Planning* could benefit from preliminary findings of this CEC-funded research.

Duan, S., P.A. Ullrich, and L. Shu. 2020. "Using Convolutional Neural Networks for Streamflow Projection in California." *Frontiers in Water*. Available at: https://www.frontiersin.org/article/10.3389/frwa.2020.00028

Gershunov, A., Guzman Morales, J., Hatchett, B. et al. 2021. "Hot and cold flavors of Southern California's Santa Ana winds: their causes, trends, and links with wildfire." *Clim Dyn* 57**,** 2233–2248. Available at: https://link.springer.com/article/10.1007/s00382-021-05802-z

Pierce, D.W., L. Su, D.R. Cayan, M.D. Risser, B. Livneh, and D.P. Lettenmaier. 2021. "An Extreme-Preserving Long-Term Gridded Daily Precipitation Data Set for the Conterminous United States." *J. Hydrometeorology*, 22(7) 1883-1895.

Pierce, D. W., and D. R. Cayan. 2019. "Future projections of hourly surface temperature in California." A report in partial fulfillment of a grant by the CEC: 48 pages available at: https://cirrus.ucsd.edu/~pierce/tmp/Hourly_data_interpolation_2019-05-23.pdf

Pierce, D.W., L. Su, D.R. Cayan, M.D. Risser, B. Livneh, and D.P. Lettenmaier. 2021. "An extreme-preserving long-term gridded daily precipitation data set for the conterminous United States." *J. Hydrometeorology*, 22(7) 1883-1895.

Schreiner-McGraw, A.P., H. Ajami. 2022. "Combined impacts of uncertainty in precipitation and air temperature on simulated mountain system recharge from an integrated hydrologic model." *Hydrology & Earth System Sciences Discussions*. Available at: https://hess.copernicus.org/articles/26/1145/2022/hess-26-1145-2022.pdf.

Schreiner-McGraw, A.P., H. Ajami. 2021. "Delayed Response of Groundwater to Multi-year Meteorological Droughts in the Absence of Anthropogenic Management." *Journal of Hydrology 603(B)*. Available at: https://doi.org/10.1016/j.jhydrol.2021.126917

Schreiner-McGraw, A.P., H. Ajami. 2020. "Impact of Uncertainty in Precipitation Forcing Datasets on the Hydrologic Budget of an Integrated Hydrologic Model in Mountainous Terrain." *Water Resources Research*, Available at: https://doi.org/10.1029/2020WR027639

Shu, L., P.A. Ullrich, and C.J. Duffy. 2020. "Simulator for Hydrologic Unstructured Domains (SHUD v1. 0): numerical modeling of watershed hydrology with the finite-volume method." *Geoscientific Model Development 13* (6), 2743-2762. Available at: https://doi.org/10.5194/gmd-13-2743-2020.

Walton, D., Neil Berg, David Pierce, Ed Maurer, Alex Hall, Yen-Heng Lin, Stefan Rahimi, Dan Cayan. 2020. "Understanding Differences in California Climate Projections Produced by Dynamical and Statistical Downscaling." *Journal of Geophysical Research*: *Atmospheres*, 125(19) doi: 10.1029/2020JD032812.

4.4 Conference Presentations and Posters

- Ajami, H., A. Schreiner-McGraw. 2020. "Characterizing Groundwater Response Time to Droughts Across the United States." *European Geosciences Union, 2020 online meeting*.
- Ajami, H., A. Schreiner-McGraw. 2019. "Characterizing Mountain System Recharge Processes from Headwaters to Groundwaters." Invited Presentation. *American Geophysical Union, 2019 Fall Meeting*, San Francisco, California.
- Ajami, H., A. Schreiner-McGraw. 2019. "Characterizing Mountain System Recharge Processes and Variability - A recent synthesis." Invited Presentation. *Geological Society of America 2019 Annual Meeting*, Phoenix, Arizona.
- Ajami, H., A. Schreiner-McGraw. 2019. "Quantifying Groundwater Response Time to Droughts Across the United States." Oral presentation, *American Geophysical Union, 2019 Fall Meeting,* San Francisco, California.
- Duan, S, PA Ullrich, L Shu, D Hall. 2019. "Predicting daily streamflow with a dilated convolutional neural network." *American Geophysical Union, 2019 Fall Meeting Abstracts*, *H33L-2133*.
- Harris, A., E., Martin, A., and L. DeHaan. 2019. "Evaluating the Seasonal Cycle of Low Clouds in a New Hybrid High Resolution Downscaling for Current and Future Climates."

6th Annual Climate Change and Aerosol Research REU Symposium, August 30. Portland, Oregon.

- Palmer, J., A. Schreiner-McGraw, H. Ajami. 2019. "Characterizing Aquifer and Meteorologic Controls on Groundwater Response Time to Droughts." Poster Presentation, *American Geophysical Union, 2019 Fall Meeting,* San Francisco, California.
- Pierce, D.W., and D.R. Cayan. 2019. "Downscaling IPCC scenarios to the hourly level: Projected changes in energy demand and chill hours in California." Poster Presentation for Session A51Q-2839, *American Geophysical Union, 2019 Fall Meeting*, San Francisco, California. (The methods and results for hourly wind downscaling at station locations were presented.)
- Schreiner-McGraw, A.P., H. Ajami. 2020. "Propagation of Meteorological Variability from Atmosphere to Groundwater." Online Poster Presentation, *American Geophysical Union, 2020 Fall Meeting*.
- Schreiner-McGraw, A., H. Ajami. 2019. "Delayed Response of Groundwater to Droughts and Implications for a Warmer Climate." Oral Presentation*, Geological Society of America 2019 Annual Meeting,* Phoenix, AZ.
- Schreiner-McGraw, A., H. Ajami. 2019. "Propagation of Surface Changes Through the Critical Zone to the Groundwater. Oral Presentation, *W3188 Multistate Annual Meeting,* Riverside, California.
- Schreiner-McGraw, A. and H. Ajami. 2018. "Drought Impacts on Hydrologic Connectivity of a Coupled Mountain Agricultural System." E-Lightening Presentation, *American Geophysical Union, 2018 Fall Meeting,* Washington, DC.
- Shu, L., P.A. Ullrich, and C.J. Duffy. 2020. "rSHUD v1.0. An R package to support unstructured domain modeling in hydrology." *AGU Fall Meeting Abstracts 2020, H197-0018*.
- Shu, L., P.A. Ullrich, P. A., and C.J. Duffy. 2019. "Quick and reproducible automated watershed modeling with the SHUD: Essential data, simulation, applications and visualization." *American Geophysical Union,* 2019 *Fall Meeting,* San Francisco, California.
- Shu, L., and P.A. Ullrich. 2018. "Model simulated spatial distribution and the variation of groundwater level in Sacramento Watershed, California from 1985 to 2017." *American Geophysical Union, 2018 Fall Meeting*, Washington, DC.

CHAPTER 5: Conclusions/Recommendations

California's investor-owned electricity utilities need greater specificity in climate and weather events that drive both trends and extreme impacts on energy supply, demand, and reliability. Additionally, IOUs and decision makers in a variety of sectors need improved information on deliveries of water and other vital resources to the state. Key findings that underpin California's Fourth Climate Change Assessment follow.

It is widely recognized that regional dynamical model downscaling of high volumes of GCM simulations can be impractical because of high computational resource costs. The quality of dynamical and statistical downscaling is dependent upon the availability of global or regional modeling output to provide large-scale guidance on projected or historical patterns and high-resolution historical data for either validation or training statistical models. Input data may be sets of direct observations, analyzed observations, or model generated data such as global and regional reanalyses. Even statistical downscaling of the broad emerging suite of CMIP6 simulations will require substantial computer resources and data storage. Procuring necessary computer resources for comprehensive hybrid dynamical/statistical downscaling is a critical requirement for such an effort.

Observed training or validation data is represented with varying quality and uneven spatial and temporal coverage for different variables. Observational datasets invariably contain some degree of sampling and instrumental errors. As described in Section 3.1.3, the precipitation training dataset used for LOCA downscaling in the Fourth Assessment used a technique of adjusting for different stations' time of observation, which decreased the maximum 1-day precipitation, increased the wet-day fraction, and decreased the mean precipitation on wet days. The reduction in daily extreme precipitation is an important limitation because, for example, it would cause hydrological model estimates of flooding to be under-predicted. A new version of the gridded precipitation training dataset constructed to avoid this time adjustment resulted in a 27 percent greater annual maximum for one-day precipitation (area averaged over the conterminous U.S.). When applied to the Variable Infiltration Capacity land surface/hydrological model, annual maximum one-day runoff increased 38 percent, annual mean runoff increased 17 percent, evapotranspiration dropped 2.3 percent, latent heat flux dropped 2.2 percent, and the surface shortwave insolation increased 3.3 percent.

Some observational datasets are relatively short or confined to a limited domain (such as the winds and humidity datasets obtained from SDG&E), and thus may be inadequate for region-wide statistical downscaling training datasets. However, such data should not be dismissed because it may provide extremely valuable evaluation or calibration of downscaled methods and results.

There are a number of variables for which statistical downscaling procedures have not been developed (here and elsewhere), because these variables are not routinely observed and, in some cases, do not have wide ranges of use cases. A noteworthy example is a set of variables

of interest to the wildfire prevention and management community that may be available from regional dynamical models but not from statistical downscaling techniques. This underscores the value of dynamic models, via atmospheric reanalyses, climate GCMs, and dynamic downscaling in producing a full suite of dynamically consistent atmospheric variables. Since some atmospheric variables have not been and are currently not consistently observed, the output provided by dynamic models may provide a dataset that can be employed in statistical downscaling. This research provided an 11-year dynamically downscaled reanalysis from which statistical downscaling experiments and various diagnoses can be conducted. Dynamical modeling of some phenomena (for example, marine boundary layers and coastal clouds) is problematic with standard regional-model codes (Section 3.2). The effects of influences such as aerosols on California's coastal marine clouds are furthermore not well understood and new modeling and diagnostics studies are ongoing and needed. Sensitivity tests allowed selection of a WRF configuration that best represents the observed magnitude of cloud cover, while accurately preserving other key climate properties of California climate such as sea-level pressure and temperature. This configuration nonetheless suffers from significant biases in the inland extent, seasonal and interannual cycles of cloud cover that require further refinement. In part, these deficiencies are related to fundamental physics such as turbulent moisture fluxes in the boundary layer. But cloud-cover deficiencies may also be partially remedied by addressing lateral boundary conditions or the impact of aerosols on cloud albedo. These potential updates might improve future versions of WRF-CA-CLC. However, as with clouds simulated by any dynamical model, important biases are likely to remain. As suggested in Section 3.2.2, bias correction can effectively increase skill in modeling weather variables, and should reduce biases in downwelling shortwave radiation, a variable strongly related to CLC presence. WRF-CA-CLC may thus benefit from similar statistical bias corrections when applied to projections of California's future climate.

From Section 3.2.5, WRF hourly temperatures are closely matched to observations over the limited time period available for comparison, although with a systematic underestimation of hourly timescale variability. When compared to the station observations, the WRF simulations are not much better or worse in simulating hot extremes, cold extremes, periods of large variability, or periods of small variability. The spatial coherence of hourly temperature variability in the WRF simulation is similar to observations in the Central Valley, the Bay Area, and parts of near-coastal Southern California. It is greater than observed in Northern California and the extreme interior southeast part of the state. It is less than observed along the coast between San Luis Obispo and Oxnard. These geographical patterns of similarities and differences are not sensitive to the exact timescale of hourly variability.

The evaluation carried out here showed a general overestimation in the magnitude of the WRF simulated winds that vary by month (bias increases towards later months in the year) and location (larger bias concentrated on the most eastern locations). Wind speed overestimations are also observed during the inspected Santa Ana wind event. In addition, WRF simulations exhibits diurnal differences and longer event duration relative to observations. Nonetheless, the complete assessment of systematic bias should be carried over a longer simulation period as well as over a larger number of Santa Ana wind events.

In both dynamical and statistical models, the ideal bias correction procedure would jointly adjust multiple variables using a full multivariate approach. In other words, a model may not produce uniform biases in T and P in simulating warm and cool precipitation events. The existing LOCA bias correction scheme (Pierce et al., 2015) addresses this using conditional bias correction. For example, the bias correction of temperature is conditional upon the presence or absence of precipitation so that the differing impacts of snow and rain are better captured in the final result. Also, as described in section 3.1.3, it was found that the addition of sea level pressure to regional wind patterns added skill when LOCA downscaling wind over the California region. Because of the complex dynamics governing many atmospheric variables such as precipitation and wind, bias correction using a multivariate bias approach would ideally be conducted. However, this requires computational resources, amounting to an increase by about a factor of 30 over single variable bias correction; and thus, is not feasible for high volume downscaling under present computational constraints. There is no clear path forward to reduce the large time demands of the multivariate bias correction. Since it is an iterative process, it is accepted that there may be no way around this, and it will have to be evaluated whether the 30-fold increase in time needed to do this form of multivariate bias correction is worthwhile and acceptable given our need to process all of California for multiple models, ensemble members, and scenarios. This might largely be determined by how many models, ensemble members, and emissions scenarios are desired in forthcoming CMIP6 downscaling effort.

Hydrologic models contain another set of techniques, advantages, and drawbacks. Tradeoffs between model sophistication and model simplicity and efficiency arise because of limitations in computational resources. Surface water and groundwater resources, which are often treated as separate systems in climate impact assessments, ideally should be treated as linked components of the same hydrologic system. In Section 3.4 a fully coupled surface-subsurface hydrologic model was developed (SHUD) that was specifically designed for the challenging hydrologic environment in California. Since only two model layers are used to represent the subsurface, the computational expense of the model is substantially less than a fully coupled 3D hydrologic modeling system. Further, this system uses advanced numerical methods that enable relatively large time step sizes even in regions of steep slopes and a shallow subsurface. Nonetheless, as with any hydrologic modeling system, substantial calibration is needed to ensure good results as a result of surface and subsurface heterogeneity. As a process-based model, this model has the potential to provide deep insight into California's hydroclimate system. Work is now underway to employ it for modeling of the entire Sacramento River watershed, and future work will extend it for use over the entire state of California.

The primary application targeted in the hydrological modeling component of this study is future projection of streamflow in California. With historical precipitation and streamflow for calibration, and future precipitation from CMIP5/6 models, our coupled hydrologic modeling system can be used to project future streamflow response. These simulated stream flows can then be used for training an advanced statistical model for downscaling of streamflow (for instance, using machine learning and deep neural networks). Nonetheless, many challenges remain on this front, the most significant of which being the fact that precipitation, temperatures, and radiation in the future are not in the same regime as the historical period.

Consequently, this research builds up tools and techniques for validating that the models are performing reasonably even when the input data is outside of the input data used in the training period.

In a related part of this study, sensitivity of water-budget partitioning was quantified to variable precipitation and temperature forcings as simulated by an integrated surface water-groundwater model. Results indicate that topography exerts a large impact on propagating uncertainty in simulated hydrologic fluxes. Analysis of model performance metrics indicates that merging multi-source precipitation products improves simulated hydrologic fluxes compared to averaging simulated hydrologic fluxes from multiple models. Uncertainty in air temperature forcings amplifies the impact of uncertain precipitation forcings on the simulated water budget. This amplification is caused by air temperature controls on the rain/snow precipitation partitioning.

Although the ParFlow.CLM modeling approach, both in general and more specifically as applied to the Kaweah watershed in this project (Section 3.5), is computationally expensive relative to simpler hydrologic models commonly applied for climate change impact assessment, there are important advantages. Using a process-based integrated modeling approach to simulate the climate change impacts on water resources has the advantage that the model performance is not tied to historical conditions. By representing the processes via which water moves through a landscape, changes in meteorological conditions will be propagated through the system via physically based equations that describe shallow surface water and subsurface flow, rather than empirical methods derived from the statistical analysis of historic data. The second advantage of the approach used in this research is that it uses a 3D representation of groundwater, coupled with a land-surface model. This allows the impacts of hydrologic connectivity between the Sierra Nevada mountains, where most of the precipitation falls, and the Central Valley aquifer, where most of the water use is being studied. Furthermore, it is possible to assess the impacts of pumping, irrigation, and snowmelt processes in a fully integrated manner.

Modeling groundwater variation and change statewide using integrated groundwater-land surface models is possible via the project approach. The benefits of such an approach are in capturing hydrologic processes from the atmosphere to the bottom of the aquifer, removing the need for implementing multiple hydrologic models to capture different aspects of the system. Assuming that climate projections require 2,500 years of simulation time (25 GCMs with 100 years of data), this would require ~1 million CPU hours. This equates to about one month of run time on 1,500 computational nodes. Therefore, this approach is feasible for the entirety of California with sufficient computational resources. A tradeoff could be to use fewer than 25 scenarios of 100-year duration. If 100 years of simulation for a historical period were run in addition to three projected climate (representing low, median, and high) precipitation projections, fewer computational resources would be needed.

Landcover types and irrigation practices vary considerably over California's complex landscape, and in some areas are changing rapidly. However, while such land-use impacts produce substantial impacts in surface and subsurface hydrology (Levy, et al., 2020), landcover parameters and irrigation practices are not commonly represented in most hydrologic models

suited for climate impact assessment and would require further development. ParFlow.CLM has the irrigation scheme of CLM but further refinements are needed to represent crop parameters, irrigation types, and scheduling relevant to California agriculture. Other human manipulations such as dams, diversions, and managed flows furthermore affect the hydrology of many catchments in California yet are not represented broadly across California's landscape, so separate models are used to represent them. These water management options should be incorporated in integrated hydrologic models like ParFlow.CLM to represent hydrologic processes of intensively managed watersheds in a fully integrated manner.

CHAPTER 6:
Benefits to Ratepayers

This project produced advances in dynamically informed statistical techniques to downscale relatively coarse-scale climate model simulations, which are of use to California's electrical utilities and a broad set of other stakeholders. The hydrological modeling techniques are vital to translate the meteorological data into impacts over the land surface, including quantitative characterizations of floods, runoff, drought, and groundwater stocks that feed into the supply and demand of electricity, and thus, the well-being and maintenance of the state's electrical infrastructure. The datasets describing California's surface weather and hydrology require higher spatial (3 km x 3 km) and temporal (hourly) resolution as needed by California's electrical utilities and a broad set of other stakeholders. Projected climate data, available from a large set of global climate models, needs to be downscaled to fine spatial and temporal resolution to prepare for climate changes including high-impact extreme weather events and compound weather-and-hydrological events that potentially lead to extreme impacts on the electrical system. Such data will also be important in disentangling long-term trends resulting from global anthropogenic climate change from those resulting from natural variability, regional, or local effects.

The techniques developed as part of this project will help advance the downscaling of projected climate data, available from a large set of global climate models, to find spatial and temporal resolutions that enable the state to prepare for extreme climate changes that could impact the electrical system. Learnings from the development of the hybrid techniques in this project are also being applied to another CEC-funded project, EPC-20-006: *Development of Climate Projections for California and Identification of Priority Projections*. That project will integrate the latest bias correction and downscaling approaches (dynamical and hybrid statistical-dynamical) to application of the recently produced GCMs from CMIP6, together with an engagement process involving IOUs and other key California stakeholders. As part of EPC-20-006, some key observed datasets that were developed or explored in this project, such as precipitation, cloud albedo, and wind records, will provide important resources for validation, bias correction, and statistical model training. This linked set of activities will develop a robust, usable, set of climate projections for California.

Conclusions from development of the hybrid techniques are already being applied to two other CEC projects, which will advance development of a robust and usable set of climate projections for California. The first, PIR-19-007: *Development and Evaluation of a 2-km hourly historical climate dataset for California,* will build on this project's findings on dynamical modeling of coastal clouds and winds and will incorporate validation techniques and observed datasets employed here. Using a modern global atmospheric reanalysis dataset, PIR-19-007 will produce a 2km x 2km hourly simulation of historical weather and climate over California and the surrounding region that can be used to describe past weather and climate events. The second project, EPC-20-006: *Development of Climate Projections for California and Identification of Priority Projections,* will integrate the latest bias correction and downscaling

approaches (dynamical and hybrid statistical-dynamical) applied to the recently produced GCMs from CMIP6 with an engagement process to develop a robust, usable, set of climate projections applicable for California.

GLOSSARY AND LIST OF ACRONYMS

Term	Definition
AET	Actual evapotranspiration
AGL	Above ground level
BL	Boundary Layer
CCN	Cloud condensation nuclei
CEC	California Energy Commission
CLC	Coastal Low Clouds
CLM 3.0	Common Land Model
CMA-ES	Covariance Matrix Adaptation - Evolution Strategy
CMIP 5/6	Coupled Model Intercomparison Project, Phase 5/Phase 6
CONUS	Continental United States
CPU	The central processing unit of a computer
CVODE	A solver for stiff and non-stiff ordinary differential equation systems
CWP	Cloud water path
Daymet	Daily gridded meteorological data at 1 km spatial resolution covering North America. Variables are: precipitation, Tmax, Tmin, downward surface shortwave radiation, water vapor pressure
DJF	December, January, and February
DRI	Desert Research Institute
ECMWF	European Center for Medium Range Weather Forecasting
ERA5	European Center for Medium Range Weather Forecasting Reanalysis, version 5
ET	Evapotranspiration
Fourth Assessment	California's Fourth Climate Change Assessment
GCM	Global Climate Model
GOES	Geostationary Operational Environmental Satellite
Gridmet	Daily 4-km surface meteorological data covering the contiguous US from 1979. The dataset includes the following variables: precipitation, Tmax, Tmin, downward shortwave radiation, and vapor pressure.
GW	Groundwater
hPa	Hectopascal pressure unit 1 hPa is equal to one millibar
IOU	Investor-owned Utilities

Term	Definition
JJA	June, July, and August
KBFL	Symbol for the Meadows Field Airport in Bakersfield, California
LOCA	Localized Constructed Analogs
LWP	Liquid water path
MERRA2	Modern-Era Retrospective analysis for Research and Applications, Version 2
MJJAS	May, June, July, August, and September
mm	Millimeter
MSc	Marine Stratocumulus clouds
NARR	North American Regional Reanalysis
NASA	National Aeronautics and Space Administration
Nc	The number of cloud droplets per unit volume of the atmosphere
NCAR	National Center for Atmospheric Research
NLDAS	North American Land Data Assimilation System
NLDAS-2 meteorology	North American Land Data Assimilation System provides hourly metrological forcing and fluxes over central North America.
NOAA/NCEP	National Oceanic and Atmospheric Administration National Centers for Environmental Prediction
ParFlow	ParFlow is a parallel, integrated hydrology model that simulates spatially distributed surface and subsurface flow, as well as land surface processes including evapotranspiration and snow.
ParFlow.CLM	An integrated groundwater-land surface model that simulates surface water and groundwater flow processes at large scale. It is ParFlow coupled to CLM, the Community Land Model.
ParFlow.WRF	An integrated groundwater-land surface model coupled to the Weather and Research Forecasting model.
PIHM	Pennsylvania State Integrated Hydrologic Model
PRISM	Parameter-elevation Regressions on Independent Slopes Model (PRISM) daily gridded dataset at 4 km resolution for precipitation, temperature, and dew point temperature.
RAWS	Remote Automatic Weather Stations
Reanalysis	In this project, a dynamical weather model rendition of historical weather that is produced over the global atmosphere using an array of historical weather observations.
RCP	Representative Concentration Pathway
RMSE	Root Mean Square Error

Term	Definition
rSHUD	SHUD R Toolbox
SDG&E	San Diego Gas & Electric
SGI	Standardized groundwater index is an index for characterizing groundwater droughts using groundwater level observations.
SHUD	Simulator for Hydrologic Unstructured Domains
SLP	Sea level pressure
SPI	Standardized precipitation index is a precipitation-based index for characterizing meteorological droughts.
SW	Sacramento River watershed
SWE	Snow water equivalent
TB	terabyte
TEMF	Total Energy – Mass Flux
TKE	turbulent kinetic energy
Tmin/ Tmax	Minimum and maximum daily temperature
TOA	top of atmosphere
TopoWx	'TopoWx ('Topography Weather') dataset at 800-m resolution includes daily minimum and maximum topo climatic air temperature for the CONUS from 1948-present.
U,V	Zonal and meridional components of the wind near the surface
UCLA	University of California, Los Angeles
UCSD	University of California, San Diego
USGS	United States Geological Survey
UTC	Universal Coordinated Time
v0, v2, v4	Refer to versions of WRF-CA-CLC labeled and examined during this research (see Table 2 in report)
VIC	Variable Infiltration Capacity land surface/hydrological model.
WRF	Weather Research and Forecasting model, from the National Center for Atmospheric Research (NCAR) in Boulder, CO.
WRF-CA–CLC	WRF - California - Coastal Low Clouds: The standard WRF configuration that was used in the project to dynamically downscale coastal low cloud amount in the historical climate period.
WRF-Chem	WRF coupled with predictive models for atmospheric chemistry and aerosols (https://ruc.noaa.gov/wrf/wrf-chem/). Herein, only the code module "mixactivate" is used to predict given a prescribed aerosol cloud condensation nuclei concentration.

REFERENCES

Abatzoglou, J. T., 2013. "Development of gridded surface meteorological data for ecological applications and modelling." *International Journal of Climatology*, 33(1), 121–131. https://doi.org/10.1002/joc.3413.

Ajami, H., M.F. McCabe, J.P., Evans, S. Stisen. 2014. "Assessing the impact of model spin-up on surface water-groundwater interactions using an integrated hydrologic model." *Water Resources Research*, 50, 2636–2656. https://doi.org/10.1002/2013WR014258.

Albrecht, Bruce A. 1989. "Aerosols, Cloud Microphysics, and Fractional Cloudiness." *Science* 245 (4923), pp.1227-1230.

Ashby, S. F., R.D. Falgout. 2017. "A Parallel Multigrid Preconditioned Conjugate Gradient Algorithm for Groundwater Flow Simulation." *Nuclear Science and Engineering*, 124:1, 145-159, DOI: 10.13182/NSE96-A24230.

Auger, A., N. Hansen., 2005. "A restart CMA evolution strategy with increasing population size." 2005 IEEE Congress on Evolutionary Computation (Vol. 2, pp. 1769-1776).

Bloomfield, J.P. and B.P. Marchant. 2013. "Analysis of groundwater drought building on the standardised precipitation index approach." *Hydrology and Earth System Sciences*, 17 (12), 4769–4787, https://hess.copernicus.org/articles/17/4769/2013/

Brown, T. J., Mills, G., Harris, S., Podnar, D., Reinbold, H. J., Fearon, M. G. 2016: "A bias corrected WRF mesoscale fire weather dataset for Victoria, Australia 1972-2012." *Journal of Southern Hemisphere Earth Systems Science*, 66(3), 281-313.

Cannon, A. J. 2018. "Multivariate quantile mapping bias correction: an N-dimensional probability density function transform for climate model simulations of multiple variables." *Clim Dyn*, 50, 31-49. Doi 10.1007/s00382-017-3580-6.

Cao Y. and R.G. Fovell. 2016. "Downslope Windstorms of San Diego County Part I: A Case Study." Mon Weather Rev 144(2):529–552. https://doi.org/10.1175/MWR-D-15-0147.1

Chaney, N.W., E.F. Wood, A.B. McBratney, J.W. Hempel, T.W. Nauman, C.W. Brungard, N.P. Odgers. 2016. POLARIS: "A 30-meter probabilistic soil series map of the contiguous United States." *Geoderma*, 274, 54–67. https://doi.org/10.1016/j.geoderma.2016.03.025.

Clemesha, R.E., Gershunov, A., Iacobellis, S.F., Williams, A.P. and Cayan, D.R. 2016. "The northward march of summer low cloudiness along the California coast." *Geophysical Research Letters*, 43(3), pp.1287-1295.

Clemesha, R.E.S., A. Gershunov, S.F. Iacobellis and D.R. Cayan. 2017. "Daily variability of California coastal low cloudiness: A balancing act between stability and subsidence." *Geophysical Research Letters*, 44(7), 3330–3338, doi:10.1002/2017GL073075.

Dai, Y., X. Zeng, R.E. Dickinson, I. Baker, G.B. Bonan, M.G. Bosilovich, et al. 2003. "The Common Land Model." *Bulletin of the American Meteorological Society*, 84(8), 1013–1024. https://doi.org/10.1175/BAMS-84-8-1013.

Daly, C., M. Halbleib, J.I. Smith, W.P. Gibson, M.K. Doggett, G.H. Taylor, et al. 2008. "Physiographically sensitive mapping of climatological temperature and precipitation across the conterminous United States." *International Journal of Climatology*, 28(15), 2031–2064. https://doi.org/10.1002/joc.1688.

Duffy, C.J. 1996. "A Two-State Internal-Balance Model for Soil Moisture and Groundwater Dynamics in Complex Terrain." *Water Resources Research*, 32(8), 2421-2434.

Farthing, M.W., F.L. Ogden. 2017. Numerical Solution of Richards' Equation: A Review of Advances and Challenges." *Soil Science Society of America Journal*, 81(6), pp.1257-1269, https://doi.org/10.2136/sssaj2017.02.0058

Guo, Q., J. Chen, X. Zhang, M. Shen, H. Chen, S. Guao. 2019. A new two-stage multivariate quantile mapping method for bias correcting climate model outputs. *Clim Dyn*, 53: 3603-3623. https://link.springer.com/article/10.1007/s00382-019-04729-w.

Han, Q., W.B. Rossow, J. Chou, and R.M. Welch. 1998. "Global Survey of the Relationships of Cloud Albedo and Liquid Water Path with Droplet Size Using ISCCP." *Journal of Climate.* 11(7), pp.1516-1528.

Hansen, N. 2006. "The CMA Evolution Strategy: A Comparing Review." In: Lozano, J.A., Larrañaga, P., Inza, I., Bengoetxea, E. (eds) Towards a New Evolutionary Computation. Studies in Fuzziness and Soft Computing. vol 192. Springer, Berlin, Heidelberg. https://doi.org/10.1007/3-540-32494-1_4

Hersbach, H.,B. Bell,P. Berrisford,S. Hirahara,A. Horányi, J. Muñoz Sabater, et al. 2020. "The ERA5 global reanalysis." *Quarterly Journal of the Royal Meteorological Society.* 146(730), 1999–2049. https://doi.org/10.1002/qj.3803.

Hinkelman, L. 2019. "The Global Radiative Energy Budget in MERRA and MERRA-2: Evaluation with Respect to CERES EBAF Data. *Journal of Climate*. 32(6), 1973-1994, doi:10.1175/JCLI-D-18-0445.1.

Iacobellis, S. F., and D. R. Cayan. 2013. "The variability of California summertime marine stratus: Impacts on surface air temperatures." *Journal Geophysical Research Atmospheres*. 118(16), 9105–9122, doi:10.1002/jgrd.50652.

IPCC (Intergovernmental Panel on Climate Change). 2014. "Summary for policymakers." *Climate Change 2013*: The Physical Science Basis. Contribution of Working Group I to the Fifth Assessment Report of the Intergovernmental Panel on Climate Change. T.F. Stocker, D. Qin, G.-K. Plattner, M. Tignor, S.K. Allen, J. Doschung, A. Nauels, Y. Xia, V. Bex, and P.M. Midgley, Eds. Cambridge University Press, pp. 1-30, doi:10.1017/ CBO9781107415324.004.

Jones, J.E., C.S. Woodward. 2001. "Newton–Krylov-multigrid solvers for large-scale, highly heterogeneous, variably saturated flow problems." *Advances in Water Resources*, 24(7), 763–774. doi:10.1016/S0309-1708(00)00075-0.

Levy, M. C., W.R. Neely, A. A. Borsa, J.A. Burney. 2020. "Fine-scale spatiotemporal variation in subsidence across California's San Joaquin Valley explained by groundwater demand."

Environmental Research Letters, 15(10), 104083. https://doi.org/10.1088/1748-9326/abb55c.

Livneh, B., E.A. Rosenberg, C. Lin, B. Nijssen, V. Mishra, K.M. Andreadis, et al. 2013. "A Long-Term Hydrologically Based Dataset of Land Surface Fluxes and States for the Conterminous United States: Update and Extensions." *Journal of Climate*, 26(23), 9384–9392. https://doi.org/10.1175/JCLI-D-12-00508.1.

Livneh, B., Bohn, T., Pierce, D. W. et al. 2015. "A spatially comprehensive, hydrometeorological data set for Mexico, the U.S., and Southern Canada 1950-2013. *Sci Data* 2, 150042. https://doi.org/10.1038/sdata.2015.42.

Kollet, S. J., R.M. Maxwell. 2008. "Capturing the influence of groundwater dynamics on land surface processes using an integrated, distributed watershed model." *Water Resources Research*, 44(2), doi:10.1029/2007WR006004.

Kumar, M. and C.J. Duffy. 2009. "Detecting hydroclimatic change using spatio-temporal analysis of time series in Colorado River Basin." *Journal of Hydrology*, 374(1-2), pp.1-15, https://doi.org/10.1016/j.jhydrol.2009.03.039.

Margulis, S. A., G. Cortés, M. Girotto, M. Durand, 2016. "A Landsat-Era Sierra Nevada Snow Reanalysis (1985-2015)." *Journal of Hydrometeorology*, 17(4), 1203–1221. https://doi.org/10.1175/JHM-D-15-0177.1.

Martin, A., Clemesha, R., DeHaan, L., and D. Cayan, (*in-prep*) "Hybrid Downscaling of California Coastal Cloudiness at Decadal and Longer Timescales." *Journal of Climate*.

Martin, A.C., Cornwell, G.C., Atwood, S.A., Moore, K.A., Rothfuss, N.E., Taylor, H., DeMott, P.J., Kreidenweis, S.M., Petters, M.D. and Prather, K.A. 2017. "Transport of pollution to a remote coastal site during gap flow from California's interior: impacts on aerosol composition, clouds, and radiative balance." *Atmos. Chem. Phys*, 17(2), pp.1491-1509. https://doi.org/10.5194/acp-17-1491-2017

Mathiesen, P., J. M. Brown, and J. Kleissl. 2012. "Geostrophic Wind Dependent Probabilistic Irradiance Forecasts for Coastal California." In *IEEE Transactions on Sustainable Energy*, 4(2), 510-518 doi:10.1109/TSTE.2012.2200704.

Matsui, T., S. Q. Zhang, S.E. Lang, et al. 2020. "Impact of radiation frequency, precipitation radiative forcing, and radiation column aggregation on convection-permitting West African monsoon simulations." *Clim Dyn*, 55,193-213. doi:10.1007/s00382-018-4187-2.

Maxwell, R.M., L.E. Condon, and S.J. Kollet. 2015. "A high resolution simulation of groundwater and surface water over most of the continental US with the integrated hydrologic model ParFlow v3." *Geoscientific Model Development*, 8(3), 923-937. doi:10.5194/gmd-8-923-2015.

Maxwell, R. M., M. Putti, S. Meyerhoff, J.F. Delfs, I. M. Ferguson, V. Ivanov, J. Kim, et al. 2014. "Surface-subsurface model intercomparison: A first set of benchmark results to diagnose integrated hydrology and feedbacks." *Water Resources Research*, 50(2), 1531–1549, doi:10.1002/2013WR013725.

Mesinger, F., DiMego, G., Kalnay, E., Mitchell, K., Shafran, P.C., Ebisuzaki, W., Jović, D., Woollen, J., Rogers, E., Berbery, E.H. and Ek, M.B. et al. 2006. "North American Regional Reanalysis." *Bulletin of the American Met. Society*. 87(3), 343-360. doi:10.1175/BAMS-87-3-343.

Molod, A., Takacs, L., Suarez, M., and Bacmeister, J. 2015. "Development of the GEOS-5 atmospheric general circulation model: evolution from MERRA to MERRA2." *Geosci. Model Dev.*, 8(5), 1339–1356, https://doi.org/10.5194/gmd-8-1339-2015,

Morrison, H., G. Thompson, V. Tatarskii. 2009. "Impact of Cloud Microphysics on the Development of Trailing Stratiform Precipitation in a Simulated Squall Line: Comparison of One– and Two–Moment Schemes." *Mon. Wea. Rev.*, 137(3), 991–1007. doi:10.1175/2008MWR2556.1.

NOAA (National Oceanic and Atmospheric Administration, National Centers for Environmental Information). Website: https://www.ncei.noaa.gov/products/weather-climate-models/reanalysis, last accessed September 2023.

Oyler, J.W., A. Ballantyne, K. Jencso, M. Sweet, S.W. Running. 2014. "Creating a topo climatic daily air temperature dataset for the conterminous United States using homogenized station data and remotely sensed land skin temperature." *Int. J. Climatol.* http://dx.doi.org/10.1002/joc.4127.

Pan, M., X. Cai, N.W. Chaney, D. Entekhabi, E.F. Wood. 2016. "An initial assessment of SMAP soil moisture retrievals using high-resolution model simulations and in situ observations." *Geophysical Research Letters*, 43(18), 9662–9668. https://doi.org/10.1002/2016GL069964

Paniconi, C., M. Putti, 2015. Physically based modeling in catchment hydrology at 50: Surveyand outlook, Water Resources Research, 51, 7090–7129, doi:10.1002/2015WR017780.

Pierce, D. W., D. R. Cayan, and B. L. Thrasher. 2014. "Statistical Downscaling Using Localized Constructed Analogs (LOCA)." *Journal of Hydrometeorology*, 15(6), 2558-2585, doi:10.1175/JHM-D-14-0082.1 Note: For more information on LOCA, see https://loca.ucsd.edu/

Pierce, D. W. and D. R. Cayan. 2016. "Downscaling humidity with Localized Constructed Analogs (LOCA) over the conterminous United States." *Clim Dyn*, 47, 411-431. doi 10.1007/s00382-015-2845-1.

Pierce, D. W., D. R. Cayan, E. P. Maurer, J. T. Abatzoglou, and K. C. Hegewisch. 2015. "Improved bias correction techniques for hydrological simulations of climate change." *J. Hydrometeorology*, 16, 2421-2442. doi: http://dx.doi.org/10.1175/JHM-D-14-0236.1.

Pierce, D. W., J. F. Kalansky, and D. R. Cayan. 2018. "Climate, Drought, and Sea Level Rise Scenarios for California's Fourth Climate Change Assessment." California's Fourth Climate Change Assessment, California Energy Commission and California Natural Resources Agency. CCCA4-CEC-2018-006. Available at: https://cirrus.ucsd.edu/~pierce/tmp/Pierce_et_al_2018_CA_climate_scenarios.pdf

Pierce, D. W., and D. R. Cayan. 2019. "Future projections of hourly surface temperature in California." A report in partial fulfillment of a grant by the California Energy Commission, 48 pp. Available at: http://cirrus.ucsd.edu/~pierce/tmp/Hourly_data_interpolation_2019-05-23.pdf.

Pierce, D. W., Su, L., Cayan, D. R., Risser, M. D., Livneh, B., Lettenmaier, D. P. 2021. "An Extreme-Preserving Long-Term Gridded Daily Precipitation Dataset for the Conterminous United States." Journal Of Hydrometeorology, 22(7), 1883-1895. doi: 10.1175/JHM-D-20-0212.1.

Premoli, A., P. Tavella. 1993. "A revisited three-cornered hat method for estimating frequency standard instability." *IEEE Transactions on Instrumentation and Measurement*, 42(1), 7–13. https://doi.org/10.1109/19.206671

Qu, Y. 2004. "An integrated hydrologic model for multi-process simulation using semi-discrete finite volume approach." PhD thesis, Pennsylvania State University.

Sapsis, D., Brown, T. J., Low, C. 2016. "Mapping Environmental Influences on Utility Fire Threat." 55 pp., Final report to the California Public Utilities Commission Pursuant to R.08 - 11-005 and R.15-05-006.

Schreiner-McGraw, A.P., and H. Ajami, *in revision*. "Impact of uncertainty in precipitation forcing datasets on the hydrologic budget of an integrated hydrologic model in mountainous terrain." *Water Resources Research*.

Schreiner-McGraw, A.P. and H. Ajami, *in review.* 'Delayed response of groundwater to droughts." *Geophysical Research Letters*.

Schreiner-McGraw, A.P., H. Ajami, A. AghaKouchak, *in preparation.* "Propagating combined precipitation and temperature uncertainties in integrated hydrologic models." *Water Resources Research.*

Schreiner-McGraw, A.P., H. Ajami, and J. Palmer, *in preparation.* "Quantification of aquifer and meteorologic controls on groundwater response to drought." *Water Resources Research.*

Schwartz, R. E., A. Gershunov, S.F. Iacobellis, and D.R. Cayan. 2014. "North American west coast summer low cloudiness: Broadscale variability associated with sea surface temperature." *Geophysical Research Letter*s. 41(9), 3307–3314, doi:10.1002/2014GL059825.

Shen, C. and M.S. Phanikumar. 2010. "A process-based, distributed hydrologic model based on a large-scale method for surface–subsurface coupling." *Advances in Water Resources*, 33(12), 1524-1541, https://doi.org/10.1016/j.advwatres.2010.09.002.

Shu, L., P.A. Ullrich, and C. Duffy. 2020. "Simulator for Hydrologic Unstructured Domains (SHUD v1.0): numerical modeling of watershed hydrology with the finite volume method." *Geosci. Model Dev.*, 13(6), 2743–2762, 2020. https://gmd.copernicus.org/articles/13/2743/2020/.

Skamarock, W. C., Kl;emp, J.B. et al. 2008. "A description of the Advanced Research WRF version 3." *University Corporation for Atmospheric Research (NCAR)*. doi:10.5065/D68S4MVH

Thornton, P. E., S.W. Running, M.A. White. 1997. "Generating surfaces of daily meteorological variables over large regions of complex terrain." *Journal of Hydrology*, 190(3–4), 214–251. https://doi.org/10.1016/S0022-1694(96)03128-9.

Twomey, S. 1977. "The Influence of Pollution on the Shortwave Albedo of Clouds." *Journal of the Atmospheric Sciences,* 34(7), 1149-1152. doi: 10.1175/1520-0469

Vanderstraeten, D. and R. Keunings. 1995. "Optimized partitioning of unstructured finite element meshes." *International Journal for Numerical Methods in Engineering*, 38(3), 433-450. https://doi.org/10.1002/nme.1620380306.

Vauclin, M., D. Khanji, G. Vachaud. 1979. "Experimental and numerical study of a transient, two-dimensional unsaturated-saturated water table recharge problem." *Water Resources Research*, 15(5), 1089-1101, https://doi.org/10.1029/WR015i005p01089.

Viviroli, D., R. Weingartner. 2004. "The hydrological significance of mountains: from regional to global scale." *Hydrology and Earth System Sciences*, 8(6), 1017–1030. https://doi.org/10.5194/hess-8-1017-2004.

Williams, J.L. III, and R.M. Maxwell. 2011. "Propagating Subsurface Uncertainty to the Atmosphere Using Fully Coupled Stochastic Simulations." *Journal of Hydrometeorology*, 12(4), 690-701, doi:10.1175/2011JHM1363.1.

Wood, R. 2012. "Stratocumulus Clouds." *Monthly Weather Review*, 140(8), 2373-2423. Doi: 10.1175/MWR-D-11-00121.1

CALIFORNIA ENERGY COMMISSION

CALIFORNIA NATURAL RESOURCES AGENCY

ENERGY RESEARCH AND DEVELOPMENT DIVISION

Appendix A: WRF Aerosol Sensitivity Simulations

February 2024 | CEC-500-2024-012

APPENDIX A:
WRF Aerosol Sensitivity Simulations

Susceptibility of Coastal Low Clouds to Particulate Matter Pollution

Atmospheric aerosols can modulate cloud reflectivity through aerosol indirect effects (Twomey et al., 1977; Albrecht et al., 1989). Aerosol indirect effects and other feedback caused by the interaction between clouds and aerosols are the largest source of uncertainties in the effort to estimate climate sensitivity to greenhouse gases (IPCC, 2013, e.g., Chapter 7, p. 573). WRF-CA-CLC assumes a fixed global background number of aerosols available to participate in cloud nucleation, but aerosol concentration in the real atmosphere exhibits great spatiotemporal variability. Concentrations are also expected to change with population and economic activity in future climates. Therefore, simulations are needed to estimate the sensitivity of CLC reflectivity to aerosol concentration.

The change in cloud albedo (α_c) to the change in cloud droplet concentration (N_c) is known as susceptibility. Broadly, it is expected that MSc will be most susceptible when baseline liquid water path (LWP) is robust, free atmosphere humidity is high, drizzle rate is low, and baseline aerosol concentration is low. In general, doubling of N_c (75 to 150 cm^{-3} at constant LWP ~ 150 g m^{-3}) leads to a 0.06 increase in cloud albedo. In this research experiments were performed to estimate susceptibility in WRF by enabling dynamic evolution of α_c for N_c=70 cm^{-3}, 300 cm^{-3} (marine, polluted conditions). Observational data (Martin et al., 2017) for marine cloud albedo susceptibility in the northern California coastal zone were used to verify that the model preserves correct relationships.

Particulate matter (atmospheric aerosols) can modify cloud properties and the radiative properties of clouds through the so-called aerosol-indirect effects. The most well-known of these is the aerosol indirect effect, first described by Twomey (1977), whereby increasing aerosol concentration causes clouds to become more reflective to sunlight (a.k.a. "brightening"). Other aerosol indirect effects exist, and feedbacks between aerosol concentration and cloud dynamics can cause unexpected or hard to measure changes (e.g., Han et al., 1998). As a result, the net impact of aerosol concentration on CLC albedo is unknown. This project attempts to develop methods to estimate the impact of pollutant aerosols on CLC albedo, and thus the reduction of downwelling solar radiation in the California coastal zone as part of the larger hybrid downscaling effort (EPC-16-063).

The dynamical downscaling model, WRF-CA-CLC, (Section 3.2) was used as the primary methodological tool to simulate both CLC and their brightening in response to increasing aerosol concentrations. Two simulations were run to represent clean and polluted particulate matter scenarios. The aerosol concentrations (150 cm^{-3}/ 600 cm^{-3}) representing each scenario were drawn from previously published observations at the California coast (Martin et al., 2017) and are, therefore, representative of the current climate and current particulate matter regulatory frame in California. Aerosol susceptibility, defined as the relative change in albedo

in response to an increase in aerosol concentration (see Methods section below) was used as the primary metric to estimate the response in cloud brightness to particulate matter. The results obtained, described below, indicate that polluted conditions increase warm season (MJJAS) CLC albedo 15 to 20 percent along the California coast. This magnitude of increase is similar to the relative interannual variability in albedo found for the period 2009 to 2018 of ~25 percent. The change in simulated albedo diurnal cycle in response to polluted conditions is small relative to its amplitude. CLC are most susceptible to polluted conditions in the month of July. Thinner clouds (by water path below 700 hPa) are more susceptible to pollutant aerosols than are thick clouds (CWP700 > 0.1 mm), while the spatiotemporal variability in susceptibility is also greatest for thin clouds. It was also demonstrated that the modelling methods used herein to allow dynamically varying cloud effective radius in response to changing aerosol concentration produce more realistic relationships between cloud water amount and albedo, and that the default approach used before applying our methods produces clouds that are too bright, even for many polluted clouds. These results help inform future regional downscaling efforts whose aim is to investigate coastal low clouds and their impact on surface insolation.

Methods

Definitions

Albedo	Reflectivity of a cloud-containing atmospheric column as measured by the ratio of upwelling to downwelling solar radiative flux at the top of the atmosphere α =(F_TOA^↑)/ (F_TOA^ ↓)
	Typical albedo values for summer clear and cloudy sky conditions over the California coast are 0.15 and 0.6, respectively.
Susceptibility	Defined as the relative change in albedo following a systematic change in cloud properties (e.g., number of aerosols or cloud droplets) S= 〖 α -α〗 _0/α_0. That is, a measure of the sensitivity to aerosol loading.
Cloud Water Content	The total mass of cloud water in an atmospheric column, including liquid and ice phases. M_c
	For stratocumulus clouds over the California coast, Mc is typically near 0.4 grams per cubic meter of air.
Cloud Number Concentration	The number of cloud droplets (Nc) per unit volume of the atmosphere. N_c
	In near-coastal stratocumulus conditions, Nc, typically ranges between 100 and 1000 cloud droplets per cubic centimeter of air.
	In general, the greater the number of cloud droplets, the more reflective cloud tops are, gaining a higher albedo for a constant Mc.
Cloud Water Path (CWP)	The integrated amount of cloud water mass between the earth's surface and the top of the atmosphere. Also, the integrated amount between the earth's surface and a pressure equal to 700 hPa. CWP700. Typically, CWP700 is between 0.01 and 0.3 mm when stratocumulus clouds are present.

Cloud Droplet Effective Radius	The ratio of the third to second moments of the cloud droplet size distribution, describing the scattering efficiency of clouds in most atmospheric radiative transfer models, r_e.
	Typical values of re are between 5 and 30 micrometers. Smaller re tends to result in more efficient scattering, analogous to the impact of raising Nc on cloud albedo.
Cloud Optical Depth	The total extinction of radiation (here, solar) in an atmospheric layer containing cloud. τ_c.
	Typical values of τ_c are between 1 and 50.
	Thicker optical depth yields lower penetration of radiation to the surface and higher albedo.

Models

- WRF-CA-CLC: the standard WRF configuration that was used to dynamically downscale coastal low cloud amount in the historical climate period. See Section 3.2.
- WRF/CHEM: WRF coupled with predictive models for atmospheric chemistry and aerosols (https://ruc.noaa.gov/wrf/wrf-chem/). Herein, only the code module "mixactivate" is used to predict N_c given a prescribed aerosol cloud condensation nuclei concentration.
- Morrison 2-Moment Microphysics: Cloud microscale physics model running interactively with WRF in WRF-CA-CLC configuration. The Morrison 2-moment microphysics model (Morrison et al., 2009) allows N_c and M_c to evolve independently, thus enabling CLC susceptibility experimentation.
- Goddard Radiative Transfer Model: Atmospheric radiative transfer model running interactively with WRF in WRF-CA-CLC configuration. The Goddard radiative transfer model (Matsui et al., 2018) uses M_c, r_e, and other atmospheric variables to predict τ_c and α.
- Model Susceptibility Process (1 -> 2 -> 3 in Figure A-1): As configured by the developers, the standard Goddard radiative transfer model does not ingest a dynamically varying r_e from the Morrison 2-moment microphysics model. Instead, a fixed value of r_e=10 μm is used for all clouds. Thus, even when the standard WRF/CHEM is activated to provide clean and polluted scenarios for Nc; the albedo of clouds, the subsequent cloud top cooling, and resulting boundary layer turbulence depicted in Figure A-1 cannot respond to a change from clean to polluted conditions. For this study, the Morrison 2-moment microphysics model and the Goddard radiative transfer model components of WRF/CHEM were modified so that the dynamically varying value of r_e is used to compute cloud optical depth and thus albedo, radiative heating and cooling at cloud top. This version is called "modified WRF-CA-CLC".

Figure A-1: Updates to the WRF-CA-CLC sub-models governing CLC simulation to allow albedo susceptibility

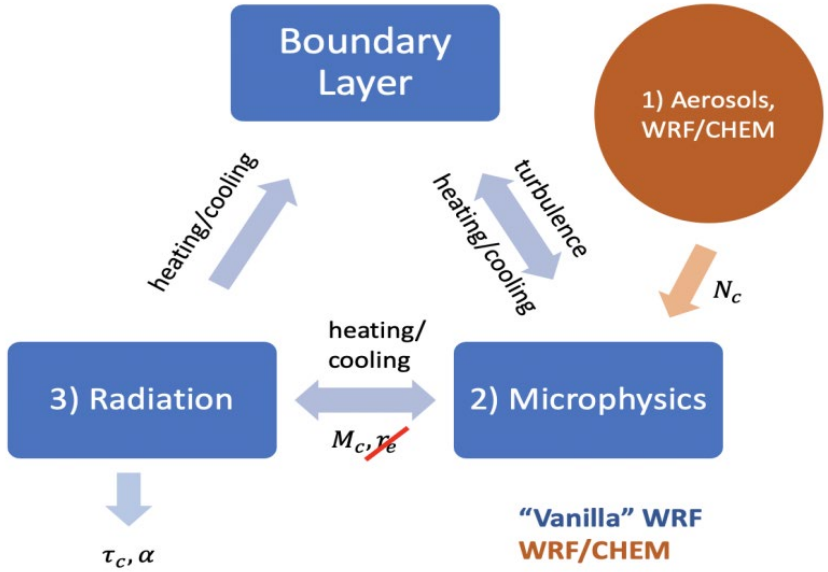

N_c, M_c, τ_c, α and steps 1, 2, 3 are defined in the text under "Definitions" and "Models," respectively. Red slash indicates that WRF does not, by default, pass the cloud effective radius (r_e) to the radiation model, making susceptibility simulations impossible. Updating WRF code to allow effective radius to pass to the radiation model was a technical achievement of this project.

Sources: from analyses herein, see text for additional details.

Historical Period

The warm season, defined as May through September (MJJAS, was re-simulated using the modified WRF-CA-CLC code for 2011 and 2015. Years 2011 and 2015 were chosen for susceptibility simulations because they represented very cloudy and clear conditions for the warm season in the primary WRF-CA-CLC dataset (e.g., Figure 12) and as confirmed by GOES and airport cloud observations. Model domain, initial and boundary condition data followed the 2011 and 2015 historical period simulations described in the primary EPC-16-063 report. Re-simulating unusually cloudy and unusually clear summer cases gave additional bounding on the estimated CLC susceptibility because, as will be shown, the susceptibility is related to the cloud water amount.

Defining Clean and Polluted Conditions

The activated cloud droplet concentration (N_c) for Clean and Polluted scenarios were drawn from Martin et al. (2017). Therein, the authors measured aerosol number concentration and the concentration of cloud condensation nuclei (CCN) at Bodega Bay, California during January through March 2015. CCN, as the authors measured it, is compatible with the definition of N_cin WRF/CHEM as used herein. During clear weather at Bodega Bay, wind is primarily onshore, bringing a clean marine airmass with low aerosol number concentration to the measurement site. However, episodes of offshore wind are created by a mesoscale weather phenomenon known as gap wind. During gap wind events, the authors measured much higher

aerosol concentrations and were able to chemically associate the particulate matter with secondary aging processes that occur over the California Central Valley, the airmass source region during gap wind. Therefore, the onshore period mean CCN concentration, 150 cm^{-3}, and gap wind mean CCN concentration, 600 cm^{-3}, were used to represent California coastal clean and polluted conditions for this study.

Cloud Screening

Albedo susceptibility is used as the primary metric in this study, but the standard method for calculating albedo from both WRF-CA-CLC and satellite observations cannot discriminate whether the reflective surface is a low or high cloud. If high clouds overtop CLC in the model or observations, spurious values of albedo and susceptibility may occur. Cloud screening was performed to remove model grid points containing high clouds from the WRF-CA-CLC output. The differential high water content, defined as CWP - CWP700 was used to detect the presence of high clouds. If the ratio CWP - CWP700 / CWP700 was greater than 0.01, the grid point was excluded from analysis.

Results

Relationship of Susceptibility to Cloud Water Amount

Figure 19 shows the relationship between CWP700 and albedo for WRF-CA-CLC warm season CLC in the California coastal zone for both clean and polluted simulations. The California coastal zone was defined as the set of model grid points nearest the land/sea boundary while retaining a land-surface type. This analysis serves as a validation of the model procedure and experimental method used herein (see "model susceptibility process" discussed above). Overlaid on Figure 19a are lines from the theoretical model of Han et al., (1998), whose authors explored the global relationship between liquid water path and albedo for liquid clouds. The approximate boundaries albedo can take for a given value of liquid water path (herein equivalent to CWP700) follow the line labelled "max" and the line for re = 35 μm. Figure 19a shows that WRF-CA-CLC clouds follow these bounds well. Figure 19a further shows that the effect of exchanging clean aerosol (blue) for polluted aerosol (red) conditions is to restrict the majority of clouds such that re does not exceed 20 μm. By contrast, clean conditions allow the albedo curve for clouds with re = 35 μm to be accessed in the model. Finally, both clean and polluted simulations produce clouds with albedo indicative of re > 10 μm for a given CWP700. Recall from the model susceptibility process section, that the Goddard radiative transfer model assumes re = 10 μm. Figure 19a demonstrates that allowing dynamic variation of re within a dynamical downscaling model allows a more realistic range of albedo for a given cloud water amount, and allows less bright clouds to develop, even for polluted aerosol conditions. Thus, projects attempting to dynamically downscale CLC should consider using a dynamically varying cloud effective radius, as used herein to produce realistic cloud albedos. Figure 19b shows the relationship between susceptibility and CWP700, essentially the fractional difference between the two populations in Figure 19a. Thinner clouds experience a much higher range of susceptibility for a given value of CWP700 than for thicker clouds, as expected by varying re within the Han et al., 1998 theoretical curves. However, on average

susceptibility is greater for thinner clouds than for thicker clouds, as will be seen in the results that follow.

Mean Warm Season Susceptibility

Figure 20 depicts the mean clean condition albedo and low cloud susceptibility for WRF-CA-CLC warm season (MJJAS) simulations, including cloudy (2011) and less cloudy (2015) years. During 2011 (Figure 20a), albedo is elevated ($\alpha>0.3$) over nearly the entire coast, with pockets of very high ($\alpha>0.5$) albedo. By contrast, elevated and very high albedo are confined primarily to the central and southern coasts in 2015 (Figure 20c). Low cloud susceptibility is higher in 2015, with a value of 0.21 compared to 0.16 in 2011. Han et al., 1998 discuss the relationship between CWP, r_e and α (see their Figure 1). Changes in re impact α more as CWP decreases. Thus, if coastal clouds were thinner on average during 2015, as is suggested by Figure 20c, then an increase in aerosol concentration from clean to polluted conditions would be expected to brighten clouds more, as is shown in Figure 20b, d. As seen in the main document, a susceptibility of 0.16 - 0.21 compares favorably to the relative interannual variability found in both WRF-CA-CLC and GOES (~0.25). Thus, the impact of polluted aerosol conditions on cloud brightening or reduction of solar insolation in the heavily populated California coastal zone may be approximately equivalent to the difference between a less cloudy warm season and a cloudier, warm season.

Susceptibility by Month and by Day

Figure 21 depicts the mean clean condition albedo and low cloud susceptibility by month for WRF-CA-CLC warm season simulations, including both 2011 and 2015. A clear seasonal pattern in coastal and offshore albedo is visible, wherein clouds (and elevated albedo) are widespread during May, confined to the south coast largely south of point Conception in June, begin marching northward along the coast in July, reach their northernmost coastal extent in August, and retreat southward along the coast again in September. The widespread elevated ($\alpha>0.3$) albedo in May, including over the Central Valley and inland desert regions could be indicative of deep, precipitating clouds driven by synoptic weather systems as found by previous authors (e.g., Clemesha et al., 2016).

Albedo susceptibility (Figure 22) follows the mean albedo seasonal cycle, as it is only calculated where CLC are present. However, the value of coastal mean susceptibility (where defined) shows no such marked seasonality. The exception is for May, where mean susceptibility is relatively less at 0.15, compared to 0.19, 0.2, 0.18, and 0.18 for JJAS.

As discussed, the susceptibility is larger for thinner clouds (by CWP), and the potential for deep precipitating clouds in May to contain much higher CWP may explain why the May susceptibility is lower than the late summer. Heat waves and clear skies are less common during May for most of the populated coastal zone, thus the impact of particulate matter in reducing insolation through cloud brightening may be greater later in the summer when low clouds are thinner and more susceptible.

Figure 23 shows the mean albedo diurnal cycle (daylight hours: 14 UTC to 01 UTC) for the warm season 2011 WRF-CA-CLC clean and polluted simulations alongside the diurnal cycle from GOES observations of albedo in the California coastal zone (coastal zone points as in

Figures 20-22). Visually following the difference between the curves for clean and polluted simulations reveals that there is very little diurnal cycle in susceptibility, except that which may be caused by the variation in clean albedo (e.g., the denominator of the susceptibility equation). In other words, polluted clouds show no systematic increase in reflectivity based on time of day. Also seen in Figure 23, the amplitude of the WRF-CA-CLC warm season diurnal cycle is significantly less than the GOES diurnal cycle (12 percent compared to 18 percent), and the model simulations prescribe a rebound of cloudiness in the evening, while the observational data does not show a systematic rebound. It should also be noted that the higher albedo level at all times of day shown in Figure 23 is consistent with the interannual timeseries for 2011 from Figures 11 and 12. Not shown in Figure 23 is the mean albedo diurnal cycle derived from 2015 warm season simulations, which are very similar in shape and amplitude, but differ somewhat in albedo absolute value. In particular, WRF-CA-CLC mean warm season albedo was less than GOES in 2015 instead of more than as in 2011.